ASSESSING PERIPHERAL NERVE FUNCTIONAL RECOVERY: RETHINKING A MODEL FOR THE RAT COMMON PERONEAL NERVE

A Thesis

Presented to the Faculty of the Graduate School of Cornell University

College of Veterinary Medicine

In Partial Fulfillment of the Requirements for the Degree of

Master of Science in Comparative Biomedical Sciences

by

Eric Alison Yeager

August 2015

ABSTRACT

Peripheral nerve injury is common, with annual incidence rates of 300,000 in the United States. Not surprisingly, a large volume of research exists regarding nerve injury, repair, and regeneration. However, functional outcomes of repair are typically disappointing. Full recovery rarely occurs in spite of recent advances, representing significant personal and societal burdens, and maintaining the importance of continued research. There are various methodologies for assessing peripheral nerve regeneration. However, relatively few useful clinical tests for determining functional recovery exist that are not either invasive or destructive. The most used animal model for peripheral nerve injury research is the common laboratory rat, with the sciatic nerve most frequently studied. Walking track analysis is the most widely used method of assessment in this model. Walking tracks are created by using ink on the rat's feet to make prints on paper, though many variations of both "ink" and "paper" have been used historically. Measurements of various aspects of the prints (e.g. print length or distances between digits) are calculated into a sciatic function index (SFI) that represents dysfunction on a scale of 0 to -100 (with -100 being absolute dysfunction). This method has also been used in the laboratory rat for the branches of the sciatic, the tibial (TFI) and common peroneal (PFI) nerves. Unfortunately, this method is also plagued with difficulties (in any of these nerve models), including autotomy, contracture of injured limbs, and difficulties in obtaining prints (smearing or contamination). Recently, a new method, called skilled locomotion, has been used successfully in assessing recovery from central nervous system damage. In this method, rats traverse either a ladder with alternately missing rungs or a tapered beam. They are then scored based on the accuracy of their steps. This method has been suggested, but not validated, for use in peripheral nerve recovery studies. The present study used both sciatic nerve and common peroneal nerve transection models to compare SFI and PFI to skilled locomotion. Retrograde labels were also used to detect motor neurons that had successfully regenerated from the proximal to the distal nerve stump in order to provide an anatomic correlation of recovery. Our SFI results were consistent with the literature,

showing approximately a 20% recovery. However, our analysis of individual factors disagrees with the current literature. Specifically, we show that the distance to the opposite foot is significantly affected by nerve injury and recovery, that there is a lack of significant changes in print length, and an inability to differentiate toe spread and intermediate toe spread among post-surgical groups. The traditional PFI did not work as expected for our data. Analysis of measured components, including distance to the opposite foot and deviation angle of the foot (previously discarded as too variable of inconsequential) allowed us to create new models for common peroneal functional index. Using these models, we also addressed other perceived problems with the historical indices, including the use of contralateral limb data to normalize experimental limb data, and the use of the longest individual measurement for each trial in the final analysis. Skilled locomotion analysis of the surgical limb revealed a higher estimate of recovery (41-43%) than SFI (20%) in the sciatic nerve model. Our data also revealed that Sprague-Dawley rats slow down significantly when presented with either difficult terrain or nerve injury, and that they apparently learn to tread more carefully in all limbs under these conditions. Skilled locomotion analysis revealed that slip rates did not vary significantly for the common peroneal model. Finally, motor neuron counts were shown to correlate well with SFI ($p = 0.011$) and skilled locomotion ($p = 0.010$) in the sciatic nerve model.

BIOGRAPHICAL SKETCH

Eric Yeager is a ‘non-traditional’ student who started attending college after being in the workforce for over a dozen years following his secondary school education. He has worked and trained in many areas including the military, awning and sign fabrication, electronics assembly, line cook, retail sales and collections (among others), though he also has interests in computer programming, woodworking/fabrication, backpacking, horseback riding, electronics, mechanics, cooking, writing poetry and fiction, mathematics, and, of course, science and medicine. Eric completed an Associate of the Sciences degree in a Liberal Arts program at Finger Lakes Community College in Canandaigua, NY in 2005. His undergraduate work was completed in 2010 at the State University of New York at Oswego and culminated in a Bachelor of Science degree in Zoology with a minor in Chemistry. At the time of the writing of this thesis, he was a recent graduate of Cornell University’s College of Veterinary Medicine that was simultaneously completing this degree in Comparative Biomedical Science. Eric intends to continue in graduate education to pursue a Ph. D. in preparation for a career in academia. His ultimate goal is to design and implement an alternative school. He currently lives in Ithaca, NY, with his fiancée, Sarah, two dogs, Duchess and Phoebe, and a cat, Whiner.

Dedicated to Sarah Elizabeth Harris

Without you there is… nothing.

ACKNOWLEDGMENTS

Amanda Jones (substantial intellectual and practical assistance)

Emilija Zygelete (rat handler extraordinaire and substantial practical assistance)

Megan Lee (confocal microscope guru)

Allegra Terhorst (long nights counting motor neurons)

Matt Martin (practical assistance and general sounding board)

Sean Reining and Bob Doran (general rodent surgical principles, surgical suite construction)

Kevin Yager (rat husbandry and facilities)

Cherie Brown (rat cones, other)

Bryant Blank (veterinary care, when warranted)

Dr. Germaine Rivard (rat behavior)

And especially Dr. Jon Cheetham, who has gone to bat for me on multiple occasions and allowed this project to be my own while contributing active and gentle support when I needed it most.

The project described was supported by Grant Number T32RR018269 from the National Institute of Health. The content is solely the responsibility of the authors and does not necessarily represent the official views of the National Institute of Health.

Imaging data was acquired in the Cornell BRC-Imaging Facility using the shared, NIH-funded (S10RR025502) Zeiss LSM 710 Confocal.

TABLE OF CONTENTS

LIST OF FIGURES

LIST OF TABLES

LIST OF ABBREVIATIONS

Abbreviation	Meaning
BMH	Bain-Mackinnon-Hunter
CNS	Central nervous system
CP	Common peroneal nerve
IP	Intraperitoneal
IT	Intermediate toe spread (between digits II and IV)
LF	Left forelimb
LH	Left hindlimb
MN	Motor neuron
OCT	Optimal cutting temperature compound
PFI	Common peroneal function index
PL	Print length
PNS	Peripheral nervous system
RF	Right forelimb
RH	Right hindlimb
RT	Retrograde tracer
SC	Subcutaneous
SFI	Sciatic function index
SL	Skilled locomotion
SN	Sciatic nerve
SR	Slip rate
STS	Stationary toe spread
STSF	Stationary toe spread factor
TFI	Tibial function index
TIB	Tibial nerve
TOF	Distance to the opposite (contralateral) foot (from tip of digit III to tip of digit III)
TS	Toe spread (between digits I and V)

CHAPTER ONE

Peripheral Nerve Development, Degeneration, and Regeneration

Peripheral nerves, in general, are composed of the axons of efferent motor neurons (whose cell bodies lie in the ventral spinal cord) and afferent sensory neurons (whose cell bodies lie in dorsal root ganglia). Dependent on the specific nerve, they may also contain axons of afferent and/or efferent autonomic neurons (whose cell bodies lie in various peripheral ganglia). Each axon is surrounded by a basal lamina that is secreted and maintained by Schwann cells, the glia of the peripheral nervous system. In this way, Schwann cells form a sheath around all neuronal axons. Depending on the specific fiber type, Schwann cells may or may not produce a myelin coating that is responsible for saltatory conduction but they always produce the basal lamina sheath around each axon[1]. The axons are further covered in a series of connective tissue layers (Figure 1). The innermost is the endoneurium, which covers individual axons. Mast cells[2], fibroblasts, and the capillaries supplying vital nutrients and waste removal can also be found within the endoneurium[3]. These coated axons are bundled into a complex of interwoven and interconnected fascicles that are further sheathed by perineurium. Neither individual axons nor fascicles are randomly arranged. Instead, they are organized into approximations of their eventual tributary branches within yet another sheath, the epineurium[4], despite forming regularly dividing plexuses within the epineurium[5]. An extensive longitudinal arrangement of nutrient vessels is also organized within the epineurium and provides critical blood supply to the fascicular capillaries.

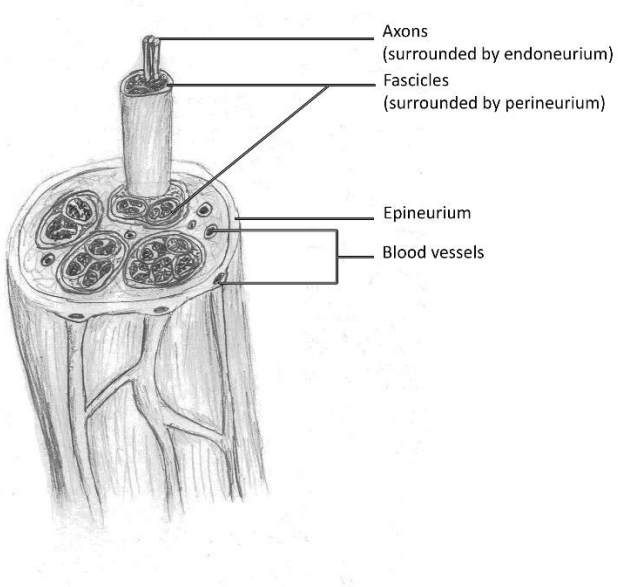

Figure 1: Typical structure of a peripheral nerve
Typical peripheral nerve with axons bundled into fascicles including connective tissue sheaths.

Degeneration of the peripheral nerve following injury follows a predictable pattern in terms of a basic immunologic and inflammatory response. However, understanding the subsequent regenerative processes requires defining basic concepts of innervation from an embryologic perspective, since they share similarities at the cellular and molecular levels. This understanding must be tempered with the knowledge that only half of the genes found to be functioning in regenerating nerves are present during development, indicating that there are also clear differences in these processes[4]. Furthermore, the extracellular environment surrounding axons during development is very different from the environment surrounding axons undergoing repair in the mature animal[6].

The nervous system is quite complex, and the size and locations of the important anatomic components of peripheral nerves also must be considered. Damage to a nerve fiber peripherally assuredly means that changes occur centrally, in the spinal cord where the neuron's soma is located, and to the nerve's synaptic interface with its target organ. Therefore, any therapy should consider the involved cell(s) as a whole - not just the grossly visible site of the lesion[7].

Peripheral Nerve Development

The relationship of peripheral motor neuron regeneration to peripheral motor neuron development is limited to the events that occur following embryologic neurulation, and specification of the neurons of the central nervous system (CNS) and peripheral ganglia. During development, a motor neuron's position within the spinal cord and its embryologic 'birthday' (the time at which it splits from its progenitor) are the generally accepted factors that accomplish neuronal specification prior to the initiation of axonal extension. The neuron, along with a group of neurons in its vicinity, will then begin to extend their axons toward a specific target. In part, this is a result of axonal chemorepellant receptors expressed secondary to Lim protein expression and as a function of the neuron's location and embryologic birthday. Certain chemorepellant molecules direct the axons dorsally in the limb bud while others direct them ventrally[8]. From this point, axonal specificity is typically divided into three sequential steps: pathway selection, target selection, and address selection.

During embryogenesis, the extending axon has a locomotory apparatus, called the growth cone, that is capable of sensing its environment and altering its migration based on identified signals. The growth cone is composed of numerous filopodia, called microspikes. Microspikes contain microfilaments that are arranged in parallel with the long axis of the axon and are anchored to the microtubules that provide the primary structural component of the axon. Movement of the growth cone is mediated via elongation of the microspikes, their attachment to the substrate of the extracellular matrix (especially laminin), and their subsequent contraction to draw the rest of the axon forward. Receptors on the microspikes sample the chemical composition of the environment and respond locally to detected molecules, being either attracted towards or repulsed from advancement. Additionally, these receptors also report back to the neuron soma via retrograde transport.

Regeneration of peripheral nerves recapitulates development beginning at the stage in which neurons choose targets and extend their axons over great distances through the periphery to innervate their target organs, a process known as axonal guidance[8]. The neuron itself takes no part in the guidance of the axon, and connection to its target organ will occur even in the absence of neural activity. Instead,

guidance is based on a variety of factors. The first is the presence of adhesive molecules (such as laminin) upon which the axonal growth cone will selectively advance. Additionally, proteins (from the ephrin, semaphorin, netrin, and Split families) within the matrix upon which the axon travels provide both attractive and repulsive cues to the growth cone. Groups of neurons express receptors for certain attractant proteins, while others express different receptors for certain repellant proteins. It is important to note that an attractant to one group of axons may be repellant to another. Diffusible molecules (such as netrin-1, netrin-2, and Slit) also may play a role in directing the extending axons. Some of these soluble molecules are also able to intimately interact with the extracellular matrix and potentially further alter its activity (from attractive to repulsive or vice-versa).

Target selection is similar, in that the expression of receptors by the axon growth cone guide the interactions of an axon with its intended target. Proteins expressed by the target tissue interact with the receptors of the extending axon in order to 'attach' it. In addition, neurotrophins (such as nerve growth factor [NGF], brain-derived neurotrophic factor [BDNF], and neurotrophins 3 and 4/5 [NT3, NT4/5]) produced by target cells also form the final chemotactic gradients that attract the growth cones to their final destinations. The final attachment can be digital (strongly molecule specific resulting in neuron-specific attachment) or analog (many axons may bind the molecule on the target and the amount of the molecule appears to be important), though it is likely a combination of these factors[8].

When forming a neuromuscular synapse, the axon adheres to the muscle cell membrane and begins to produce vesicles containing neurotransmitter. The cell membranes thicken and the intervening space is filled with a specialized extracellular matrix that is composed of laminin produced by the muscle cell and, sometimes, N-cadherin from the growth cone. This matrix also serves as a signal to other growth cones to stop migrating and attach to the muscle cell. A minimum of two neurons transiently attach and form a synapse with the muscle. However, through a competitive process of 'address selection' (based on the activity level of the neuron's synapse), all neurons except the most active are retracted. The retraction and eventual apoptotic death of the neurons that fail to attach is likely mediated by the relative absence of neurotrophic factors to support them.

Peripheral Nerve Degeneration

Neuron cell body

Following peripheral nerve injury, there is a period of glial cell proliferation near the neuron cell body, which results in isolation of the affected neuron via removal of the synaptic connections by the glia[2]. If the damage to the peripheral nerve is extensive or very close to the origin of the axons, apoptotic cell death is a possibility. Damage to the nerve that is more severe or in closer proximity to the cell body increases the likelihood of cell death, which is also more likely as age increases[9]. Additional changes take place in the soma but most are either related to preparation for repair and growth or are mediated by signals that start at the site of injury.

Site of Insult

Trauma to a peripheral nerve causes immediate damage to axons, supportive cells and the connective tissue sheaths at the site of the insult. In transected fascicles (or whole nerves), the elastic endoneurium causes retraction of the severed nerve ends, while hemorrhage and edema results from compromise of the local vasculature and, in turn, permits an increased inflammatory response[2]. However, a number of factors also have a direct immediate and possibly long term damaging effect on the traumatized peripheral nerve stumps including ion shifts, penetration of free calcium into the axoplasm, and outflow of axoplasmic contents[10]. Fibrin can be deposited as a result of disruption of local vasculature and can act to inhibit regeneration[4]. Immediately following transection of the nerve, electrical activity of the nerve stimulates increases in the concentration of intracellular calcium at both the soma and the site of injury[4]. Calcium is an important mediator of Wallerian degeneration, a well-documented process in which the axons in the distal nerve stump degenerate and their myelin sheaths degrade[11]. Within 48 to 96 hours, any remaining axonal continuity is lost. Fragmentation of neurons can take up to 44 hours to be detectable in rats under light microscopy and proceeds visibly in an anterograde direction at variable rates (10-24 mm/hour)[12]. The degenerative process can take up to 8 weeks to complete[2].

A similar degeneration occurs within the proximal nerve stump, though it is usually limited in comparison to the degeneration observed in the distal stump and its extent is dependent on the type of damage to the nerve[2, 3]. The axons of the proximal stump will also decrease in diameter, which will in turn reduce conduction velocity[2].

Early in the degenerative process, Schwann cells in the distal stump start to phagocytose debris that results from the injury and initial axonal fragmentation. However, having lost their innervation, they begin to proliferate and their de-differentiated daughters align themselves within the existing basal lamina sheaths to form Bands of Büngner[12]. Macrophages are recruited to assist Schwann cells while endoneurial mast cells release serotonin and histamine, further enhancing the influx of macrophages. Removal of myelin and myelin-associated glycoprotein is essential to regeneration as they act directly to inhibit regeneration of severed axons, and may also play a role in complement activation that results in formation of membrane attack complexes on intact axons in the vicinity of the lesion[12]. Fibroblasts begin to proliferate to form a fibrous scar. Overall, the process of removing the axonal remnants and myelin debris can take days to months[2]. Macrophage infiltration, which peaks at 7 days[13,14], is also critical to proliferation of Schwann cells[15], which fail to proliferate and dedifferentiate when non-resident macrophages are excluded from the site of injury[17,16].

Cytokines and chemokines play key roles in the events following peripheral nerve injury. Prior to macrophage infiltration, cytokines and chemokines expressed by resident denervated Schwann cells and fibroblasts are typical of inflammation. Examples include tumor necrosis factor alpha (TNFα), interleukins 1-alpha and 1-beta (IL-1α and IL-1β), granulocyte macrophage colony-stimulating factor (GM-CSF), monocyte chemoattractant proteins 1 and 1-alpha (MCP-1/CCL2 and MIP-1α/CCL3), and matrix metallopeptidase 9 (MMP-9). Conversely, the later phase of Wallerian degeneration (following macrophage recruitment) is characterized by increases in production of anti-inflammatory cytokines, primarily interleukins 10 and 6 (IL-10 and IL-6) and reduced production of the pro-inflammatory cytokines[12]. Neurotrophic factors, such as nerve growth factor (NGF), brain-derived neurotrophic factor (BDNF), neurotrophin-4 (NT4), and IL-6, are responsible for promoting neuronal survival and axon

growth, and are up-regulated in resident fibroblasts during normal Wallerian degeneration[12]. Finally, ciliary neurotrophic factor (CNTF), a neuropoietic cytokine, is transported in retrograde fashion to the neuron cell body, functioning as an injury factor and stimulating the early activation of Signal Transducer and Activator of Transcription-3 (STAT3), which is responsible for early activation of nerve regeneration via Growth Associated Protein 34 (GAP43)[4].

The environment of the transected neuron fills with serum shortly following surgical transection and over the next few days the serum is replaced by a more solid fibrin matrix. Furthermore, macrophages and neutrophils invade, as do fibroblasts and Schwann cells. Fibroblasts begin to replace the fibrin matrix with the more durable collagen, and Schwann cells begin to lay down laminin[4].

Target Organ

While the formation of motor end-plates is an important aspect of the embryologic development of motor neuron connections and to the survival of the motor neurons, there is a relative paucity of literature that discusses the effects of transection to the distal nerve stump all the way to the level of the synapse or neuromuscular junction. Degeneration of the motor endplate is time-dependent[3], and the denervated muscle clearly becomes atrophic over time. However, while the normal muscle is only responsive to acetylcholine at the neuromuscular junction, the denervated muscle becomes sensitive to it over its entirety. Fibrosis from chronic denervation diminishes the probability of functional reinnervation[18].

Peripheral Nerve Regeneration

Neuron cell body

Chromatolysis refers to dispersal of Nissl bodies (dissolution of ribosomes), one of several morphologic changes of a neuron cell body in response to injury, also including swelling, eccentric nucleus and nucleolus, and nucleolar enlargement[4]. These changes signify the beginning of the transition from a functional neuron to one that is growing (or repairing)[19], and are also thought to be related to the isolation of the neuron initiated by the glia of the CNS[2].

Genes that are up-regulated include actin, tubulin, and GAP43 – all of which are related to axon extension and the generation of a growth cone. In contrast, the genes related to neurofilament production (related to axonal diameter) are down-regulated[20], as are those coding enzymes related to neurotransmitter synthesis[4]. This, too, is a recapitulation of processes noted in embryologic development[21]. Interestingly, the antegrade transport of the up-regulated gene products down the axon to the injury site occurs at a rate of approximately 5-6 mm/day, which is roughly the limit of daily axonal elongation[22,3].

Most, but not all, neurotransmitters and neuropeptides are down-regulated. For example, calcitonin gene-regulated peptide (CGRP) is up-regulated in axotomized motor neurons and may be related to vasodilation and thus promoting infiltration of macrophages at the site of injury as well as to formation and maintenance of neuromuscular junctions[19]. The activity of the axotomized motor neuron is also supported by the production of pro-inflammatory cytokines (i.e. IL-1, IL-2, IL-6, TGF-β, and IFN-γ)[19]. Finally, production of both neurotrophins and neurotrophic receptors suggests autocrine/paracrine support of local axonal growth and neuronal survival[19].

Site of Insult

In the transected peripheral nerve, the loss of structure, formation of scar tissue, infiltration of phagocytic cells, distance between the transected stumps and progressive degeneration of the distal stump all present challenges to the regeneration of functional axons. Regeneration begins within hours of transection, starting with sprouts being generated at the most distal, yet still viable, nodes of Ranvier in the proximal stump. Sprouts grow down the endoneurial tubes toward their target and may split or branch distal to the site of transection, although many of these branches will not survive[21]. The growth cone of the regenerating axon moves and acts exactly as the growth cone of the developing axon, except they grow between the basal lamina and the outer surface of a Schwann cell membrane[23] (which are not formed yet in embryologic development). There are commonly multiple sprouts from each severed axon, and if a gap exists, sprouts may encounter chemical signals or physical impediments that misdirect their growth[2,4].

It has been well demonstrated that living Schwann cells, and not simply the basal lamina that they secrete (although it is also important), are an absolute requirement for axonal regeneration[21]. Schwann cells proliferate in the proximal stump and migrate along the regenerating axon, presumably due to influences from the growing axons themselves[1]. The Schwann cells surround the axons in groups but later sort them into individual axons and form a myelin sheath around each axon. Finally, they produce a new basal lamina while the old basal lamina (if still present) is degraded. Axon sprouts extend beyond the basal lamina of the proximal stump, cross the connective tissue and debris between the stumps and enter the distal nerve stump into the Bands of Büngner. Studies of various nerve models have shown both preferential and random connections to the distal stump[24].

After a few months, the regenerating nerve compartmentalizes the axons into 'mini-fascicles' to re-establish normal endoneurium. Similar to embryologic development, the number of axons (and branches) that have extended to the distal stump is thinned to only those that have formed the most competent reconnections at the target organ[23].

Growth rates have been reported in a range between 0.5 and 9 mm per day, dependent on species, distance of the regenerating axon tip from the soma, and the technique used to estimate the growth[2,25]. This rate of axonal outgrowth has been correlated with the faster of the 'slow component' mechanisms of anterograde axonal transport responsible for delivery of structural proteins necessary for building or repairing microtubules and microfilaments[26–28].

Target Organ

There appears to be selective reinnervation of denervated end-plates[3], which is likely related to the phenomenon of 'bridging' by Schwann cells at the neuromuscular junction which act as channels to guide reinnervation of previously denervated junctions[29,30]. If a functionally unrelated end-organ or an end-organ that has degenerated beyond recovery is encountered, the development and maturation of the axon is aborted[2].

CHAPTER TWO

Comparison of Functional Recovery Assessment Methods

Introduction

Peripheral nerve injuries are common, with annual incidences of 300,000[31] in Europe and 360,000[32] in the United States. Although the majority of peripheral nerve injuries are of traumatic origin (87-93%)[33–35], iatrogenic surgical injury also plays a prominent role (7.5%), followed by etiologies that do not involve limb trauma (7-7.5%). Incidence is generally found to be higher in men (74%) and within relatively young age ranges (32.4-34.6)[36,35]. Additionally, approximately 50% of patients require support services and/or rehabilitation[37], representing massive societal and personal costs[38].

Despite the large volume of research in peripheral nerve regeneration and advances made in microsurgical technique, currently used methods of repair produce moderate results that rarely achieve ideal axonal regeneration rates of 1 mm per day in patients with transected nerves[4,39]. Functional outcomes are disappointing and full functional recovery is seldom achieved[18,41,40]. Furthermore, peripheral nerve injuries are commonly complicated by neuropathic pain, which can be a significant source of morbidity[42,32].

There are numerous methods for measuring physiologic and/or anatomic outcome of peripheral nerve repair in experimental models. These include histological measurements of axon count[43,42], neuron cell body count[45,44], and motor endplate count[46], as well as motor unit number estimation[48,47], evoked potential measurement[49–51], muscle contractile force[53,52,54], and muscle wet weight[57,56,55], among others. However, relatively few methods of assessing functional recovery from peripheral nerve injury have been used[20]. Classically, tests for the measurement of functional recovery have been behavioral in nature and include walking track analysis[58–60], sensory function[61,55], photographic studies of kinematics[64,62,63], and ground reaction force (measured using force transduction plates)[67,66,65].

The ability to measure functional recovery is essential to assess outcomes of any therapy directed at improving peripheral nerve repair. In addition, clinical assessment of functional recovery is useful for

the serial study of peripheral nerve repair in animal research models, as it reduces the number of animals required for experimentation. It also minimizes some of the variability in testing by allowing repeated measurements on the same experimental subjects (i.e. longitudinal studies), rather than subjecting all or part of a group of research subjects to terminal or invasive methods of assessment.

Among models of peripheral nerve injury and repair, the sciatic nerve (or one of its distal branches) in the laboratory rat represents a relatively easy surgical target in a convenient animal model and has a well-established body of available work to support its use[20]. Among these studies, the most common test of functional recovery is that of walking track analysis[20]. Numerous variations in methodology have been used for obtaining walking tracks, including grease and paper[68], x-ray film or photographic paper with developer[58], poster paint and paper[69], bromophenol blue treated paper with tap water[70], and India type ink with plain paper[71], among others. However, the general methodology involves the application of some ink-like media to the hind feet of the rat and allowing them to traverse a paper-like substance upon which they leave their hind paw prints.

Measurement of morphologic changes reflected in walking tracks of rats that were otherwise demonstrated to have consistent and reliably quantified locomotion was proposed by Hruska, et al. in the late 1970s[68]. De Medinaceli, et al. developed specific measurements for print length (PL, distance from heel to digit III), total toe spread (TS, the distance between digits I and V), intermediate toe spread (IT, the distance between digits II and IV) and distance to the opposite foot (TOF, distance from digit III of the measured print to digit III of the next contralateral print, Figure 2)[58]. Measurements were taken of the prints on both the experimental limb (E) and the contralateral (C) limb (e.g. EPL, ETS, EIT, and ETOF for the experimental limb and CPL, CTS, CIT, and CTOF for the contralateral limb), which de Medinaceli called ‘normal’. These measured components were used to normalize the experimental limb measurements against the contralateral limb using a variant of percent change, and into ‘factors’(Figure 3). The calculation of these factors differs for some components, although a clear rationale for the differences was not provided.

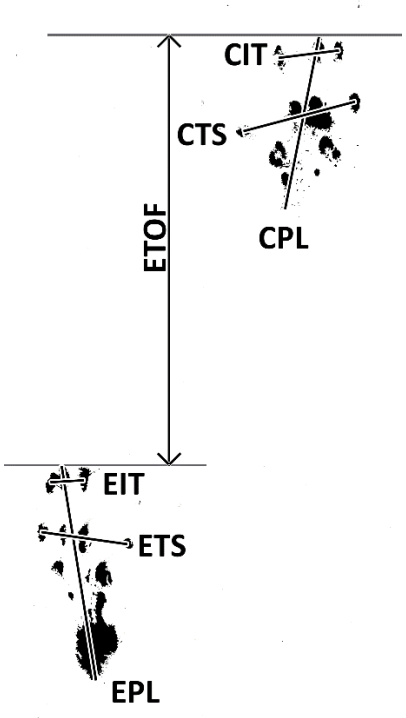

Figure 2: Example measurements for traditional SFI.

The traditional measurements for SFI include print length (the distance between cranial extent of digit III and caudal extent of the print), the total spread (the distance between the centers of paw pad I and paw pad V), intermediate toe spread (the distance between the centers of paw pad II and paw pad IV), and distance to the opposite foot (the vertical distance between the cranial aspects of contralateral prints). CTOF is not shown here but would be measured in the same way from the right print to the next sequential left print.

Equation(s) for factors in de Medinaceli SFI:

$$TOF\ factor = \left(\frac{ETOF - CTOF}{CTOF}\right)$$

$$PL\ factor = \left(\frac{CPL - EPL}{EPL}\right)$$

$$TS\ factor = \left(\frac{ETS - CTS}{CTS}\right)$$

$$IT\ factor = \left(\frac{EIT - CIT}{CIT}\right)$$

Figure 3: Calculation of factors from measured walking tracks
Calculations of 'factors' using the measurements taken from walking track prints. These equations are variations of percent change and use measurements of the contralateral limb to normalize the experimental measurements. Note that the calculation of the print length (PL) factor differs from the other factors.

The factors were then weighted equally to produce an empirical formula (Figure 4) that provided an 'index' (called the Sciatic Function Index, or SFI[58,72]) that used a scale of 0 to -100, where 0 represents absolute nerve function (no deficit) and -100 reflects absolute nerve dysfunction (complete deficit, as in a transected nerve).

de Medinaceli SFI equation (1982):

$$SFI = \left(\frac{ETOF - CTOF}{CTOF}\right) + \left(\frac{CPL - EPL}{CPL}\right) + \left(\frac{ETS - CTS}{CTS}\right) + \left(\frac{EIT - CIT}{CIT}\right) \times 2.2 \times \frac{100}{4}$$

Bain-Mackinnon-Hunter (BMH) SFI equation (1989):

$$SFI = -38.3\left(\frac{EPL - CPL}{CPL}\right) + 109.5\left(\frac{ETS - CTS}{CTS}\right) + 13.3\left(\frac{EIT - CIT}{CIT}\right) - 8.8$$

Figure 4: Established Sciatic Function Index (SFI) equations
The de Medinaceli equation for SFI and its successor, introduced by BMH seven years later. Interestingly, the BMH SFI does not use TOF at all.

Later, Carlton et al.[73] and Bain-Mackinnon-Hunter (BMH)[59] further revised the de Medinaceli formula using multiple linear regression on a subset of the original measurements [omitting TOF as insignificant]. All factors were normalized by BMH using an equivalent percent change calculation (Figure 4). At the same time, BMH introduced separately and similarly derived formulae for the Tibial Function Index (TFI) and the (common) Peroneal Function Index (PFI) for use with peripheral nerve injury models using the distal branches of the sciatic nerve (Figure 5).

Bain-Mackinnon-Hunter PFI and TFI equations (1989):

$$PFI = 174.9\left(\frac{EPL - CPL}{CPL}\right) + 80.3\left(\frac{ETS - CTS}{CTS}\right) - 13.4$$

$$TFI = -37.2\left(\frac{EPL - CPL}{CPL}\right) + 104.4\left(\frac{ETS - CTS}{CTS}\right) + 45.6\left(\frac{EIT - CIT}{CIT}\right) - 8.8$$

Figure 5: Established Peroneal Function Index (PFI) and Tibial Function Index (TFI) equations
Equations established via multiple linear regression analysis of measured walking tracks by Bain et al. (1989) for estimation of functional recovery following injury and repair of their respective nerves. Note that the print length (PL) factor is calculated the same as all other factors vs. the de Medinaceli SFI equation (Figure 4).

Finally, BMH suggested an alternative stationary measurement for toe spread (TS) to account for recovery in rats that had deformities (e.g. contracture or autotomy) that disrupted normal footprint formation in the earliest study time points[73,59]. In this method, the rat was held stationary about the chest and allowed to lightly rest its feet on a sheet of paper or acetate. With its weight as evenly distributed as possible, the distance between the first and fifth toes was manually marked with a fine-tipped pen[59]. Again, the experimental limb was normalized against the contralateral limb using a percent change calculation (or factor, Figure 6). This use of stationary toe spread (TS) has also been used independently as a method of assessing functional recovery[74–76], including in species other than the rat[75].

Bain-Mackinnon-Hunter Toe Spread Factor equation (1989)

$$STSF = \frac{ESTS - CSTS}{CSTS}$$

Figure 6: Established Stationary Toe Spread Factor (STSF) equation
Equation created by BMH (1989) for normalizing stationary toe spread measurements taken to account for functional recovery in rats that were unable to make measurable prints using standard walking tracks, usually due to some deformity (e.g. contracture or autotomy).

SFI is widely used in studies of peripheral nerve regeneration[81,54,86,85,87–91,77,79,80,78,82,83,43,84]. However, there are numerous problems reported with sciatic function index (SFI). Failure of experimental subjects to make readable tracks is common[59,92,60], often requiring multiple trials to obtain 'usable' prints, due to print smearing, dragging the tail or contamination with ink on other feet[58,93,94]. This can be further complicated by autotomy[92] or contracture[95] resulting from the lesions themselves. Problems can also occur if the rat pauses during a trial, especially if they stand only on their hindlimbs[96]. Weight gain and specific rat strain are also factors that must be considered. For example, autotomy is notable absent in Lewis rats following sciatic injury[60]. Finally, non-selective innervation of fascicles from the mixed grouping of tributaries of the tibial and common peroneal branches of the sciatic nerve due to axonal misdirection can result in altered activation patterns of the muscle groups during locomotion[52]. This would be more likely in the short term, as neural plasticity would allow for some correction over longer periods[97]. The common peroneal model is less prominent in the literature (we found only four

examples[60,78,98,99]). Furthermore, it is often described as difficult or impossible to assess via walking track analysis due to problems with contracture, which is presumably related to loss of function of tarsal flexor/digital extensor muscles[60,98,99].

Recently, skilled locomotion analysis over either a ladder or a tapered beam has been suggested as a means to evaluate recovery from peripheral nerve injury in rodent models[100,63]. Previously, this technique has only been used to assess recovery from central nervous lesions in rodent models[103,101,102,63,55], and has not yet been validated for use with peripheral nerve regeneration models. In its most complex form, the creators of this method (Metz et al.) described a complicated approach that assigned categorical scores to a variety of step-fault characteristics[101,102]. Each step was scored and the summation for each trial was given as a 'fault score'. These scores were then averaged across 5 trials. Kemp et al. simplified this method by using only the 0 and 1 'fault scores' described by Metz. et al. to count as a 'slip' and created a 'slip rate'[63,55] (Figure 7). Additionally, Kemp et al. expressed results only in terms of the experimental limb, whereas the Metz group analyzed measurements from all four limbs.

Kemp et al. Slip Rate equation (2010):

$$\text{Slip Rate (SR)} = \frac{\text{Total slips}}{\text{Total steps}}$$

Figure 7: Equation used by Kemp et al. to calculate Slip Rate for Skilled Locomotion Analysis
Total slips are divided by total steps (slips and non-slips) to derive a slip rate for estimating functional recovery following nerve injury.

We hypothesized that analysis of skilled locomotion over a ladder apparatus would provide a superior system for evaluating functional recovery in a transected nerve model in laboratory rats when compared to walking track analysis (both SFI and PFI). Skilled locomotion analysis is attractive as an apparently simple method of assessment, utilizing relatively inexpensive equipment in a low-stress and non-invasive approach that laboratory rodents should be expected to tolerate well. A simplified scoring method, such as that used by Kemp et al., could easily be used for assessment of functional recovery without requiring extensive training of personnel and promises broader repeatability between labs. Importantly, this method of assessment eliminates some of the difficulties commonly associated with

walking track analysis (e.g. smeared or contaminated tracks). Finally, there is no reliance on normalization against the contralateral limb in skilled locomotion analysis.

Two different surgical models were used: 1) acute transection and coaptation of the sciatic nerve, and 2) acute transection and coaptation of the common peroneal branch of the sciatic nerve. The sciatic nerve model was used to validate skilled locomotion against a well-established traditional method of estimating functional recovery, in spite of the limitation of a characteristically small degree of functional recovery[60,20]. The common peroneal surgical model was chosen since we hypothesized that skilled locomotion analysis would permit estimation of functional recovery from transection of this nerve without being confounded by the difficulties posed by the PFI (e.g. smeared or unreadable prints as a result of contracture).

Velocity was measured for both walking track analysis and skilled locomotion analysis, as failure to account for velocity has frequently been implicated as one of the faults of walking track analysis[92,105,104]. Our hypothesis was that velocity would significantly change over the course of the experiment and would, therefore, significantly affect walking track analysis.

The functional indices of de Medinaceli and BMH both used factors that were derived by normalizing their experimental measurements against measurements made of non-surgical contralateral limb from the same set of walking tracks. It has been reported that the contralateral limb is 'normal' in this situation in Lewis rats[96], whereas in Sprague-Dawley rats the contralateral limb plays a more 'compensatory' role[60]. For this reason, and because we used Sprague-Dawley rats, we compared the typical normalization procedure to normalization using average time zero (pre-surgical) values for each measurement. We hypothesized that contralateral limb compensation for injury of the surgical limb would result in significantly altered contralateral limb prints, making them unacceptable for use as standards for normalization. Furthermore, we hypothesized that variation in the prints of normal rats were sufficiently small, and using these measurements to normalize all experimental measurements (on both the surgical and contralateral limbs) was a superior method.

In addition, both authors (de Medinaceli et al. and BMH) mentioned additional component measurements found to be too variable (de Medinaceli, angle of feet and width between feet) and/or not to significantly affect the regression equations (BMH, print angle and distance to the opposite foot). However, data was not presented to support these assertions. For this reason, and in consideration of our hypothesis regarding surgical limb measurement normalization methods, measurements were taken for distance to the opposite foot (TOF), print length (PL), total toe spread (TS), intermediate toe spread (IT), deviation angle (DA), and stance width (SW) in the common peroneal model. We hypothesized that these factors were, in fact, significantly variable over time in the common peroneal model and should, therefore, be considered when preparing a scaled index. Ultimately, multiple linear regression analysis was repeated using all of these measured components and a new PFI equation was defined.

For skilled locomotion over a ladder, irregularly spaced rung patterns have been suggested as a superior model since rats would be unable to 'memorize' the rung patterns. However, no data has been shown to support this concept. We collected data for the sciatic nerve study on both irregular and regular rung patterns. Similar to others, we hypothesized that the irregular patterns would show significantly higher slip rates and would, therefore, be most useful for future analysis of skilled locomotion over a ladder.

Finally, retrograde labeling of the regenerating nerves was used as a means to validate the anatomic and physiologic reinnervation. In this method, fluorescent dyes are transported in a retrograde fashion up the axons of only those axons that have regenerated a connection to a cell body, where they accumulate and are later visible histologically using a scanning laser confocal microscope. While many other methods of attempting to discern this reconnection have been used, retrograde labelling avoids error due to errors axonal sprouting or pathfinding[4,20]. We hypothesized that counts of labeled MNs would correlate well with both walking track analysis and skilled locomotion. However, we expected that the relationship between skilled locomotion and motor neuron counts to be the better of the two.

Materials and Methods

Ethics Statement

This study was performed in accordance with the Public Health Service Policy on Humane Care and Use of Laboratory Animals[106], the NIH guide for Care and Use of Laboratory Animals[107], and federal and state regulations. It was approved by the Cornell University Institutional Animal Care and Use Committee (IACUC, protocol #2012-0099). Animals were brought into the research facility and given a 72-hour acclimatization period prior to any procedure. All animals were maintained in a temperature and light controlled environment (12-hour light/dark cycle) and were permitted *ad libitum* access to water and standard laboratory rodent food (Tekland Mouse Breeder Diet; Harlan Laboratories, Madison, WI) without restriction. ARRIVE guidelines for reporting *in vivo* experiments were used throughout[108].

Experimental Subjects

A total of 52 female Sprague-Dawley rats (The Jackson Laboratory, Bar Harbor, ME), aged 12 weeks and weighing 239.41 (± 1.55) grams weeks at the time of initial surgery were used in this study. Twenty-four rats were randomly allocated into five groups based on pre-determined termination points (1, 4, 8, 12, and 16 weeks after nerve transection and repair) for the sciatic nerve functional recovery study. An additional twenty-two rats were randomly allocated into six groups based on pre-determined termination points (1, 4, 8, 12, 20, and 24 weeks after nerve transection and repair) for the common peroneal functional recovery study. Six rats were used as controls for the estimation of axon regeneration using retrograde tracers (RT); five were positive controls and one was a negative control.

Functional assessment: Training, baseline, and experimental assessments

Assessments of function were taken for each rat on the day before its initial transection and coaptation surgery (baseline, or week 0), at week 1 post-transection, and then at 4 week intervals, up to and including their pre-determined termination point. For the sciatic functional recovery study, termination points were defined at 1, 4, 8, 12, and 16 weeks post-operatively. For the common peroneal functional study, termination points were defined at 1, 4, 8, 12, 20, and 24 weeks, and additional functional assessments taken at 2, 3 and 16 weeks following surgery.

Each assessment consisted of three different methods, which were always taken in the following order: 1) skilled locomotion analysis across a level ladder, 2) stationary toe spread (TS) measurement, and 3) walking track analysis. Measurements of locomotive function were taken using a specially constructed corridor apparatus, and rats were acclimated to this apparatus prior to their baseline assessment using a 'regular' pattern of rung arrangement (9 days of acclimatization for the sciatic functional recovery study and 3 days of acclimatization for the common peroneal functional recovery study).

For the sciatic functional recovery study, assessment consisted of a minimum of 3 trials each on the 'regular' pattern and two different (randomized) 'irregular' patterns on the ladder (9 trials total). For the common peroneal functional recovery study, assessment consisted of a minimum of 3 trials each on a single (randomized) 'irregular' pattern on the ladder. The irregular patterns used were distinct between the separate functional recovery studies. Each ladder pattern was divided into three horizontal 'zones' to enable assessment of velocity at different places on the track. Rats were permitted to cross the ladder apparatus at a speed of their choosing, and were only encouraged to keep moving, not to move at a particular velocity. Timing, in order to calculate velocity, and video, used to assess validity of trials and to aid in enumeration of slips and steps for skilled locomotion, were both recorded for the entirety of each trial. The 'acceptability' of each trial was based only on whether or not the rat remained in constant motion across the apparatus. Three trials for each pattern at each time point for each rat were retained for analysis. A full description of the ladder patterns, zones and timing/video recording mechanisms is available in the Appendix.

The stationary TS was then made by holding the rat around its chest and placing each of its hind feet on a sheet of acetate paper until they laid flat on the plantar surface. The exterior-most position of digits I and V were then marked on the paper using a felt-tipped marker. Three separate stationary TS measurements (trials) were made at each time point for both the experimental (left) limb and the contralateral limb for each surviving rat and were retained for analysis.

Each rat had a minimum of three walking track assessments taken by inking their feet using an oversized inking pad (Ranger Industries, Tinton, NJ) soaked in archival quality ink (Ranger Industries,

Tinton, NJ) and then permitting them to run across a 43 cm long by 10 cm wide piece of (cut standard 20# ledger sized) paper placed on the 'floor' of the corridor apparatus. Walking track assessment only occurred in zone 1 of the apparatus. Timing, in order to calculate velocity, and video, used to assess validity of trials, were also recorded for each trial. Only three trials for each rat at each time point were retained for analysis, and rejection of a trial occurred for only one of two possible reasons: 1) the rat paused or stopped in the middle of the trial or otherwise did not maintain a relatively constant velocity over zone 1 of the corridor, or 2) the prints made were obviously unusable (poorly inked feet that did not make measurable prints, despite the animal walking on that foot as evidenced by the video recording).

General Surgical Procedures and Post-Operative Care

Prior to surgery, animals were pre-medicated with butorphanol administered SC (0.5 mg/kg; Fort Dodge Animal Health, New York, NY). General anesthesia was then induced using 5% isoflurane (Phoenix Pharmaceuticals, Saint Joseph, MO) in 100% oxygen using an induction box. Following induction, rats were removed from the induction box and general anesthesia was maintained with 1.5 – 2.0% isoflurane in oxygen using a rodent nose cone. The surgical site was clipped and prepared using standard aseptic technique and the animals were placed on an electric heating pad (ZooMed Laboratories, San Luis Obispo, CA) that was well padded with surgical drape to prevent burns for the duration of the surgery. Rats were placed in right lateral recumbency and the left hind limb and base of the tail were taped to the surgery table to eliminate movement from manipulation during surgery. The surgical site was protected with a sterile surgical drape (containing a single fenestration) that was also secured to the surgery table with tape.

All nerve transection surgeries were carried out using a stereo microscope adapted for surgical use (M60 modular stereo microscope; Leica Microsystems, Buffalo Grove, IL).

All animals received meloxicam (0.5 mg/kg; Nordbrook, Inc., Lenexa, KS), administered SC, perioperatively. Animals were allowed to recover in 100% oxygen (Airgas, Inc., Elmira, NY) in a separate recovery box.

An additional analgesic dose of meloxicam (0.5 mg/kg) was administered SC the day after surgery. A bittering agent (Bitter Apple®, Grannick's Bitter Apple Company, Norwalk, CT) was applied to the operated limb twice daily to deter autotomy of the surgical limb.

Transection and Coaptation Surgery

A linear incision was made in the lateral left thigh, using a #10 scalpel blade, that originated proximally approximately 2 mm caudal to the greater trochanter of the femur (palpable as the point of the hip) and continued distally to a point approximately 2 mm caudal to the lateral condyle of the tibia/head of the fibula (palpable on the lateral stifle). The biceps femoris muscle was elevated using rat-toothed ophthalmic forceps and a small incision was made in the caudal fascia lata using ophthalmic scissors. The incision was extended proximally and distally using a combination of blunt dissection and occasional use of the ophthalmic scissors, taking care to avoid branches of the caudal femoral artery near the trifurcation of the sciatic nerve. Magnetic retractors (Fine Science Tools, Foster City, CA) were used to reflect the biceps femoris muscle caudally, clearly exposing the sciatic nerve and its distal branches.

For the sciatic functional recovery study, blunt nerve hooks were used to elevate the sciatic nerve and to separate it from the surrounding fascia. Gentle lateral traction was placed on the sciatic nerve with a blunted nerve hook, and the nerve was transected with a #15 scalpel blade from the medial side just proximal enough to avoid the trifurcation and the small lateral cutaneous sural nerve where it crosses to enter the biceps femoris muscle.

For the common peroneal functional recovery study, blunt nerve hooks were used to separate the three branches of the sciatic nerve (the common peroneal nerve cranially, the tibial nerve caudally, and the caudal cutaneous sural nerve deep, Figure 8). The common peroneal nerve was then isolated and gentle lateral traction was applied using a blunt nerve hook, and the common peroneal nerve was transected from the medial side using a #15 scalpel blade.

The nerve stumps were gently lavaged with normal saline (0.9% saline; Abbott Laboratories, Abbott Park, IL) and immediately coapted using two interrupted nylon sutures (9-0 Ethilon™; Ethicon, Inc., Somerville, NJ) through the epineurium. Care was taken to retain the original rotational orientation

of the nerve stumps relative to each other. The coapted nerve was lavaged once more with normal saline, the retractors were removed, and the fascia lata was closed using 5-0 Monocryl Plus™ suture (Ethicon, Inc., Somerville, NJ) in a simple continuous pattern. Finally, the skin was closed using nylon suture (5-0 Ethilon™; Ethicon, Inc., Somerville, NJ) in a simple continuous pattern. Any skin sutures that were still retained were removed 14 days following surgery.

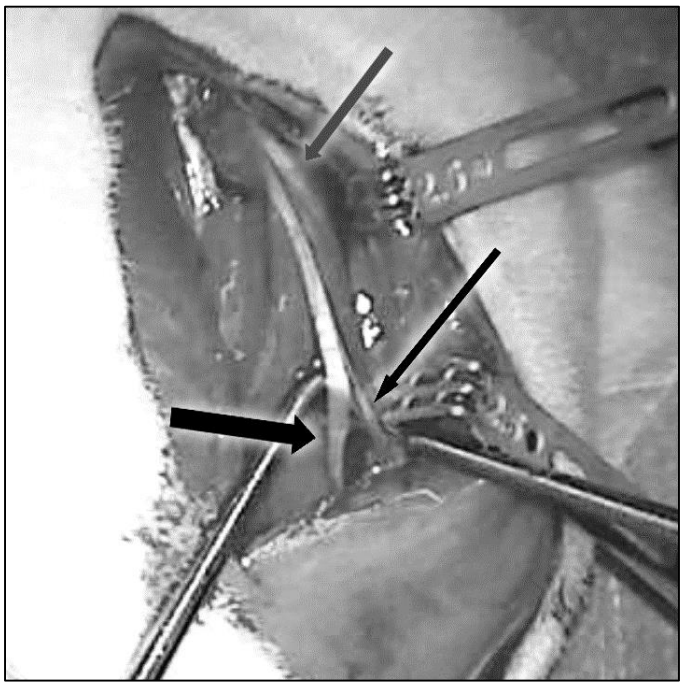

Figure 8: Sciatic nerve branches during surgery
Left lateral view of the exposed sciatic nerve and its branches (cranial left, dorsal top). In a mild anatomic anomaly, the sciatic nerve is divided very proximally, making its branches clearly visible: common peroneal (cranial, lower left), the tibial (caudal, top right), and the caudal cutaneous sural nerve (deep, lower right).

Retrograde Tracer Application

At the pre-determined termination point for each group, retrograde tracers were used to label motor neurons (MNs) of the sciatic nerve. The surgical procedure used was similar to that already described.

For the sciatic functional recovery study, in an effort to identify discrete MN pools for each branch and to detect any evidence of axonal misdirection between the branches, the left common peroneal nerve and the tibial nerve branches were individually exposed and transected separately approximately

5mm distal to the original coaptation site in order to avoid the heavily fibrotic regions of the regenerative bridge. Fluoro-Gold™ (Fluorochrome, LLC, Denver, Colorado) powder was applied to the proximal tibial nerve stump using tubes composed of modified 100 µL sterilized pipette tips (Diamond Tipack, Gilson, Inc., Middleton, WI) that were heat sealed at the small end and sterilized prior to surgery. The Fluoro-Gold™ was placed into the tube, the tube was cut to appropriate length, and the stump was gently inserted into the tube until it touched the Fluoro-Gold™ powder. The tube was then sealed with white petrolatum (Vaseline®; Unilever, Englewood Cliffs, New Jersey). A 10% solution of Fluoro-Ruby™ (Fluorochrome, LLC, Denver, CO) in 2% dimethyl sulfoxide (Neogen Corporation, Lexington, KY) was applied to the proximal stump of the common peroneal nerve branch in a similar fashion.

For the common peroneal functional recovery study, only the common peroneal nerve was transected approximately 5mm distal to the original coaptation site in order to avoid the heavily fibrotic regions of the regenerative bridge. Fluoro-Gold™ (Fluorochrome, LLC, Denver, Colorado) powder was applied to the proximal common peroneal nerve stump in the same manner as described above.

The nerve stumps were exposed to the retrograde tracers for one hour, then the tubes were removed. The stumps were lavaged twice with normal saline, then sutured to the underlying quadriceps femoris (vastus lateralis) muscle such that they were oriented away from each other in order to avoid potential cross-exposure. Muscular and cutaneous layers were closed and the animal was recovered as previously described. The retrograde tracers were given a period of 5 days to traverse their axons.

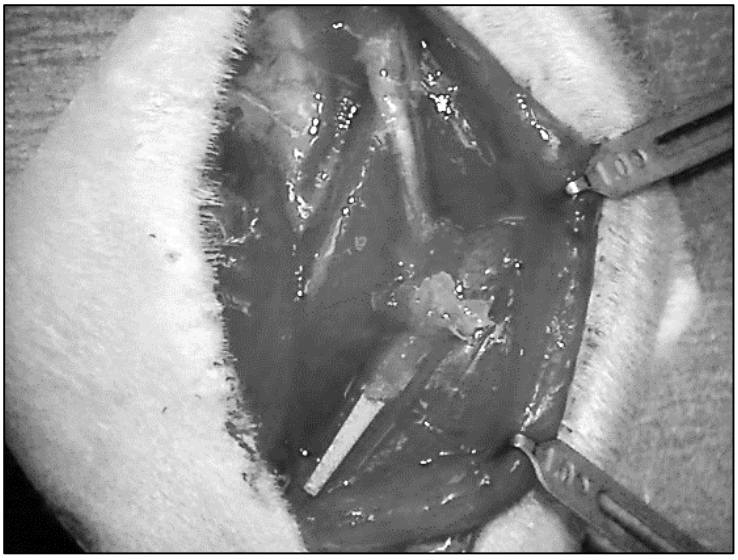

Figure 9: Rat common peroneal nerve being exposed to Fluoro-Gold™
Left lateral view of the exposed common peroneal nerve (cranial left; dorsal top). The tip of the proximal stump of the common peroneal nerve is at the junction of the very bright Fluoro-Gold™ and the sanguinous serum that is coating the remainder of the outer perineurium (circle). The whitish petrolatum 'seal' on top of the modified pipette tip can be appreciated just dorsal.

Paraformaldehyde perfusion and spinal cord harvest

Five days after the retrograde tracer exposure surgery, the spinal cords of the rats were harvested. Central nervous system (CNS) tissue generally requires fixation *in vivo* prior to harvest in order to stabilize CNS proteins and enable safe handling of this very friable tissue. Perfusion with paraformaldehyde under general anesthesia is a generally accepted procedure for collecting CNS tissue following retrograde tracer exposure, and a modification of a previously described method was used[109,110].

In brief, the rat was anesthetized (as previously described), and placed in dorsal recumbency. Incisions were made through the skin and subcutaneous tissues along the lateral thorax at a level just ventral to the axilla, from the thoracic inlet across the entirety of the rib cage. Similar incisions were made transversely at the level of the thoracic inlet and at the level of the xiphoid, connecting to the lateral incisions. The chest cavity was then opened at the level of the xiphoid process and the rib cage was removed via lateral cuts through the ribs on both sides and one transverse cut just cranial to the level of the heart using heavy Mayo scissors. The remaining bit of manubrium was clamped with a mosquito hemostat to prevent leakage from the internal thoracic arteries.

A 26-gauge catheter was then inserted through the apex of the heart into the left ventricle, the stylet was removed and the catheter was directed into the ascending aorta. A 60 mL syringe, with the plunger removed, was then attached to the catheter with an extension set and 50 mL of ice cold normal saline was allowed to gravity feed into the rat's circulatory system. The right atrium was nicked with scissors to permit controlled exsanguination and drainage of the perfusion solutions. The ice cold saline was followed immediately with 150 mL of a 4% paraformaldehyde solution (Sigma-Aldrich, Saint Louis, MO) in phosphate buffer.

When paraformaldehyde perfusion was complete, the spinal cord in the region ~15 mm on both sides of the last rib was removed using a bone rongeur. The spinal cord was then pinned at both ends to a small cork sheet (to prevent shrinkage) and was cryoprotected overnight in a 30% sucrose solution made from a 4% paraformaldehyde/phosphate buffer.

The following day, the spinal cord was embedded in optimal cutting temperature compound (OCT, Sakura Finetek USA, Inc., Torrance, CA) and snap frozen using liquid nitrogen. Prepared OCT blocks were then sectioned (50 µm thick) and mounted on Fisherbrand® *Superfrost® Plus* slides (Thermo Fisher Scientific, Inc., Pittsburg, Pennsylvania). Slides were placed on a slide warmer overnight to fix. The next day, they were washed in deionized water and permitted to dry overnight, then mounted using Cytoseal 60 (Thermo Scientific, Kalamazoo, MI) for visualization.

Imaging spinal cord sections

Spinal cord sections were imaged using a Zeiss LSM 710 laser scanning microscope in conjunction with Zen® software (Carl Zeiss Microscopy GmbH, Jena, Germany). Motor neuron cell bodies were counted at 40x magnification under ultraviolet fluorescence at barrier filters of 430 nm for FluoroGold and 580 nm for FluoroRuby. A region of interest was selected by manually setting its limits, defined by the population of fluorescing cell bodies, and the entire region was imaged and combined into a single .LSM image file format.

Skilled Locomotion Measurements and Calculations

Measurement of each ladder trial consisted of a simple system of determining 'steps' vs. 'slips', in a manner similar to the previously described method used by Kemp et al[63,55]. Slips were defined by an obvious shift of weight caused by a misstep, not necessarily a 'complete' slip of the foot off of the rung. For both the sciatic and common peroneal functional studies, using the video recordings from each time point, a single observer counted the total number of slips and the total number of steps (slips and non-slips) for each of the four limbs, within each zone, and for each trial. Slip rates (SR) were then calculated for each limb, for each zone and for each trial (Figure 6).

Walking Track Measurements and Calculations

Measurements were then made of the walking tracks, as previously described[58,59]. Briefly, the print length (PL), total toe spread (TS), intermediate toe spread (IT), and the distance to the opposite foot (TOF) were measured for prints made by both the experimental (left, E) and the contralateral (right, C) limbs.

For the sciatic functional recovery study, components used in the BMH SFI equation[59] (PL, TS, and IT) were measured by two different observers, and mean values derived from the two observations were used in subsequent calculations of the BMH SFI (Figure 4). Typically, several prints for each limb were made during each trial. However, only the longest measurement from each component for each trial was recorded for analysis. A variant of the BMH SFI calculation was made where week 0 mean measurements, rather than contralateral limb measurements, were used to normalize the measured components for *both* the experimental and the contralateral limbs at each time point (Figure 10). The distance to the opposite foot (TOF) measurements (used in the de Medinaceli equation[58]) were measured only by a single observer, so the calculated de Medinaceli SFI reflects only a single observer's measurements.

Variant (time 0 normalized) SFI factors:

$$TOF\ factor = \left(\frac{(E\ or\ C)TOF - TOF_{T0}}{TOF_{T0}}\right)$$

$$PL\ factor = \left(\frac{PL_{T0} - (E\ or\ C)PL}{(E\ or\ C)PL}\right)^{a}\ or\ \left(\frac{(E\ or\ C)PL - PL_{T0}}{PL_{T0}}\right)^{b}$$

$$TS\ factor = \left(\frac{(E\ or\ C)TS - TS_{T0}}{TS_{T0}}\right)$$

$$IT\ factor = \left(\frac{(E\ or\ C)IT - IT_{T0}}{IT_{T0}}\right)$$

Figure 10: Equations for variant time 0 normalized factors

These equations represent the variant calculation of SFI using time 0 (T0) to normalize experimentally measured data at each time point for both the experimental (E) and contralateral (C) limbs. Note that TOF is not used in the BMH SFI, and that differing factors for print length (PL) are used for the de Medinaceli SFI (a) and BMH SFI and PFI(b).

For the common peroneal functional recovery study, the measurements of these four components were also recorded. In addition, two other measurements were taken for the common peroneal functional study (only using the digitized method). They were Deviation Angle (DA, the angle of the foot, where the top of the paper = 0° as reference) and Stance Width (SW, the horizontal distance between the center of a print and the next contralateral print). Each of these measurements were taken for the experimental (left) and contralateral limbs (Figure 11).

Measurements for the common peroneal functional study were completed using two methods: 1) manual (by hand with a ruler) and 2) digitized (using Photoshop CS6® software (Adobe Systems, Inc., San Jose, CA) to measure scanned (CanoScan LiDE 110, Canon USA, Inc, Melville, NY) images of the walking tracks). For manual measurements, only the longest measurement from each component was recorded for each trial (trial maximum). For digitized measurements, all measurements for all prints were recorded (usually 2 prints per limb), then two sets of measurements were composed: a trial maximum set, derived from the largest measurement for each component (as traditionally done by de Medinaceli and BMH), and a trial average set, derived from the average measurement of each component from all ipsilateral prints for both the experimental and the contralateral limbs.

Means were calculated from the two methods of measurement that were derived from trial maximums (longest manual measurement + longest digitized measurement/2), and this mean set was used for calculation of traditional peroneal function index (PFI), as described by BMH[59] (Figure 5). A variant of the BMH PFI calculation was made where week 0 mean measurements, rather than contralateral limb measurements, were used to normalize the measured components for *both* the experimental and the contralateral limbs at each time point (Figure 10). Finally, both the traditional BMH PFI and the week 0 variant BMH PFI were applied to the trial averaged data set.

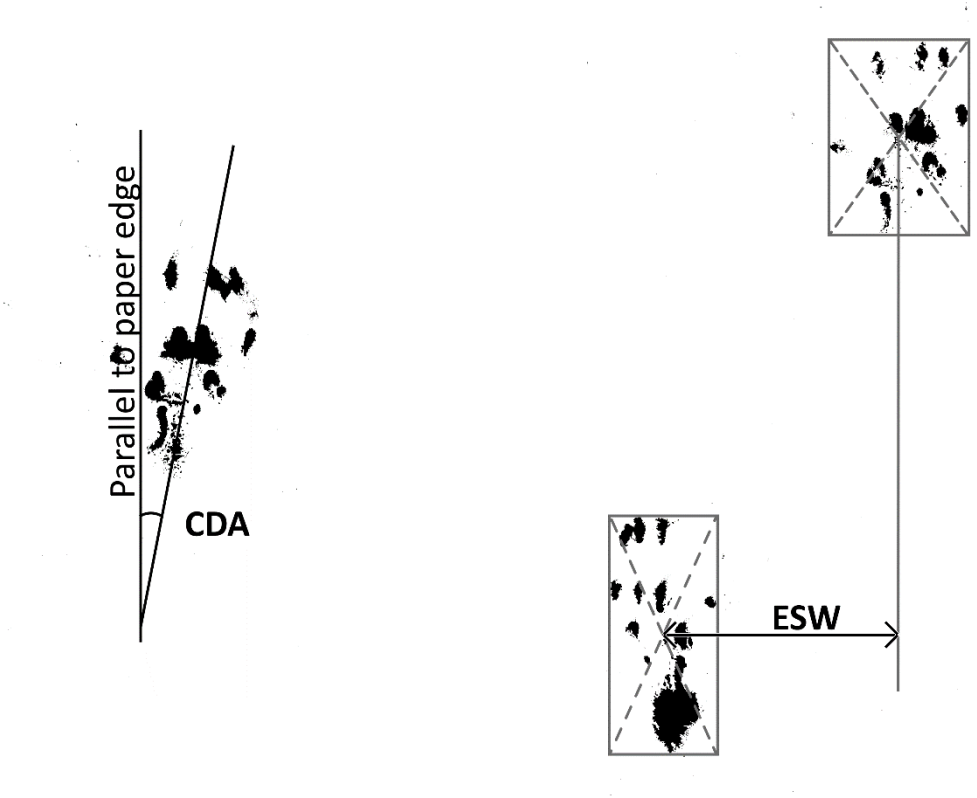

Figure 11: Examples of new measurements for additional analysis of the CP functional recovery.
New measurements included simple deviation angle (DA, the angle of the foot with respect to the edge of the paper; the top of the page = 0°) and stance width (SW, the horizontal distance between the print and the next contralateral print). Here, DA is shown only for the contralateral limb (CDA)and SW is shown only for the experimental limb (ESW).

Stationary Toe Spread Measurements and Calculations

Measurement of the stationary toe spread (STS) was carried out as previously described in a manner similar to that used by BMH[59], for all three trials at each time point. For the sciatic functional recovery study, measurement was completed by two different observers, and mean STS values derived from the two observations were used in the subsequent calculation of a Stationary Toe Spread Factor (STSF) for each trial using the method described by BMH (Figure 6). Additionally, a variant of the STSF was calculated by using mean week 0 measured STS to normalize the measured values for *both* the experimental and the contralateral limb at each time point (Figure 12). For the common peroneal functional recovery study, only a single observer carried out the measurements with which the standard and variant STSF were calculated.

Variant (time 0 normalized) stationary TS factor:

$$Stationary\ TSF = \frac{(E\ or\ C)STS - STS_{T0}}{STS_{T0}}$$

Figure 12: Equation for variant time 0 normalized stationary toe spread factor (STSF)
This equation represents the variant calculation of STSF using time 0 (T0) to normalize experimentally measured data at each time point for both the experimental (E) and contralateral (C) limbs.

Back Labelled Motor Neuron Measurements and Calculations

For both the sciatic functional recovery study and the common peroneal functional recovery study, quantitation of motor neurons (MNs) captured in .LSM files was completed using two separate methods: 1) manually (by hand), using ImageJ software (National Institutes of Health, http://imagej.nih.gov/ij/index.html), and 2) in a semi-automated way using Volocity® software (PerkinElmer, Waltham, MA).

Manual counting consisted of marking all labelled cell bodies that contained a distinct nucleus and were visualized under their respective UV fluorescent filter. Some difficulty was encountered counting sections visualized using the 430 nm filter, as the paraformaldehyde fixed tissue yielded a moderate fluorescent background at this wavelength. Therefore, some subjective interpretation of 'brightness' had to be made by the observer.

Semi-quantitative counting of motor neuron cell bodies using Volocity software required establishment of a protocol within the software. The protocol consisted of a setting limits for intensity, size of the detected object, and size at which the software should attempt to break the detected object into smaller objects. For double labelled motor neurons, the protocol also included limits using proximity of detected objects of the two labels in order to consider them co-labelled. A negative control was used to establish background intensity limits, and positively labelled controls (FR only, FG only, and double-labelled) were used to establish protocols that resulted in baseline counts that were similar to hand counts. These protocols were then used, unchanged, to count experimental images.

Mean values were then derived from the two methods and were used to generate total estimated counts for three distinct populations: 1) those with only Fluoro-Gold™, 2) those with only Fluoro-Ruby™, and 3) those with both labels.

Statistical Analysis

Slip rate (SR) analysis for the sciatic functional recovery study was carried out separately for regular pattern trials and irregular pattern trials. For both functional recovery studies, mixed effect modeling by individual limb SR, with the subject identifier as a random effect, showed no significant effect of individual trial (data not shown). However, time (weeks post-transection), zone, and velocity all had significant effects on SR. Therefore, each zone was modeled separately for each limb with velocity and week as fixed effects and subject identifier as a random effect. In addition, all zones taken together (counting the entire track as one large 'zone') was modeled, also with velocity and week as fixed effects and subject identifier as a random effect. Means resulting from these models were then tested using a Tukey's HSD for multiple comparisons.

For measured stationary TS in the sciatic functional recovery study, the two measurement sets were tested for interobserver repeatability using mean-difference analysis, as described by Bland and Altman[111,112]. For both studies, one-way analysis of variance (ANOVA) was used to assess the effect of time on each measured stationary TS and on all variations of the calculated stationary TS factors. A

Tukey's HSD (honest significant difference) test was then used for post-hoc pair-wise analysis for multiple comparisons.

For walking track analysis in the sciatic functional recovery study, the two measurement sets (for BMH SFI) were also tested for interobserver repeatability using mean-difference analysis, as described by Bland and Altman[111,112]. For the common peroneal functional recovery study, measurements obtained using both manual and digitized methods, were similarly tested for repeatability between methods using mean-difference analysis, as described by Bland and Altman[111,112]. Week 0 values were averaged for each study individually for PL, TS, IT and TOF. For both studies, the effect of time on each measured component and on the calculated indices was evaluated using ANOVA and Tukey's HSD. Calculated velocities of the SFI trials were also analyzed by ANOVA.

The components that were measured for the common peroneal functional recovery study using the digitized method (PL, TS, IT, TOF, DA, and SW) for *both* the experimental (left) and contralateral limbs were then prepared for multiple linear regression for the creation of a new CP functional index. For purposes of this analysis, measurements for all prints on each side were averaged within each trial (rather than using the longest measurement in each trial). Each component was then converted into a percent change 'factor' using the mean of that component's week 0 measurement for all rats combined (Figure 10).

For the regression analysis of the PFI factors, Week 0 data was determined to represent 'normal' function. Week 3 data was determined (via previously run ANOVA/Tukey's HSD) to represent maximum dysfunction for PL, TS, IT, and TOF. Similarly, week 4 data were determined to represent maximum dysfunction for DA and SW (also via previously run ANOVA/Tukey's HSD). Therefore, week 0 was designated as '0' and weeks 3 and 4 were both assigned as '-100' to create the independent axis for the regression analysis. Each of the component measurements were then screened for its effect on the index, using only data from weeks 0, 3, and 4. Subsequently, three independent models were constructed using multiple linear regression based on the levels of significance of the individual components ($p < 0.05$, $p <$

0.005 and $p < 0.0001$) and using the complete data set. Finally, the new PFI was calculated for each of the three models for each trial at all time points.

For both the sciatic and common peroneal functional recovery studies, the two measurement sets for MN counts were tested for repeatability between methods using a mean-difference analysis, as described by Bland and Altman[111,112]. Mean values were derived from the two methods and were used to generate total estimated counts for labelled cell bodies. The effect of time on MN count was determined using ANOVA and post-hoc Tukey's HSD tests.

Finally, bivariate analysis was used to test the relationships between MN counts and each of the calculated functional indices, as well as the relationship between MN count and SR.

All statistical analyses were carried out using JMP software (SAS Institute, Cary, NC).

Results

Exclusions

Eight rats were euthanized prematurely (seven from the sciatic functional recovery study and one from the common peroneal functional study), due to autotomy of their surgical limb, using an overdose of a barbiturate (3000 mg/kg pentobarbital; Fatal-Plus®, Vortech Pharmaceuticals, Ltd., Dearborn, MI) administered via intraperitoneal (IP) injection, and their data were not included in the final analysis. Additionally, one rat (in the common peroneal functional study) was diagnosed with and treated for a mammary adenoma during the course of the experiment, and her data was also excluded due to the possibility that the tumor functionally interfered with locomotion. A total of 17 rats were used in the final analysis of the sciatic functional recovery study, and total of 20 rats were used in the final analysis of the common peroneal functional recovery study (Table 1). Six rats were used as controls for the estimation of axon regeneration using retrograde tracers (RT); five were positive controls and one was a negative control.

Table 1: Summary of experimental subjects

Sciatic Study Group	n	Peroneal Study Group	n	Retrograde Tracer controls	n
1 week	3	**1 week**	3	**+ control**	5
4 weeks	3	**4 weeks**	3	**- control**	1
8 weeks	3	**8 weeks**	3		
12 weeks	3	**12 weeks**	3		
16 weeks	5	**20 weeks**	3		
		24 weeks	5		
Euthanized	7		2		

Sciatic Nerve Functional Recovery Group

Walking Track Analysis

Interobserver repeatability

Interobserver repeatability was high, with no clinically relevant bias noted between the two observers for any of the components used to calculate the sciatic function index (SFI) and stationary toe spread factor (TSF) as described by Bain-Mackinnon-Hunter (BMH[59], Table 2, Figure 13). On the experimental (left) limb, no trends toward bias were noted in the observed differences for experimental stationary TS (ESTS) or experimental PL (EPL) across the range of observed values. However, there were trends toward bias in experimental TS (ETS) and experimental intermediate TS (EIT). For the contralateral limb, there were no trends toward bias for print length (CPL) or intermediate TS (CIT) across the range of observed values. However, trends toward bias were observed for stationary TS (CSTS) and walking track TS (CTS). Overall, mean differences between measurements were small, with no mean difference greater than 0.25 cm. Mean differences in the measures with smaller dimensions (TS and IT) were measured in fractions of millimeters.

Table 2: Interobserver repeatability for SFI components
The mean and SE of each component used to calculate the SFI using the BMH method, with the mean and SE of the differences between observers and the trend toward bias (paired t test). E = experimental limb, C = contralateral limb, STS = stationary TS, PL = print length, TS = toe spread, and IT = intermediate toe spread.

	N	Mean (cm)	SE (cm)	Mean Difference (cm)	SE of the Mean Difference (cm)	Trend Toward Bias
ESTS	216	1.48	0.036	0.008	0.003	0.18
EPL	207	2.58	0.042	0.202	0.036	0.49
ETS	168	1.11	0.039	0.11	0.014	<0.0001
EIT	171	0.65	0.018	0.011	0.009	0.016
CSTS	216	2.22	0.017	0.012	0.003	0.0024
CPL	216	2.42	0.030	0.24	0.022	0.61
CTS	216	1.84	0.009	0.029	0.008	0.0016
CIT	216	0.91	0.006	0.026	0.005	0.36

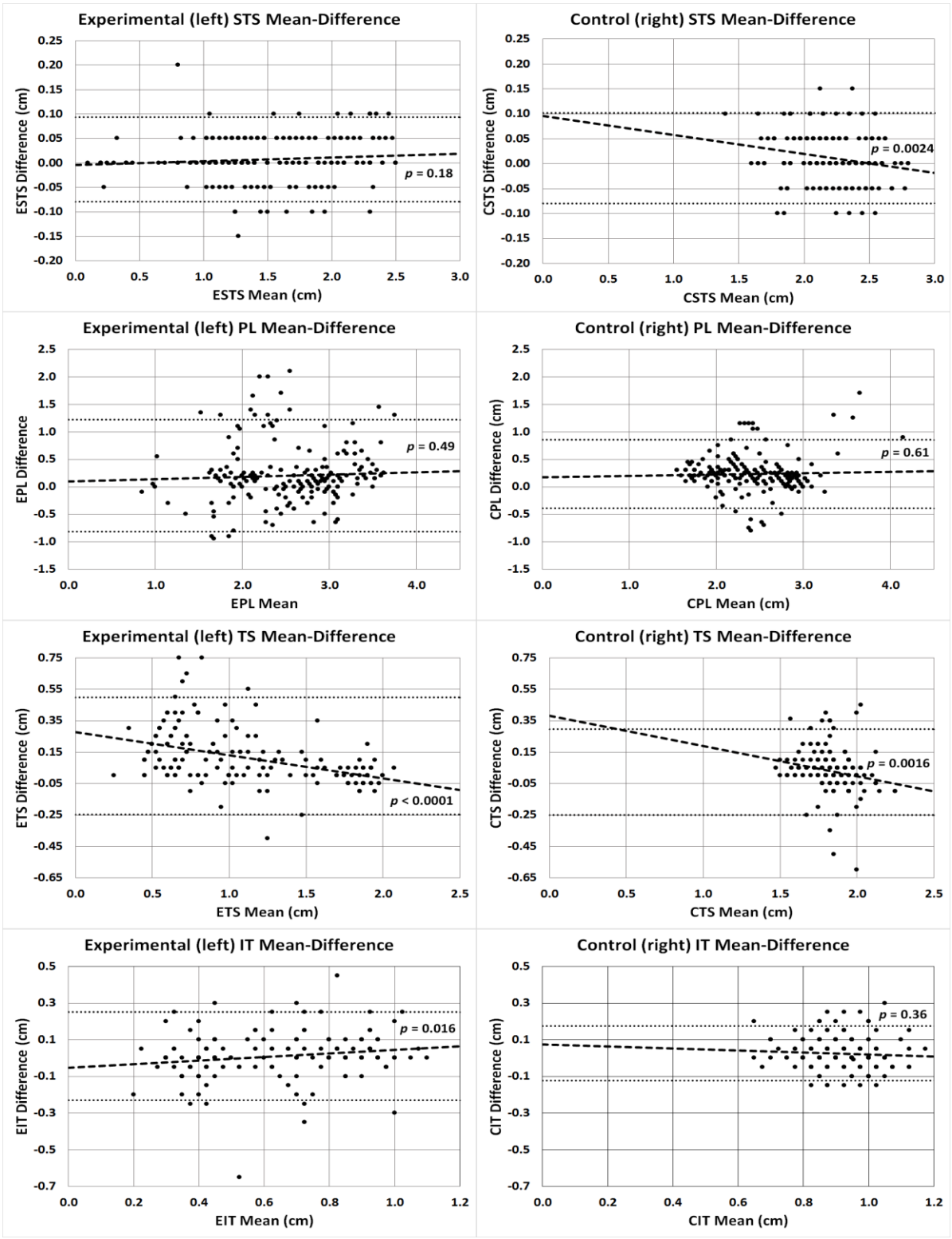

Figure 13: Bland-Altman plots for SFI component measurements.
Horizontal lines represent the limits of agreement (± 1.96 SD of the mean difference) and fitted line represents any trend over the range of the measurement (with associated p-value indicating the significance of the trend). E = experimental limb, C = contralateral limb, STS = stationary TS, PL = print length, TS = toe spread, and IT = intermediate toe spread.

Functional Index Components

For the components used in both the de Medinaceli[58] and the BMH[59] methods of calculating SFI (PL, TS and IT), significant differences over time were observed in experimental limb PL, TS, and IT (p=0.046, p<0.0001, and p<0.0001, respectively, ANOVA, Figure 14). Significant differences over time were also observed in the contralateral limb PL, TS, and IT (p=0.048, p=0.032, and p=0.040, respectively, ANOVA, Figure 14).

EPL and CPL were increased immediately following the transection-coaptation surgery before trending back toward pre-surgical print length as recovery proceeded. Interestingly, the EPL increased nearly twice as much as the CPL, with the EPL reaching its longest at 8 weeks post-surgery whereas the CPL was longest at 4 weeks post-surgery (Figure 14). ETS was significantly reduced after transection-coaptation, reaching a minimum by week four and then gradually returning towards pre-operative measurements, although these were not reached within the 16-week experimental timeline. CTS increased at weeks 1 and 4 post-surgery, returning to pre-surgical widths in the following weeks (Figure 14). EIT was widest pre-operatively and narrowest four weeks after transection-coaptation (Figure 14). Following week 4, EIT gradually returned toward pre-operative levels, although these were never achieved over the 16-week experimental timeline. In contrast, CIT was found to be narrowest pre-operatively and widest at week 1 (post-surgical), with all following time points (weeks 4-16) having means indistinct from either extreme (Figure 14).

For the additional measurement used only in the de Medinaceli[58] method (TOF), there were significant differences in both the experimental and the contralateral limbs (p=0.0001 and p<0.0003, respectively, ANOVA, Figure 14). ETOF was the longest at week 0 (pre-operative) and the shortest at 1 week (post transection-coaptation), with subsequent time points gradually increasing toward, but never reaching, pre-operative lengths. Interestingly, CTOF changed in the opposite direction, with the shortest measurement at week 0 and the longest measurement at week 4, with subsequent time points again trending back toward but never reaching pre-operative lengths (Figure 14).

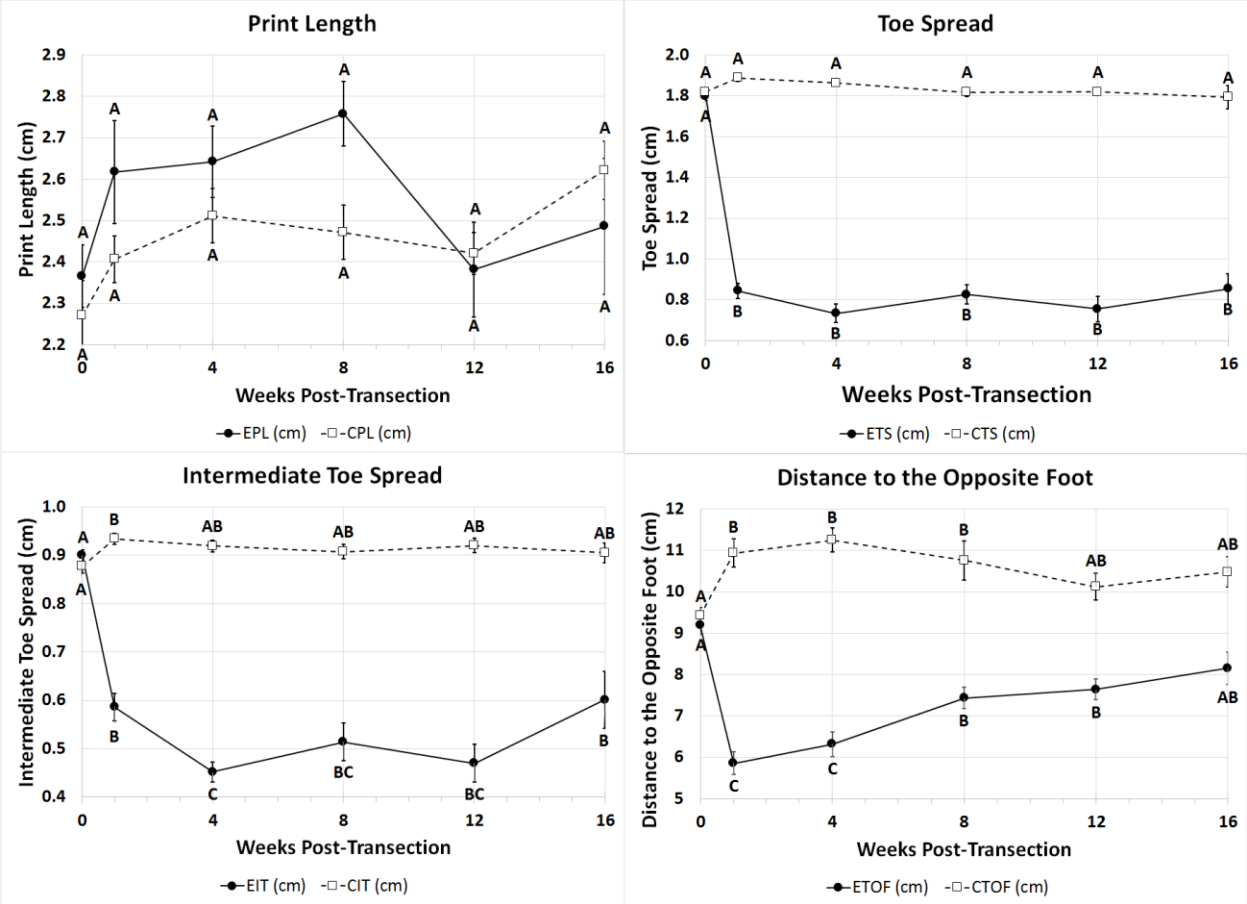

Figure 14: Variation in measured SFI components over time.
Measurements are for both experimental (E) and contralateral (C) limbs. A significant effect of time was observed on both EPL and CPL ($p=0.046$ and $p=0.048$, respectively, ANOVA), both ETS and CTS ($p<0.0001$ and $p=0.032$, respectively, ANOVA), both EIT and CIT ($p<0.0001$ and $p=0.040$, respectively, ANOVA), and both CTOF and ETOF ($p=0.0003$ and $p<0.0001$, respectively, ANOVA). Letters represent distinct groups based on Tukey's HSD test (groups not connected by the same letter are significantly distinct). Data shown are the mean and standard error (SEM).

There was no significant variation in velocity moving across the corridor apparatus over time (p = 0.26, ANOVA, Figure 15). There was a significant increase in animal weight over time (p<0.0001, ANOVA, data not shown).

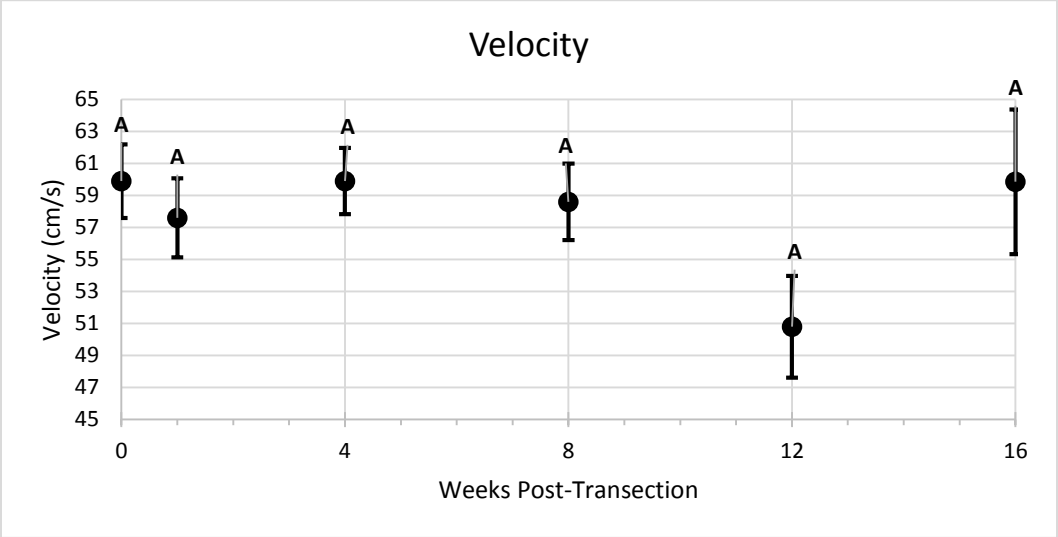

Figure 15: Variation in SFI mean velocity (V) over time.
*There was no significant effect of time, post transection-coaptation surgery, on velocity (*p*-value = 0.26, ANOVA). Letters represent distinct groups based on Tukey's HSD test (groups not connected by the same letter are significantly distinct). Data shown are the mean and standard error (SEM).*

Week 0 Measured Component Averages

There were significant differences between individual rats within the sciatic functional recovery study for the experimental limb for the TS and IT measurements (p < 0.0001 and p = 0.014 respectively, ANOVA, data not shown). There was no significant difference between rats in week 0 PL and TOF measurements (p = 0.28 and p = 0.58 respectively, ANOVA, data not shown). For the contralateral limb, there were significant differences between individual rats in week 0 PL and TS measurements (p = 0.022 and p = 0.0004, ANOVA, data not shown). However, there were no significant differences between rats for week 0 IT or TOF measurements (p = 0.070 and p = 0.14 respectively, ANOVA, data not shown).

For PL, TS, and IT measurements, the differences between measurements were small for both the experimental (left) and contralateral limbs, whereas they were somewhat larger for the TOF measurements for both limbs (Figure 16). Additionally, the week 0 average values for these measurements are very consistent between the two studies (Figure 16).

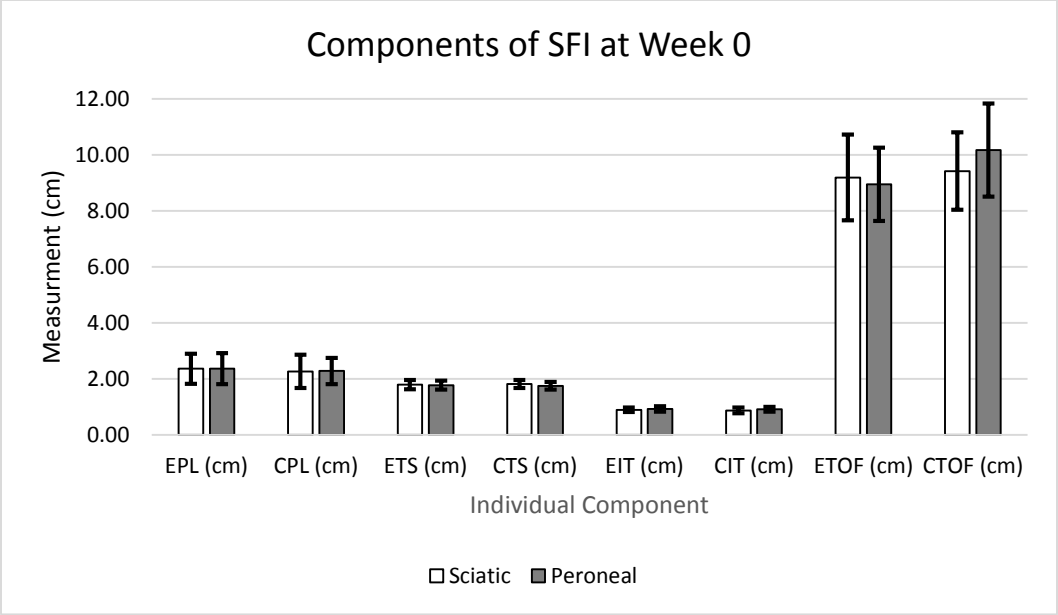

Figure 16: Mean SFI component measurements for week 0

The average measurements for components traditionally used to calculate SFI have relatively small differences between individual rats at week 0 and are consistent between the two functional recovery models (sciatic and common peroneal) for both the experimental (left) limb (E) and the contralateral limb (C). Data shown are averages of the largest measurement in each trial for all trials for all experimental subjects at week 0. Error bars represent standard error of the mean.

Calculated 'Factors' for Sciatic Function Index

Of the calculated 'factors' that were common to the de Medinaceli and BMH methods (PL, TS, and IT), only TS and IT for the experimental (left) limb were considered to be significantly affected by time ($p < 0.0001$ for both, ANOVA, Figure 17) when calculated using the traditional method (using contralateral limb measurements to normalize the experimental measurements). Time had no significant effect on the experimental (left) limb PL ($p = 0.36$, ANOVA, Figure 17). TOF, which was excluded from the BMH method, was also significantly affected by time ($p < 0.0001$, ANOVA, Figure 17) for the experimental (left) limb when calculated using the traditional method.

For the traditionally calculated factors, only the TOF had more than two statistically significant groups. The factor declined at one-week post transection and then gradually increased toward but never reached the pre-operative (week 0) value. The traditionally calculated TS and IT only differentiated between pre- and post-operative groups.

When the factors were calculated using the variant method (using week 0 average data to normalize experimental measurements), the experimental (left) limb print length was not significantly affected by time ($p = 0.10$, ANOVA, Figure 18). However, the TS, IT, and TOF factors were all significantly affected by time ($p < 0.0001$ for all three, ANOVA, Figure 18). In addition, for the contralateral limb, the PL ($p = 0.048$, ANOVA), TS ($p = 0.034$, ANOVA), IT ($p = 0.039$, ANOVA), and TOF ($p = 0.0029$, ANOVA) were all significantly affected by time (Figure 19).

Using the variant normalization calculation, the experimental limb TS and IT factors decreased immediately at one week following surgery. There was no significant distinction between post-surgical time points for either of these factors, however. The experimental limb TOF decreased at one-week post-transection and then gradually increased over the experimental time frame toward. Pre-surgical values were not achieved within the experimental period.

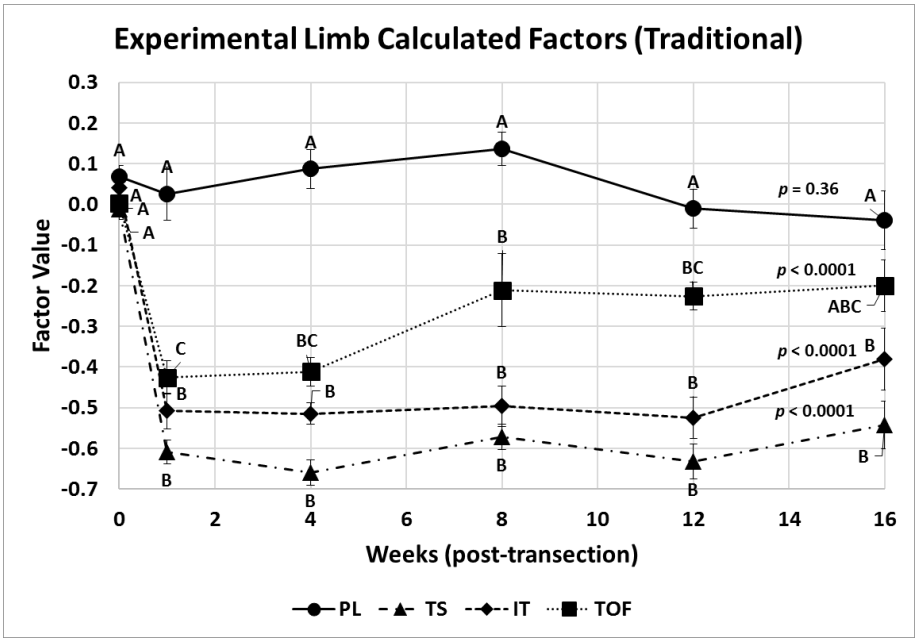

Figure 17: Calculated SFI Factors for the Experimental Limb (traditional method)
'Factors' calculated for the experimental limb using the traditional method of [(experimental limb measure – contralateral limb measure)/contralateral limb measure]. The calculated factor for TOF was significantly affected by time, whereas the PL factor was not. PL = print length, TS = toe spread, IT = intermediate toe spread, and TOF = distance to the opposite foot. Letters represent distinct groups based on Tukey's HSD test (groups not connected by the same letter are significantly distinct). Data shown are the mean and standard error (SEM).

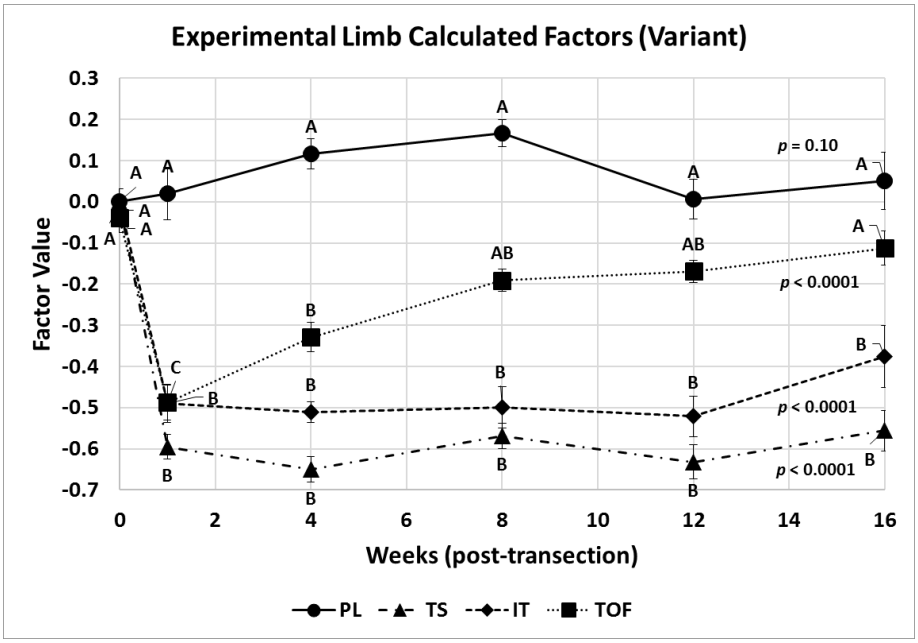

Figure 18: Calculated SFI Factors for the Experimental Limb (variant method)
'Factors' calculated for the experimental limb using the variant method of [(experimental limb measure – week 0 average limb measure)/week 0 average limb measure]. The TOF factor is the only factor affected by time significantly enough to differentiate time points post-surgery. PL = print length, TS = toe spread, IT = intermediate toe spread, and TOF = distance to the opposite foot. Letters represent distinct groups based on Tukey's HSD test (groups not connected by the same letter are significantly distinct). Data shown are the mean and standard error (SEM).

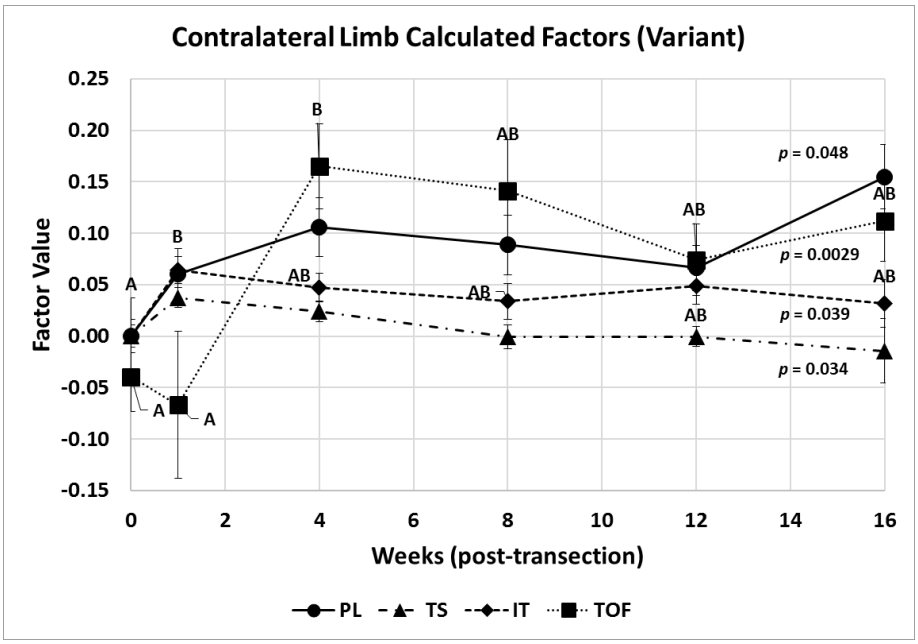

Figure 19: Calculated SFI Factors for the Contralateral Limb (variant method)
'Factors' calculated for the contralateral limb using the variant method of [(experimental limb measure – week 0 average limb measure)/week 0 average limb measure]. Connecting letters are only shown for IT and TOF, as post hoc testing of PL and TS revealed no differences in groups. PL = print length, TS = toe spread, IT = intermediate toe spread, and TOF = distance to the opposite foot. Letters represent distinct groups based on Tukey's HSD test (groups not connected by the same letter are significantly distinct). Data shown are the mean and standard error (SEM).

Calculated Sciatic Function Index

Calculated SFI varied significantly over time using both the de Medinaceli[58] and the BMH[59] calculation methods (both $p<0.0001$, ANOVA, Figure 20). However, the de Medinaceli method yielded only two distinct groups: pre-operative (week 0) vs. post-operative (all other time points). The BMH SFI was the highest at week 0 and lowest at week 4 (function and dysfunction, respectively), with a trend back toward 0 in subsequent weeks, though improvement never exceeded an index of approximately -70 within the 16-week experimental time frame.

SFI using the BMH calculated with the variant method (using time 0 measurements to normalize experimental measurements) also varied significantly over time (E (variant), $p<0.0001$, ANOVA, Figure 20). Similar to the de Medinaceli method, this method also yielded only two distinct groups: pre-operative (week 0) vs. post-operative (all other time points). Applying the same method to the right limb revealed that time also had an effect on the contralateral limb (C (variant), $p=0.022$, ANOVA, Figure 20).

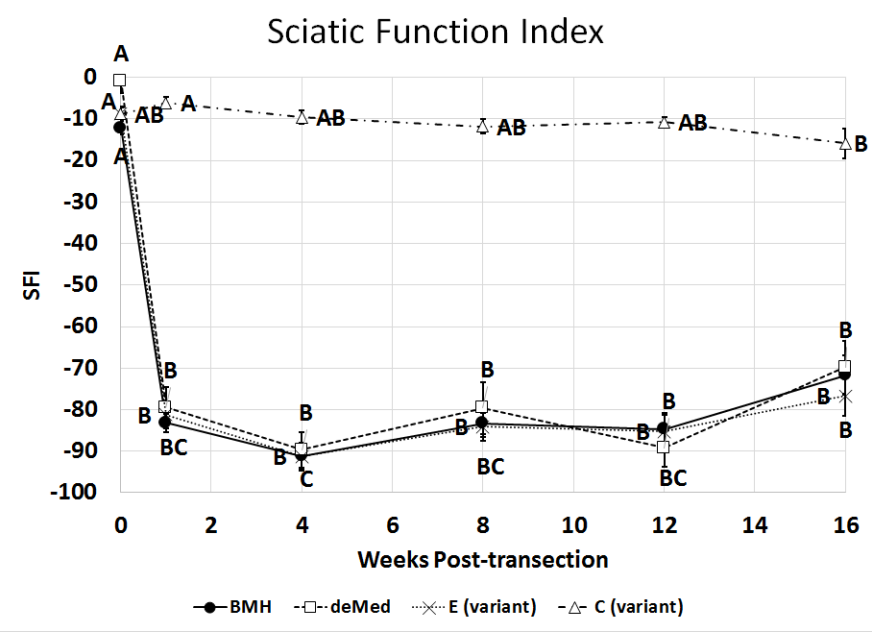

Figure 20: Variation in SFI (de Medinaceli, BMH, and BMH week 0 variant) over time.
There is a significant effect of time on the calculated indices for the experimental (left) limb, using all calculation methods ($p<0.0001$ for all). However, a Tukey's HSD test yields only two significantly distinct groups for the de Medinaceli method (deMed) and for the E (variant) (week 0 vs. all other time points in both cases). Significant differences were also noted between groups for the C (variant) ($p = 0.022$). E = experimental and C = contralateral. Letters represent distinct groups based on Tukey's HSD test (groups not connected by the same letter are significantly distinct). Letter positions by method: below = BMH SFI, above = deMed SFI, left = E (variant), and right = C (variant). Data shown are the mean and standard error (SEM).

Toe Spread Factor Components

Time had a significant effect on stationary TS, used for calculating the stationary TSF described by BMH, for both the experimental (left) limb and the contralateral limb ($p<0.0001$ and $p=0.0002$, respectively, ANOVA, Figure 21). The experimental stationary TS, similar to the toe spreads taken from walking tracks, had its widest measurement at week 0 and its narrowest measurement at week 4. However, unlike walking track toe spreads, subsequent measurements increased at first (week 8) and then become smaller again (weeks 12 and 16). For the contralateral stationary TS, week 12 measurements were significantly smaller than those in weeks 1 through 8, with week 16 measurements indistinct from either of these groups (Figure 21).

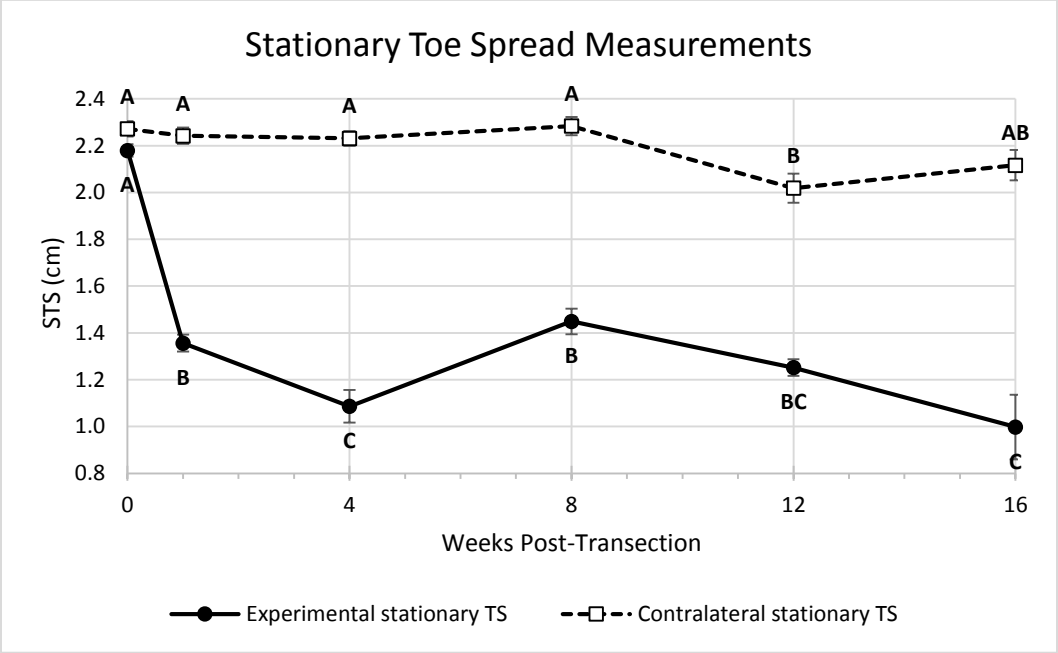

Figure 21: Variation in stationary toe spread (STS) over time for the sciatic functional recovery study. Both the experimental (left) limb (ESTS) and contralateral limb (CSTS) measurements were significantly affected by time following surgical transection and coaptation ($p<0.0001$ *and* $p=0.0002$*, respectively, ANOVA). Letters represent distinct groups based on Tukey's HSD test (groups not connected by the same letter are significantly distinct). Data shown are the mean and standard error (SEM).*

Calculated Toe Spread Factor

There was significant variation of stationary TSF (calculated using the BMH method) over time (BMH, $p<0.0001$, ANOVA, Figure 22), with a trend that was similar to the trend observed in the experimental stationary TS measurement from which it was derived. The largest measurement was at week 0 (pre-operative) and the smallest was at week 4 (post-operatively) with a trend towards improvement at week 8 which reversed back to the narrowest measurement by week 16. Stationary TSF calculated using the variant method (normalized with time 0 averages) also varied over time (E (variant), $p<0.0001$, ANOVA, Figure 22) and showed a pattern of variation with time that was similar to the standard BMH stationary TSF. The mean stationary TSF decreased significantly at weeks 1 and 4, increased again over weeks 8 and 12, and finally decreased again at week 16. Similar to the variant contralateral limb SFI, the variant contralateral limb TSF also showed significant variation over time (C (variant), $p = 0.0002$, ANOVA, Figure 22), with week 12 having a lower stationary TSF than previous weeks, and week 16 having a mean that was intermediate to the two groups.

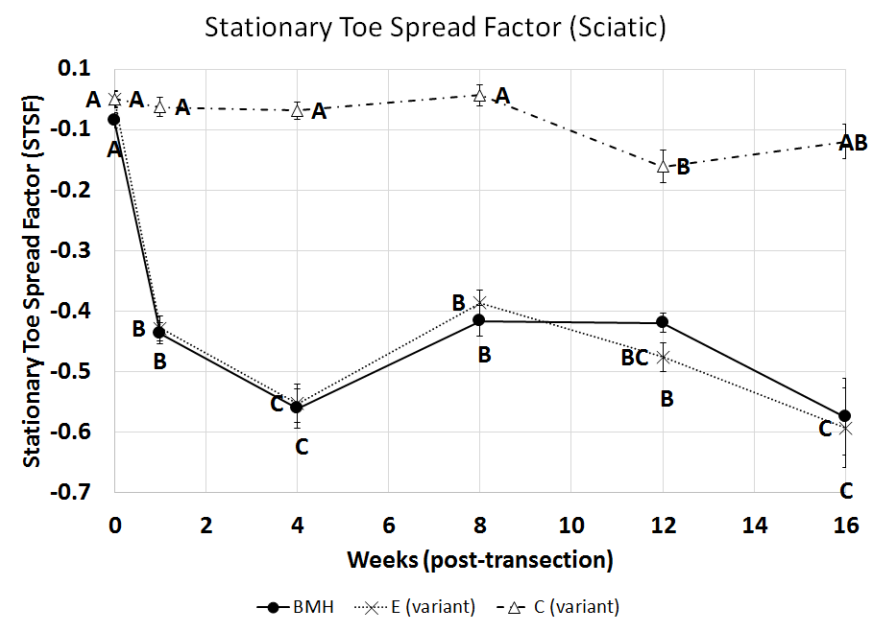

Figure 22: Variation in stationary TSF over time for the sciatic functional recovery study
Time significantly affected stationary TSF, calculated using both the BMH method and the variant method for the experimental limb (E variant) (both p<0.0001, ANOVA). There was also a significant effect of time on contralateral limb stationary TSF (C (variant), p = 0.0002). Letters represent distinct groups based on Tukey's HSD test (groups not connected by the same letter are significantly distinct). Letter positions by method: below = BMH, left = E (variant), and right = C (variant). Data shown are the mean and standard error (SEM).

Skilled Locomotion Analysis

There was significant variation in velocity over time in each zone, and in all zones taken together, for both the irregular and regular ladder patterns ($p < 0.0001$ for all, ANOVA, Figure 23). All zones showed a significant decrease in velocity following surgery (at week 1 post transection-coaptation) and a trend toward increased velocity between 4 and 8 weeks after surgery that then decreased by weeks 12 and 16 (for both pattern formats). However, zone 3 was the only zone to show a significant increase.

Fixed effect modeling of SR for zone 1 on the regular pattern showed an effect of time on the left hindlimb ($p < 0.0001$, Figure 24) but no effect on the right hindlimb ($p = 0.14$, Figure 24) or the forelimbs (RF, $p = 0.41$; LF, $p = 0.33$, Figure 24). The LH showed an increase in SR immediately following surgery (week 1) that was stable through week 4 and then decreased over the following 12 weeks. For the irregular pattern on zone 1, modeling of SR showed an effect of time on the right forelimb and left hindlimb ($p < 0.0001$ for both, Figure 24) but no effect of time on the left forelimb and right hindlimb ($p = 0.11$ and 0.080 respectively, Figure 24). Similar to the regular pattern, the LH SR increased on the irregular pattern immediately following surgery but it remained elevated through week 12 before showing a decrease at 16 weeks. Oddly, the RF SR on the irregular pattern decreased immediately following surgery and continued to trend toward 0 over the remainder of the experimental timeline.

Fixed effect modeling of SR for zone 2 on the regular pattern showed an effect of time on the hindlimbs (RH, $p = 0.0032$; LH, $p = 0.0007$, Figure 25) but no effect on the forelimbs (RF, $p = 0.56$; LF, $p = 0.65$, Figure 25). The right hindlimb on the regular pattern showed an increase in SR at week 1 that subsequently decreased by week 4 below the pre-surgical SR and then remained relatively stable over the remainder of the experimental timeline. Similar to the zone 1 changes, the LH increased sharply immediately following surgery (week 1) and then showed modest decreases from week 8 through the remainder of the experimental timeline. For the irregular pattern on zone 2, modeling of SR showed no effect of time on the left forelimb ($p = 0.67$, Figure 25), though all other limbs were affected (RF, $p = 0.027$; RH, $p = 0.030$; LH, $p < 0.0001$, Figure 25). The RF and RH SR on the irregular pattern increased at week 1 but then decreased starting at week 4 to attain a value significantly below the pre-surgical SR

by week 16. The LH SR, as observed on the regular pattern, increased at week 1 but began to decrease at week 4 through the remaining 12 weeks.

SR fixed effect modeling for zone 3 on the regular pattern showed an effect of time only on the left hindlimb SR ($p < 0.0001$, Figure 26), which increased immediately following surgery (at week 1), decreased modestly over the next 11 weeks and then sharply increased at week 16. The SR of the other limbs were not significantly affected by time (RF, $p = 0.13$; LF, $p = 0.54$; RH, $p = 0.33$, Figure 26). For the irregular pattern on zone 3, modeling of SR showed an effect of time on all limbs. The right and left forelimb, and the right hindlimb SR (RF, $p = 0.0001$; LF, $p < 0.0001$; RH, $p = 0.0007$, Figure 26) all showed similar patterns of SR changes: increased SR through week 4 following surgery that subsequently decreased below pre-surgical levels by week 12 post-surgery. The left hindlimb ($p < 0.0001$, Figure 26) showed similar patterns to other zones: a sharp increased immediately following surgery (week 1) that persisted through week 4 before modestly decreasing over the remainder of the experimental timeline.

Finally, the summation of all zones on the regular pattern showed no effect on the right forelimb ($p = 0.060$, Figure 27), though the SR of all other limbs were significantly affected (LF, $p = 0.030$; RH, $p < 0.0001$; LH, $p < 0.0001$, Figure 27). The LF and RH SR never increased but rather decreased over the entirety of the experimental time line from a pre-surgical apex. The LH SR showed an immediate post-surgical increase that was stable through week 4 and then decreased modestly over the remainder of the experimental timeline. For the summed zones on the irregular pattern, SR modeling showed an effect of time on all limbs ($p < 0.0001$ for all, Figure 27). Similar to the regular pattern all limbs showing significant changes over time, except the LH limb, showed continuous decline in SR over the experimental time frame to values that were below pre-surgical maximums. As in all other zones, the LH SR showed an immediate post-surgical increase that was stable through week 4 and then decreased modestly over the remainder of the experimental timeline.

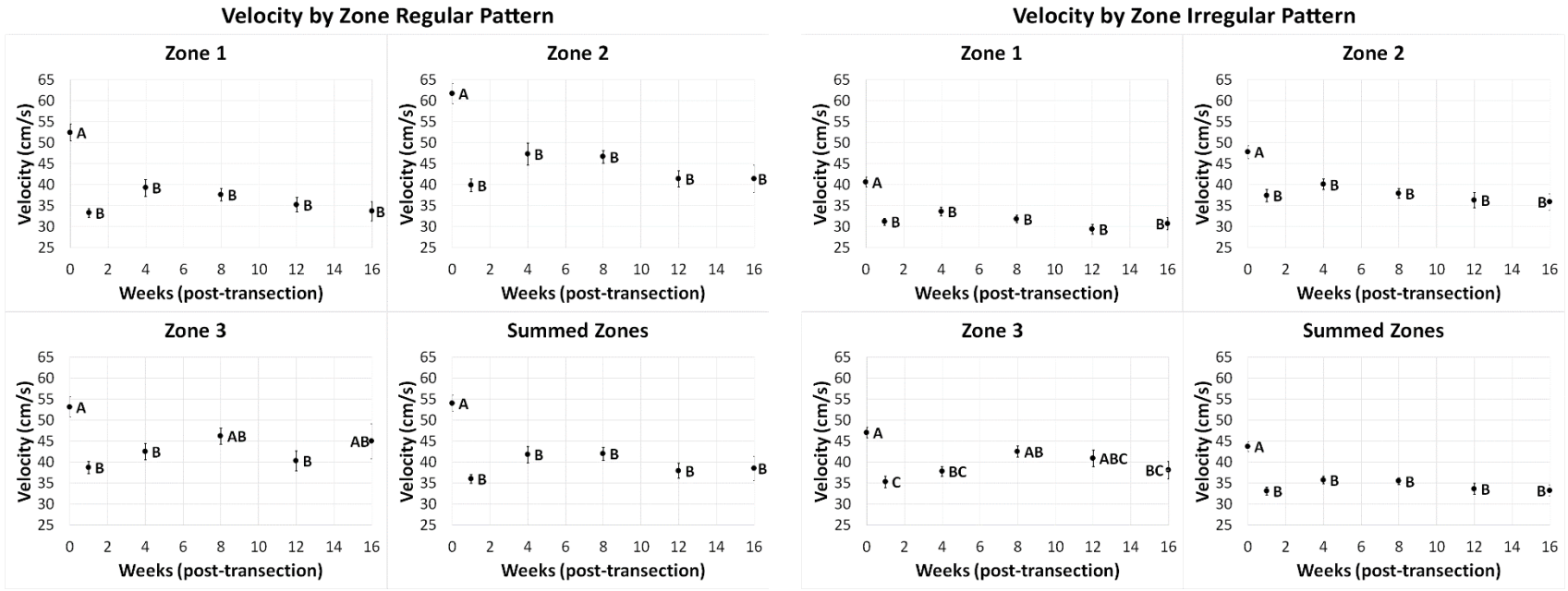

Figure 23 Variation in SL velocity (by zone and pattern) over time for sciatic recovery study.
While velocity decreased significantly in each zone (and all zones combined) on both ladder pattern styles immediately following transection and coaptation surgery, only zone 3 reflected a significant increase from the week 1 post-transection low. Letters represent distinct groups based on Tukey's HSD test (groups not connected by the same letter are significantly distinct). Data shown are the mean and standard error (SEM).

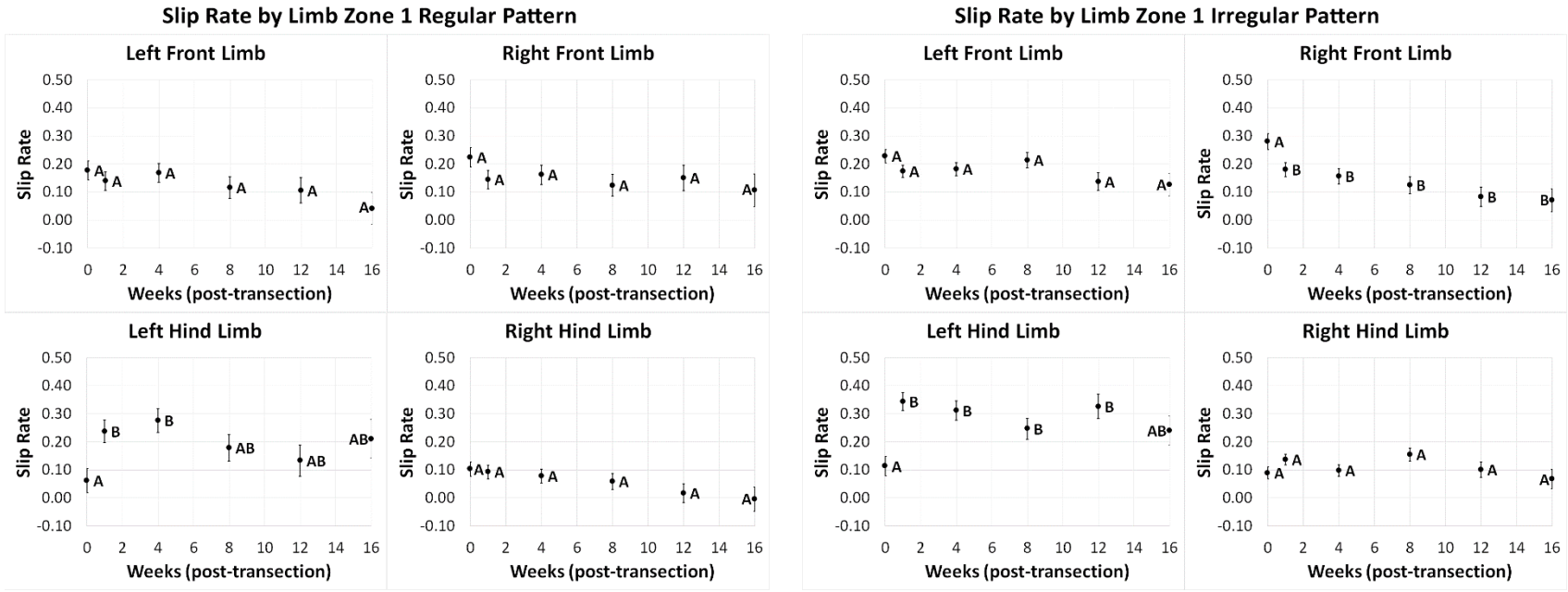

Figure 24: Zone 1 SR (by limb and pattern) for sciatic functional recovery study.
Slip rates on both ladder pattern styles in zone 1 generally decreased over time for the RF, LF, and RH limbs, although only the RF on the irregular pattern was significant ($p < 0.0001$, ANOVA). The LH limb on both ladder pattern styles showed a significant increase following transection and coaptation surgery ($p < 0.0001$, ANOVA), and trended toward decreased slip over the remainder of the experiment. Letters represent distinct groups based on Tukey's HSD test (groups not connected by the same letter are significantly distinct). Data shown are the mean and standard error (SEM).

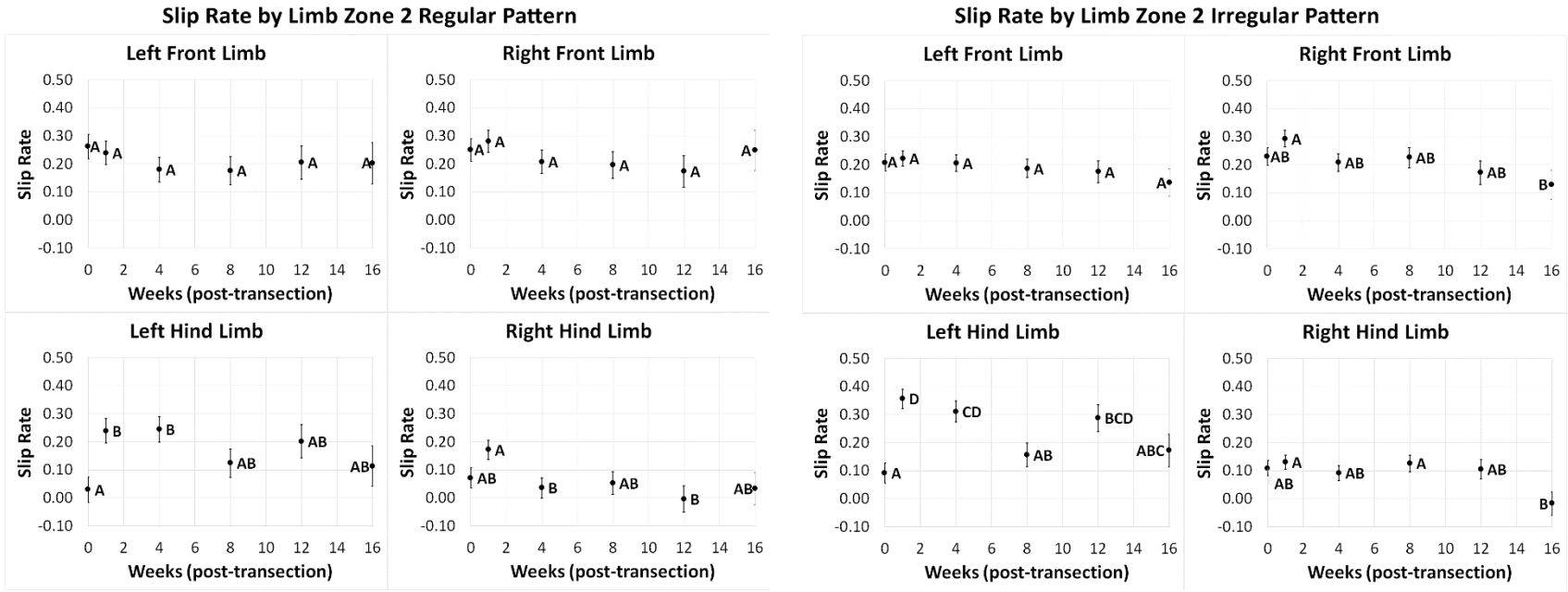

Figure 25: Zone 2 SR (by limb and pattern) for sciatic functional recovery study.
Slip rates on both ladder pattern styles in zone 2 generally decreased over time for the RF, LF, and RH limbs, although none of the decreases were significant. The LH limb on both ladder pattern styles showed a significant increase following transection and coaptation surgery (regular: $p = 0.0001$; irregular: $p < 0.0001$, ANOVA), and trended toward decreased slip over the remainder of the experiment. Letters represent distinct groups based on Tukey's HSD test (groups not connected by the same letter are significantly distinct). Data shown are the mean and standard error (SEM).

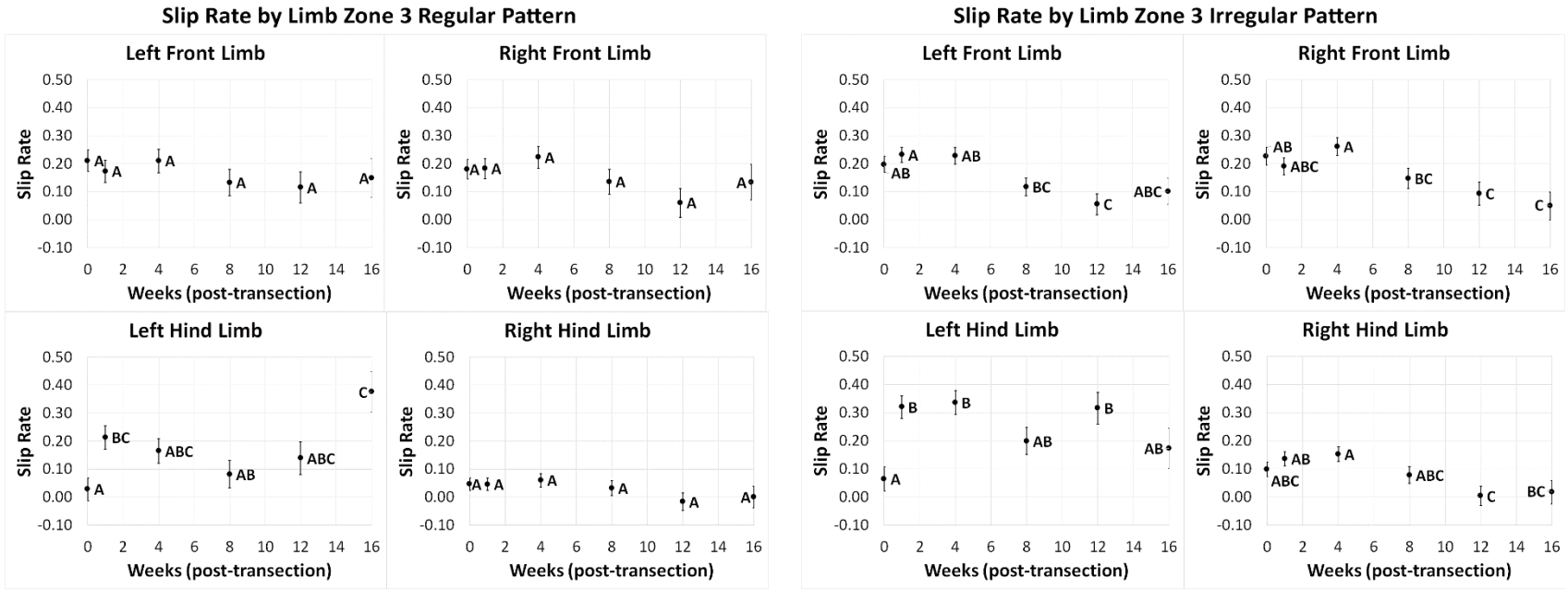

Figure 26: Zone 3 SR (by limb and pattern) for sciatic functional recovery study.
The LH limb SR on the regular pattern significantly increased following surgery ($p < 0.0001$*, ANOVA) and had a decreasing trend from week 1 to week 8, at which point it then significantly increased again. No other limbs had significant changes in SR on the regular pattern. On the irregular pattern, all limbs had significant changes in SR following surgery. The LF, RF, and RH all decreased (*$p < 0.0001$*,* $p = 0.0001$*, and* $p = 0.0007$*, respectively, ANOVA). The LH limb significantly increased at week 1 (*$p < 0.0001$*, ANOVA) then had a decreasing trend through week 16. Letters represent distinct groups based on Tukey's HSD test (groups not connected by the same letter are significantly distinct). Data shown are the mean and standard error (SEM).*

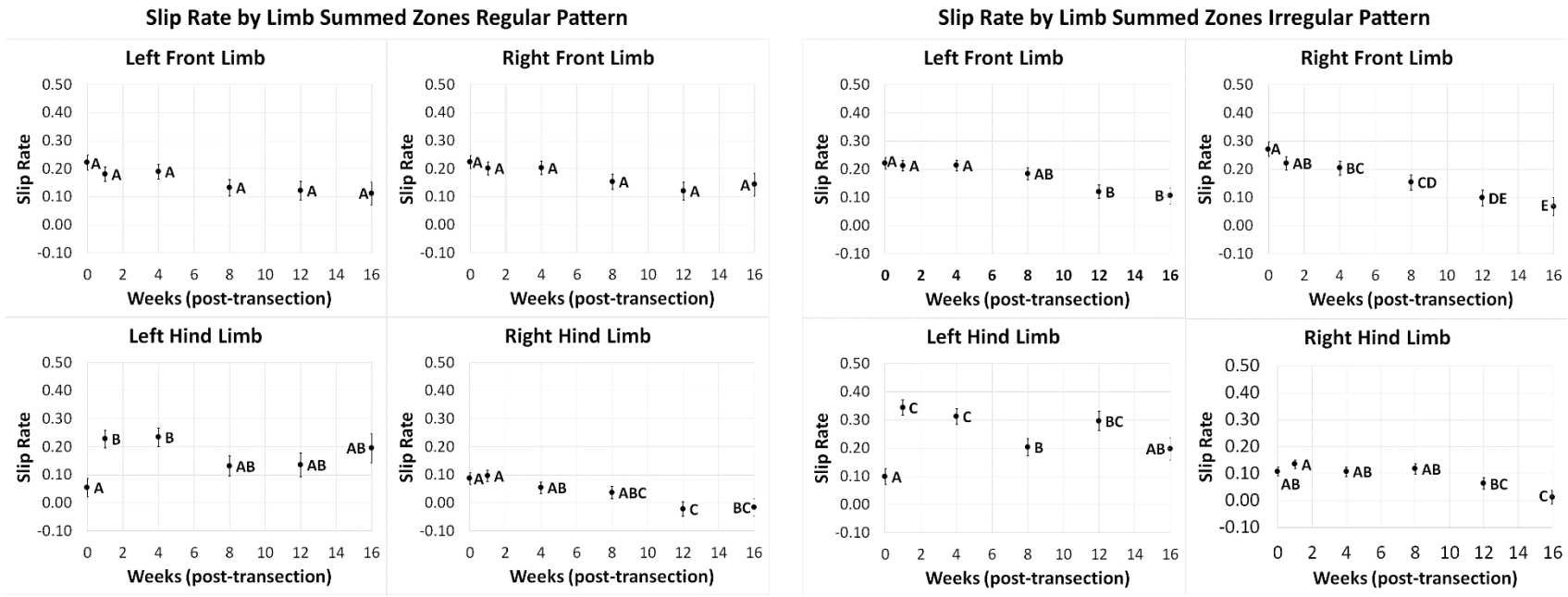

Figure 27: Combined zones SR (by limb and pattern) for sciatic functional recovery study.
Summed zone SR on the regular pattern did not significantly change for the RF or LF limb, though both had decreasing trends. Both hindlimbs significantly changed over time ($p < 0.0001$ for both, ANOVA). The RH decreased steadily, and the LH increased post-transection then decreased over the remainder of the experiment. The LF, RF and RH SR all significantly decreased over the whole experimental time frame ($p < 0.0001$ for all, ANOVA). The LH also significantly change ($p < 0.0001$, ANOVA) and showed a characteristic increase at week 1 followed by a decreasing trend through week 16. Letters represent distinct groups based on Tukey's HSD test (groups not connected by the same letter are significantly distinct). Data shown are the mean and standard error (SEM).

Motor Neuron (MN) Counts

Comparison of Counting Methods

Comparing the number of labeled motor neurons (MNs, Figure 28) using either a semi-automated algorithm (Volocity, PerkinElmer, Waltham, MA) or by manual counting, repeatability was high, with low bias between methods (Table 3, Figure 29). The trend toward increasingly larger counts using the software algorithm as MN counts increased was significant for the counts of the individual fluorescent labels (tibial – FluoroGold, $p = 0.025$; common peroneal – FluoroRuby, $p = 0.002$) but not for the double labeled MNs (representing axonal misdirection or labeling error, $p = 0.089$) and the total count of all populations taken together (representing the full sciatic nerve count, $p = 0.082$).

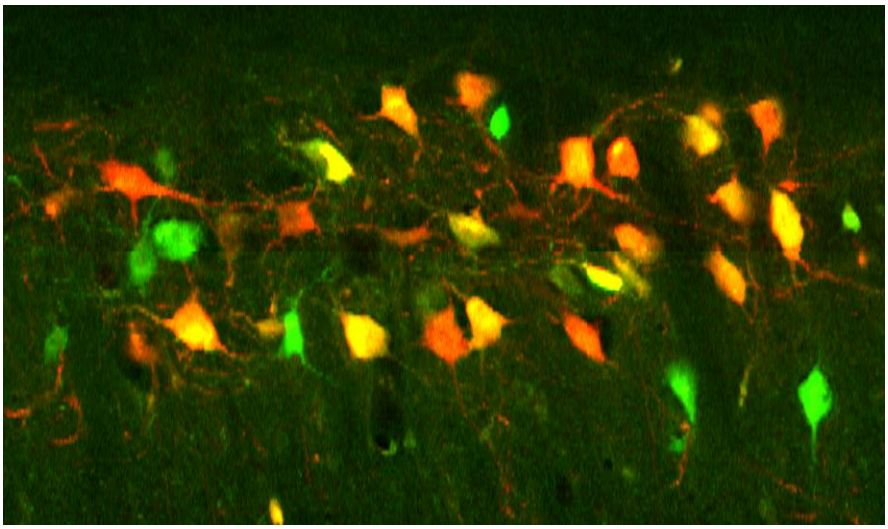

Figure 28: Typical .LSM image of back labelled motor neuron cell bodies
Partial image that is representative of the output from the Zeiss 710 confocal microscope when scanning retrograde labelled spinal cord sections of spinal cord from rats in the sciatic nerve functional recovery study (double labelled). Green cells are labelled with FluoroGold (tibial n.), red cells are labelled with FluoroRuby (common peronea n.), and cells that are double labelled appear to be yellow to orange.

Table 3: Comparison of MN counting methods (semi-automated vs. manual) for SFI study.
The mean and SE of the labeled MN counts, with the mean and SE of the difference between the counts achieved through semi-automated and manual counting methods and the trend toward bias between methods. FG = FluoroGold (tibial branch), FR = FluoroRuby (common peroneal branch), Both = double-labeled cell (axonal misdirection or labeling error), and Total = all populations taken together (the general sciatic nerve population of MNs).

	N	Mean	SE	Mean Diff	SE of Mean Diff	Trend Toward Bias
FG only	23	691	119.17	122.17	86.63	0.025
FR only	23	600	94.32	-68.74	63.10	0.002
Both	23	235	51.20	48.26	40.73	0.089
All Populations	23	1525	244.99	101.70	170.34	0.082

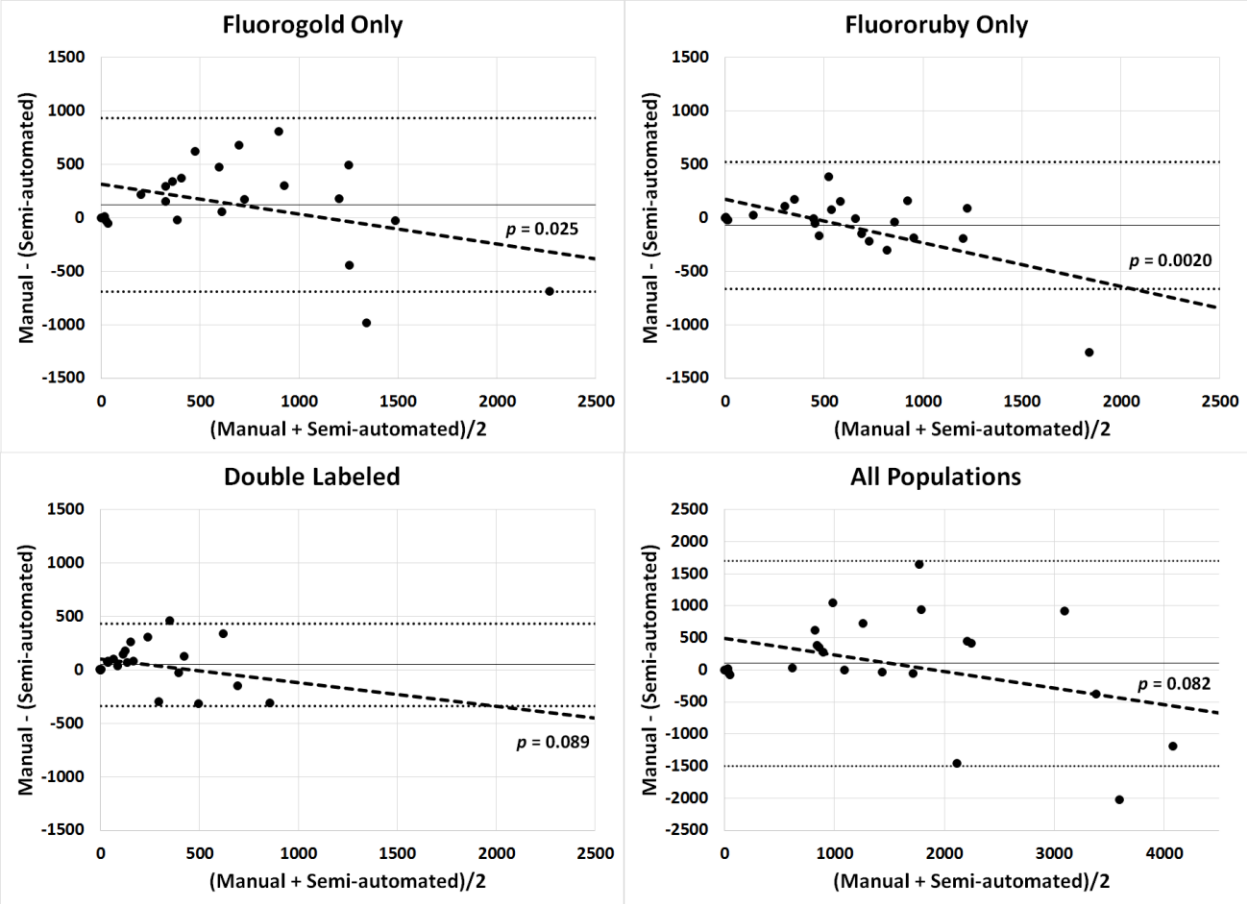

Figure 29: Mean-Difference plots for sciatic functional recovery MN counts.
Semi-automated counting trends toward increased counts as the populations increase for all populations. Mean count (solid horizontal line), limits of agreement (± 1.96 x SD, paired horizontal dashed lines), and trend toward bias (fit dashed line) for sciatic nerve MN cell bodies. FluoroGold = tibial branch of the sciatic n., FluoroRuby = common peroneal branch of the sciatic n., Double Labeled = axonal misdirection or labeling error, and All Populations = the general sciatic nerve population of MNs.

Motor Neuron Count as a Function of Time

Time had a significant effect on the number of retrograde tracer labeled MN cell bodies for each of the measured MN populations (FluoroGold - tibial branch, *p*-value = 0.0006; FluoroRuby - common peroneal branch, *p*-value = 0.0049; double-labeled - both tracers appeared in the cell body, *p*-value = 0.0044; and All Populations - sum of all individually labeled and double-labeled populations, *p*-value = 0.0002, ANOVA, Figure 30). Non-surgical controls (week 0) were significantly different than

experimental transection-coaptation subjects (week 1) in all populations. Similarly, all populations trended over time toward (but never reaching) pre-surgical levels over the experimental time period, with FluoroGold labeled populations reaching 56.7%, FluoroRuby populations reaching 70.6%, double-labeled populations reaching 53.5%, and the all populations together reaching 61% of their pre-surgical levels. Interestingly, FluoroRuby labeled cell bodies had counts that steadily increased over the course of the experiment, whereas FluoroGold and double-labeled populations increased by week 4 and again at 16 weeks (Figure 30).

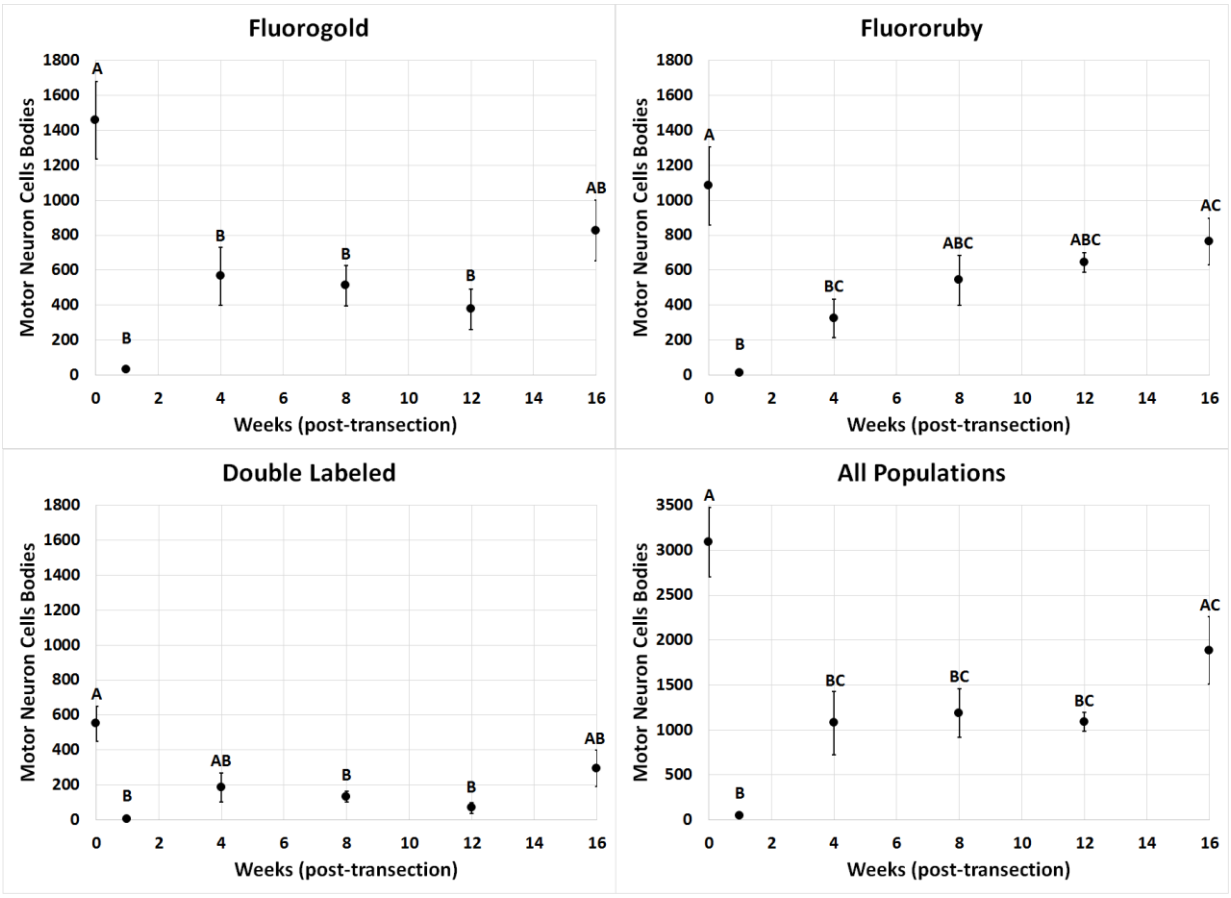

Figure 30: Variation of sciatic functional recovery MN count over time, by label.
All labeled populations show a significant difference in mean count between controls (non-surgical) and experimental (post-surgical) rats (week 0 and week 1, respectively) with a trend toward pre-surgical counts over the course of the experimental timeline. Letters represent distinct groups based on Tukey's HSD test (groups not connected by the same letter are significantly distinct). Data shown are the mean and standard error (SEM). FluoroGold = tibial branch of the sciatic n., FluoroRuby = common peroneal branch of the sciatic n., Double Labeled = dyskinesis or labeling error, and All Populations = the general sciatic nerve population of MNs.

Sciatic Function Index and Toe Spread Factor as Functions of Motor Neuron Count

Motor neuron (MN) count was found to be positively correlated with SFI in the experimental (left) limb, as calculated using the BMH method (BMH SFI, $p = 0.011$, Figure 31) and calculated using the time 0 normalized variant factors (E (variant), $p = 0.019$, Figure 31). As expected, there was no significant relationship between MN count and SFI in the contralateral limb, as calculated using the variant method, though the relationship appeared to trend toward a negative correlation (C (variant), $p = 0.095$, Figure 31). Similarly, no significant relationships were found between MN count and stationary TSF for the experimental (left) limb, as calculated using the BMH method (BMH TSF, $p = 0.96$, Figure 31) or calculated using the variant method (E (variant) TSF, $p = 0.84$, Figure 31). In the contralateral limb, the stationary TSF calculated using time 0 to normalize experimental measurements was not significantly related to MN count (C (variant) TSF, $p = 0.70$, Figure 31). Interestingly, all methods of stationary TSF calculation led to indices that appeared to trend toward a positive relationship with MN count, though this was most apparent in the calculations that used week 0 to normalize experimental measurements (and especially in the contralateral limb).

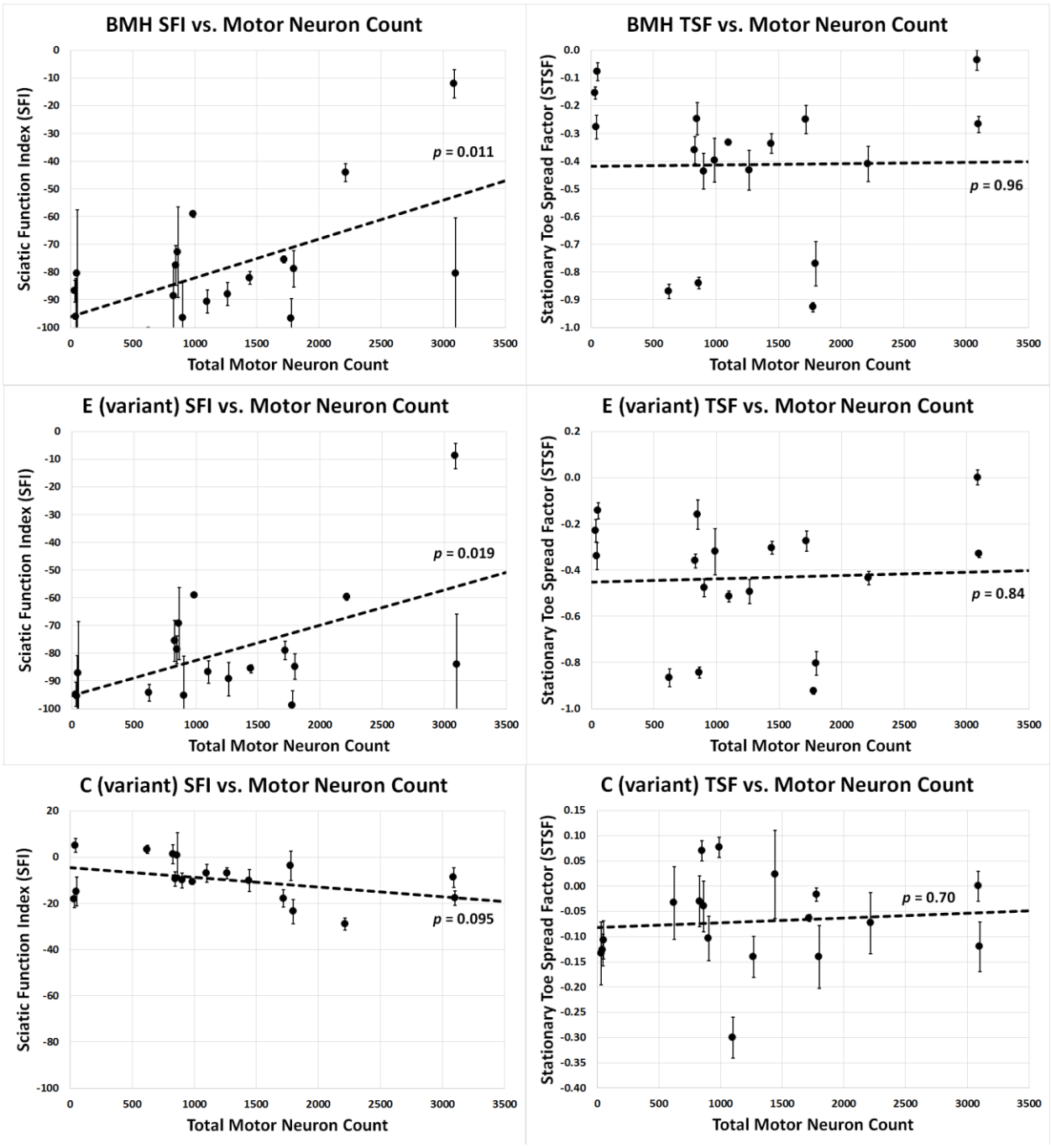

Figure 31: Variation in SFI and STSF as functions of MN count for sciatic functional recovery study. Significant positive correlations were found between MN counts and SFI for the experimental (left) limb, as calculated using the BMH method and using week 0 data as controls. There was not a significant relationship between MN count and contralateral limb SFI using week 0 controls, though the relationship trended toward a negative correlation. There were no significant correlations between MN count and STSF for either limb, using either calculation method. Data shown are the mean indices and standard error of those means (SEM).

Skilled Locomotion Slip Rate as a Function of Motor Neuron Count

Mean SR calculated for the left hindlimb, derived from fixed effect modeling using all zones summed together (as previously described), were significantly, and negatively, correlated to total motor neuron (MN) counts for trials run on the irregularly spaced ladder rungs (p = 0.010, Figure 32). A similar negative trend was observed in LH SR when correlated with total MN counts for trials run on the regularly spaced ladder rungs (p = 0.066, Figure 32).

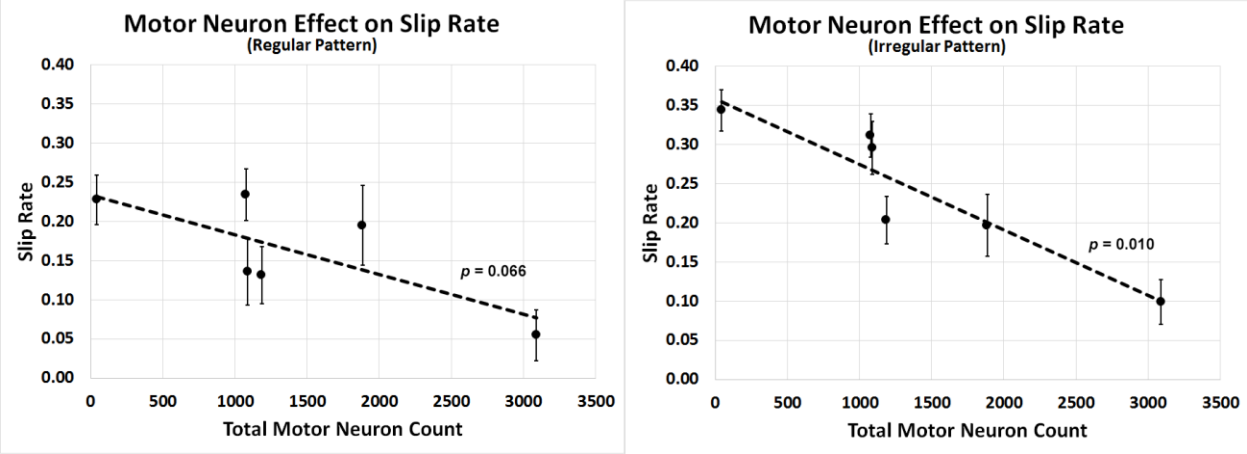

Figure 32: Variation in left hindlimb SR as a function of MN count for the sciatic study, by pattern. Both the regular and irregular patterns showed similar trends of decreased SR as MN counts increased. However, only the irregular pattern SR were considered significantly different in relation to total MN count (p = 0.010, versus p = 0.066 for regular pattern SR).

Common Peroneal Nerve Functional Recovery Group

Walking Track Analysis

Repeatability across methods

For the components typically measured for the SFI using the de Medinaceli method, repeatability between the two methods of measurement (digitized vs. ruler) was high, with no clinically relevant bias noted between them (Table 2, Figure 13). On the experimental (left) limb, no trends toward bias were noted for any of the measured components across the range of observed values. For the contralateral leg, there were no significant trends toward bias for toe spread (CTS), intermediate toe spread (CIT), or distance to the top of the opposite foot (CTOF) across the range of observed values. However, a significant trend toward bias was observed for print length (CPL) ($p = 0.0057$). Overall, mean differences between measurements were small; there was no mean difference greater than 0.15 cm, with mean differences in the measures with smaller dimensions (toe spread and intermediate toe spread) measured in fractions of millimeters.

Table 4: Repeatability between measurement methods (digitized vs. ruler) for PFI components
The mean and SE of components typically measured for the sciatic functional index using the de Medinaceli method, with the mean and SE of the differences between observers and the trend toward bias (paired t test). E = experimental limb, C = contralateral limb, PL = print length, TS = toe spread, and IT = intermediate toe spread, TOF = distance to the opposite foot.

	N	Mean (cm)	SE (cm)	Mean Difference (cm)	SE of the Mean Difference (cm)	Trend Toward Bias
EPL	406	2.82	0.026	-0.073	0.015	0.68
ETS	379	1.35	0.016	0.0039	0.0073	0.49
EIT	407	0.69	0.0095	-0.012	0.0043	0.76
ETOF	405	8.29	0.058	0.14	0.012	0.29
CPL	411	2.27	0.023	-0.13	0.010	0.01
CTS	410	1.76	0.0070	0.0037	0.0037	0.30
CIT	411	0.90	0.0044	-0.0011	0.0030	0.43
CTOF	408	10.03	0.067	-0.0080	0.013	0.21

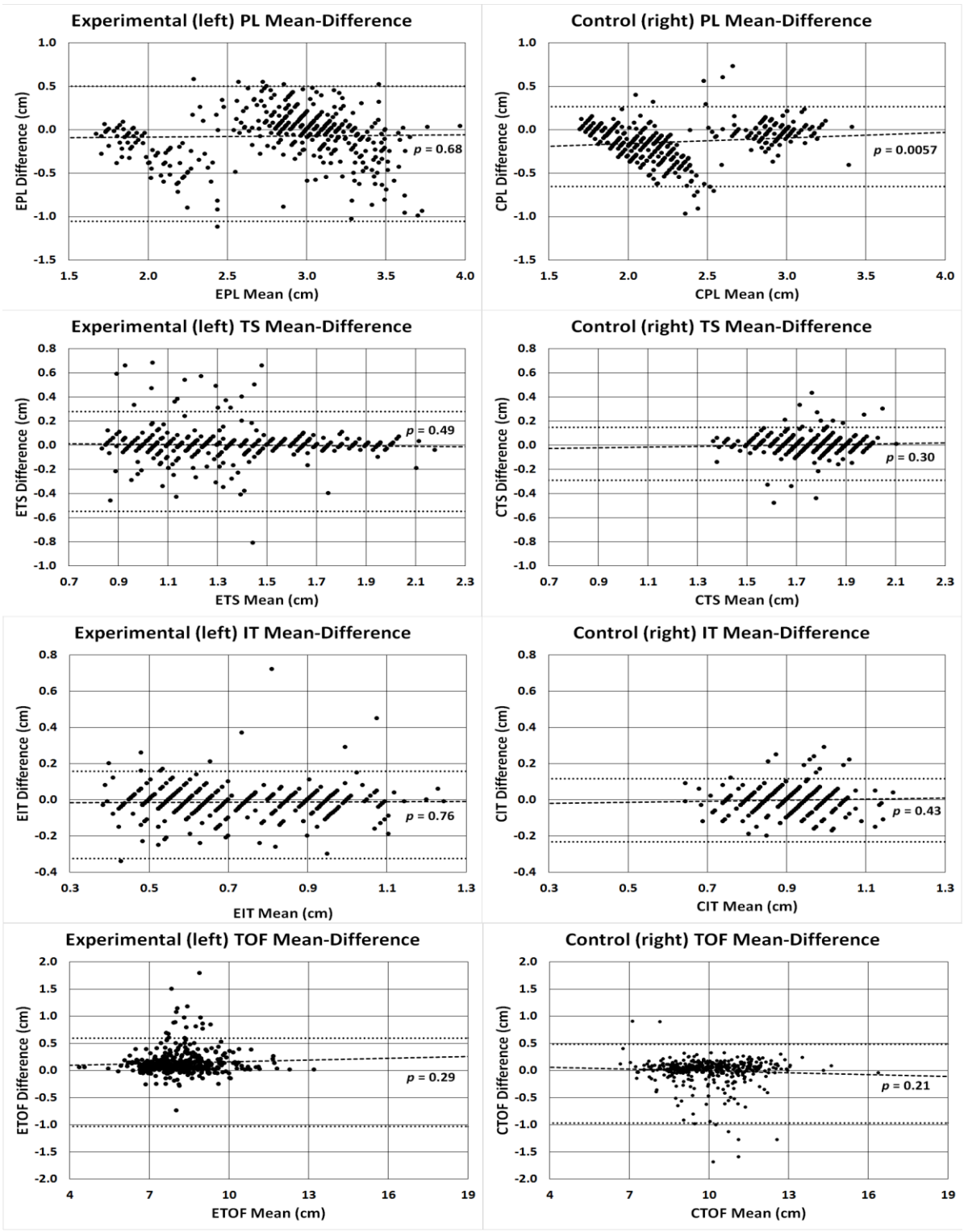

Figure 33: Bland-Altman plots for PFI component measurements.
Horizontal lines represent the limits of agreement (± 1.96 SD of the mean difference) and fit line represents trend toward bias (with associated p-value indicating the significance of the differences). Print length (PL) of the contralateral side is the only parameter showing a trend toward bias. Differences for all components are not clinically relevant. E = experimental limb, C = contralateral limb, PL = print length, TS = toe spread, and IT = intermediate toe spread, TOF = distance to the opposite foot.

Functional Index Components (Trial Maximums)

For the walking track measurements used to calculate peroneal functional index (PFI) with the BMH method (print length, PL, and toe spread, TS) and using trial maximum component measurements, there were significant differences over time in the experimental (left) limb (EPL and ETS, $p < 0.0001$ for both components, ANOVA, Figure 34). There was no significant effect of time on the contralateral limb print length (CPL, $p = 0.067$, ANOVA, Figure 34) or toe spread (CTS, $p = 0.97$, ANOVA, Figure 34). For the additional measured walking track components (not used in the BMH method of calculating PFI), there were significant differences over time for the experimental (left) limb in intermediate toe spread (EIT, $p < 0.0001$, ANOVA, Figure 34), distance to the opposite foot (ETOF, $p < 0.0001$, ANOVA, Figure 34), simple deviation angle (EDA, $p < 0.0001$, ANOVA, Figure 35), and stance width (ESW, $p < 0.0001$, ANOVA, Figure 35). In the contralateral limb, there were significant differences over time in intermediate toe spread (CIT, $p = 0.0002$, ANOVA, Figure 34) and stance width (CSW, $p < 0.0001$, ANOVA, Figure 35). There were no significant differences over time in the contralateral limb for distance to the opposite foot (CTOF, $p = 0.069$, ANOVA, Figure 34) or simple deviation angle (CDA, $p = 0.67$, ANOVA, Figure 35),.

EPL was shortest at week 0 (pre-operative) and increased over the first three weeks post-operatively. It then decreased to approach but never reached pre-operative length (Figure 34). ETS was the widest at week 0 (pre-operative) and decreased over the first three weeks post-operatively. It then increased to approach but never reached pre-operative widths (Figure 34). The mean EIT measurement was widest at week 0 (pre-operatively) and decreased to its narrowest at three weeks following surgical transection-coaptation. It widened over the next 13 weeks but never achieved pre-surgical width. Over the last 8 weeks of the experimental time period, it narrowed again. In contrast, the mean CIT widened at 1 week post-transection, then progressively narrowed to its nadir at week 24 (Figure 34). The mean ETOF measurement followed a pattern similar to EIT; it was widest at week 0 and decreased over the first three weeks post-operatively to its narrowest measurement, then widened again to nearly pre-operative width at week 12, and finally narrowed again over the last 12 weeks of the experimental time frame (Figure 34).

The mean EDA had its greatest mean value at week 0 (pre-operative), which then decreased following surgery to its lowest mean value at week 4 post operatively, then returned toward (but never reached) pre-operative values over the remaining 20 weeks (Figure 35). The mean ESW decreased significantly over the first three weeks post-operatively. Over the remaining 21 weeks of the experimental time period, the mean value increased to exceed pre-operative width by week 16 post-operatively. The mean CSW similarly decreased immediately post-operatively and reached its nadir at week 4. It also increased over the remaining 20 weeks to exceed its pre-operative width at week 20 (Figure 35).

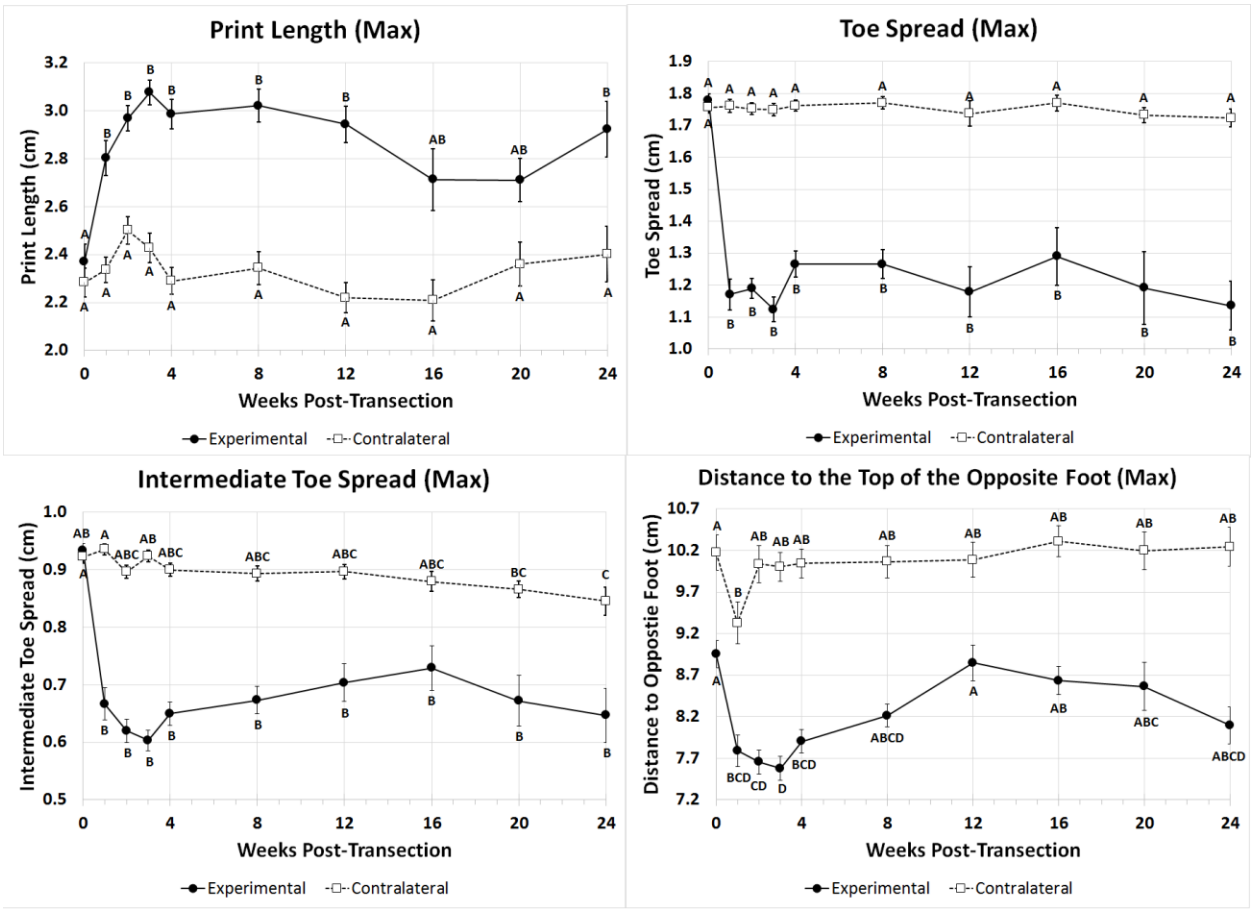

Figure 34: Variation in measured PFI components over time, trial maximums.
Measurements are for both experimental (E) and contralateral (C) limbs. There was a significant variation with time for EPL ($p < 0.0001$), ETS ($p < 0.0001$, both EIT and CIT ($p< 0.0001$ and $p = 0.0002$, respectively), and ETOF ($p < 0.0001$). There was no significant effect of time for CPL ($p = 0.067$), CTS ($p = 0.97$) or CTOF ($p = 0.069$). Letters represent distinct groups based on Tukey's HSD test (groups not connected by the same letter are significantly distinct). Data shown are the mean and standard error (SEM).

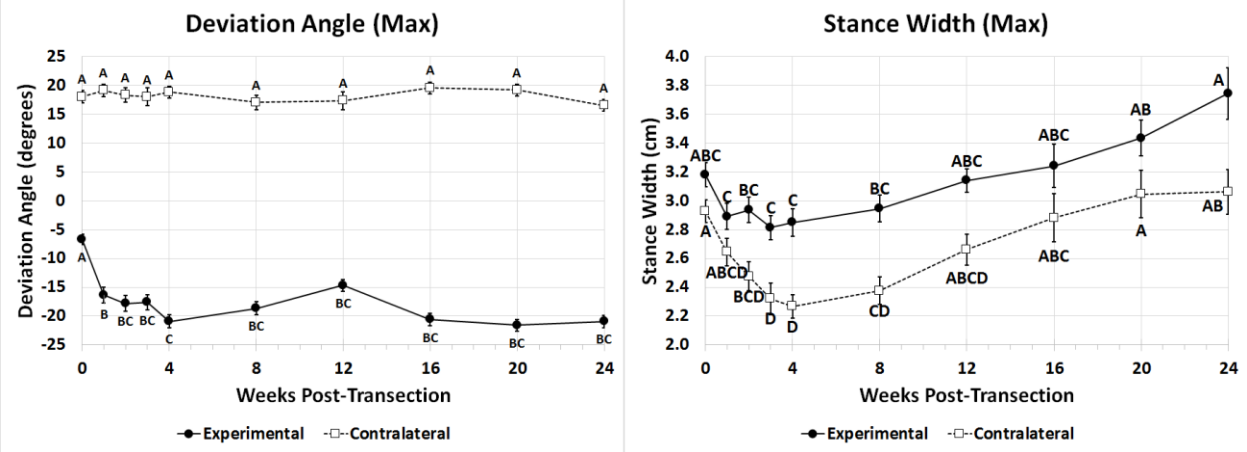

Figure 35: Variation in new PFI components over time, using trial maximum measurements.
Measurements are for both experimental (E) and contralateral (C) limbs. There was significant variation of EDA ($p < 0.0001$) but no significant change in CDA ($p = 0.86$) over time. There was a significant variation of both mean ESW and mean CSW over time ($p < 0.0001$ for both measurements). In general, the effect on the SW measured from contralateral foot to experimental foot appears larger. Letters represent distinct groups based on Tukey's HSD test (groups not connected by the same letter are significantly distinct). Data shown are the mean and standard error (SEM).

There was a significant decrease in velocity moving across the corridor apparatus over time ($p < 0.0001$, ANOVA, Figure 36). Velocity was the fastest at week 0 (pre-operative) and declined over the entire experimental timeline to its lowest value at week 24 post-operatively. Additionally, there was a significant increase in animal weight over time ($p<0.0001$, ANOVA, data not shown).

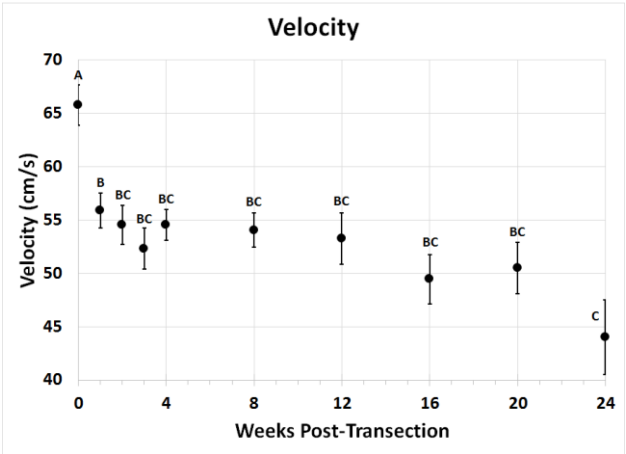

Figure 36: Variation in PFI mean velocity (V) over time.
In contrast to the SFI study, there was a significant decrease in velocity over time throughout the experimental time period ($p < 0.0001$). Letters represent distinct groups based on Tukey's HSD test (groups not connected by the same letter are significantly distinct). Data shown are the mean and standard error (SEM).

Functional Index Components (Trial Averages)

For the walking track measurements using trial averages for each component, there was a significant effect of time on experimental limb PL, TS, IT, TOF, DA, and SW (< 0.0001 for all, ANOVA Figure 37 and Figure 38). For the contralateral limb, there were significant differences over time only for PL ($p = 0.021$, ANOVA, Figure 37), TOF ($p = 0.012$, ANOVA, Figure 37), and SW ($p < 0.0001$, ANOVA, Figure 38). CTS ($p = 0.97$, ANOVA, Figure 37), CIT ($p = 0.075$, ANOVA, Figure 37) and CDA ($p = 0.97$, ANOVA, Figure 38) were not significantly affected by time.

EPL had its smallest measurement at week 0 (pre-operative) and increased over the first three weeks post-operatively to its largest measurement. It then decreased to approach but never reached pre-operative length (Figure 37). ETS was the widest at week 0 (pre-operative), decreased immediately following surgery and then had an increasing trend. However, none of the post-operative groups were differentiable throughout the remainder of the experiment (Figure 37). The mean EIT measurement was widest at week 0 (pre-operatively) and decreased to its narrowest at three weeks following surgical transection-coaptation. It widened over the next 13 weeks but never achieved pre-surgical width (Figure 37). The mean ETOF was wide at week 0 (pre-operative), and decreased immediately following surgery, with its narrowest measurement at post-operative week 1. Over the course of the remainder of the experiment, it then increased significantly to achieve pre-operative levels at week 12, only to decrease again over the remaining 12 weeks (Figure 37). CPL and CIT were considered significantly different among time points via ANOVA but post-hoc testing via Tukey's HSD failed to reveal significantly different groups (Figure 37).

For the new measurements in the experimental limb, EDA was the smallest at week 0 (pre-operatively) and increased significantly at post-surgical week 1. Though this measurement displayed an increasing trend through post-operative week 4 and after that time appeared to decrease towards pre-operative levels, the post-operative groups were not significantly differentiable (Figure 38). SW in the experimental limb was wide at time 0, and decreased in width immediately following surgery where it remained through week 12. Then, ESW increased to exceed pre-operative width by week 20 (Figure 38).

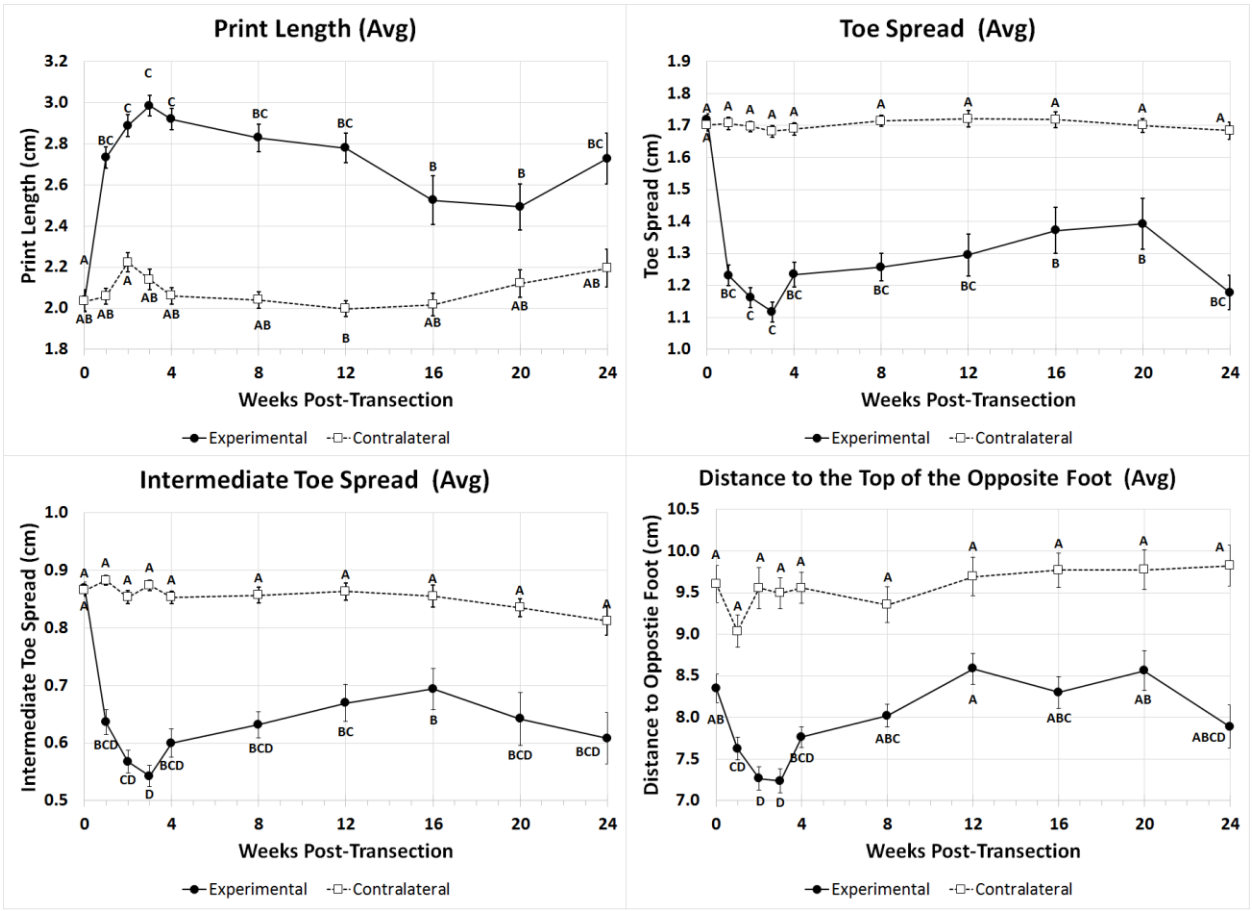

Figure 37: Variation in measured PFI components over time, trial averages.
There was a significant variation with time for EPL, ETS, EIT, and ETOF (p <0.0001 for all, ANOVA). Time had a significant effect on CPL (p = 0.021, ANOVA) and CTOF (p = 0.012, ANOVA) but not CTS or CIT (p = 0.97 and p = 0.075 respectively, ANOVA). Letters represent distinct groups based on Tukey's HSD test (groups not connected by the same letter are significantly distinct). Data shown are the mean and standard error (SEM).

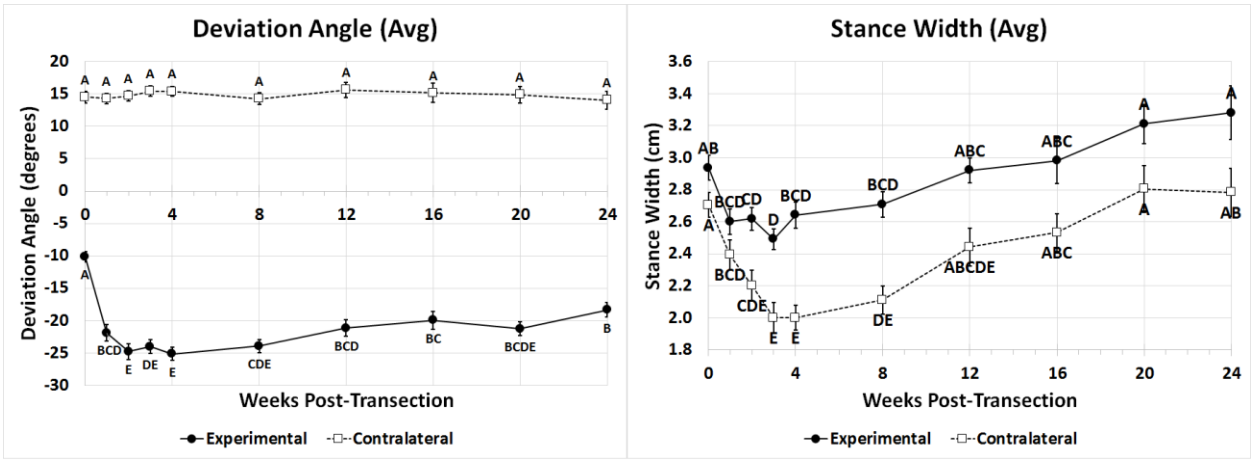

Figure 38: Variation in new PFI components over time, using trial average measurements.
There was significant variation of EDA, ESW and CSW over time (p < 0.0001 for all, ANOVA) but no significant change in CDA (p = 0.97, ANOVA) over time. Letters represent distinct groups based on Tukey's HSD test (groups not connected by the same letter are significantly distinct). Data shown are the mean and standard error (SEM).

Week 0 Measured Component Averages (Trial Maximums)

There were significant differences between individual rats within the common peroneal functional recovery study for the experimental limb for the PL, TS, and IT measurements ($p = 0.036$, $p < 0.0001$, and $p = 0.008$ respectively, ANOVA, data not shown) when the maximum measurement per trial was taken. There was no significant difference between rats in week 0 maximum TOF measurements ($p = 0.15$, ANOVA, data not shown). For the contralateral limb, there were significant differences between individual rats in week 0 maximum TS and IT measurements ($p = 0.0002$ and $p = 0.016$, ANOVA, data not shown). However, there were no significant differences between rats for week 0 maximum PL or TOF measurements ($p = 0.066$ and $p = 0.23$ respectively, ANOVA, data not shown).

For PL, TS, and IT, the differences between maximum measurements were small for both the experimental (left) and contralateral limbs, whereas they were somewhat larger for the maximum TOF measurements for both limbs (see Figure 16 in the sciatic functional recovery study results). The week 0 average values for these measurements are very consistent between the two studies (see Figure 16 in the sciatic functional recovery study results).

Week 0 Measured Component Averages (Trial Averages)

For week 0 measurements that were averaged within a trial, there were significant differences in the experimental (left) limb between individual rats for PL, TS, and IT ($p = 0.0014$, $p < 0.0001$, and $p = 0.0003$ respectively, ANOVA, data not shown). However, average TOF measurements were not significantly different between rats ($p = 0.4024$, ANOVA, data not shown). For the contralateral limb, there were significant differences in the averaged week 0 component measurements between rats for TS and IT ($p < 0.0001$ and $p = 0.0040$ respectively, ANOVA, data not shown). However, there were no significant differences in week 0 averaged component measurements between subjects for PL or TOF ($p = 0.0855$ and $p = 0.14$ respectively, ANOVA, data not shown). Overall, differences between rats for averaged week 0 components were small for PL, TS, and IT and only slightly larger for TOF for both the experimental and contralateral limbs (Figure 39).

Experimental limb week 0 measurements for simple deviation angle (DA) and stance width (SW) were significantly different between rats ($p = 0.0034$ and $p < 0.0001$ respectively, ANOVA, data not shown). For the contralateral limb, week 0 DA was significantly different between rats ($p < 0.0001$, ANOVA, data not shown). However, week 0 SW was not significantly different between individual rats in the contralateral limb ($p = 0.064$, ANOVA, data not shown). The differences in week 0 average simple DA and SW, calculated using average measurements for all prints in each trial, are small (Figure 40).

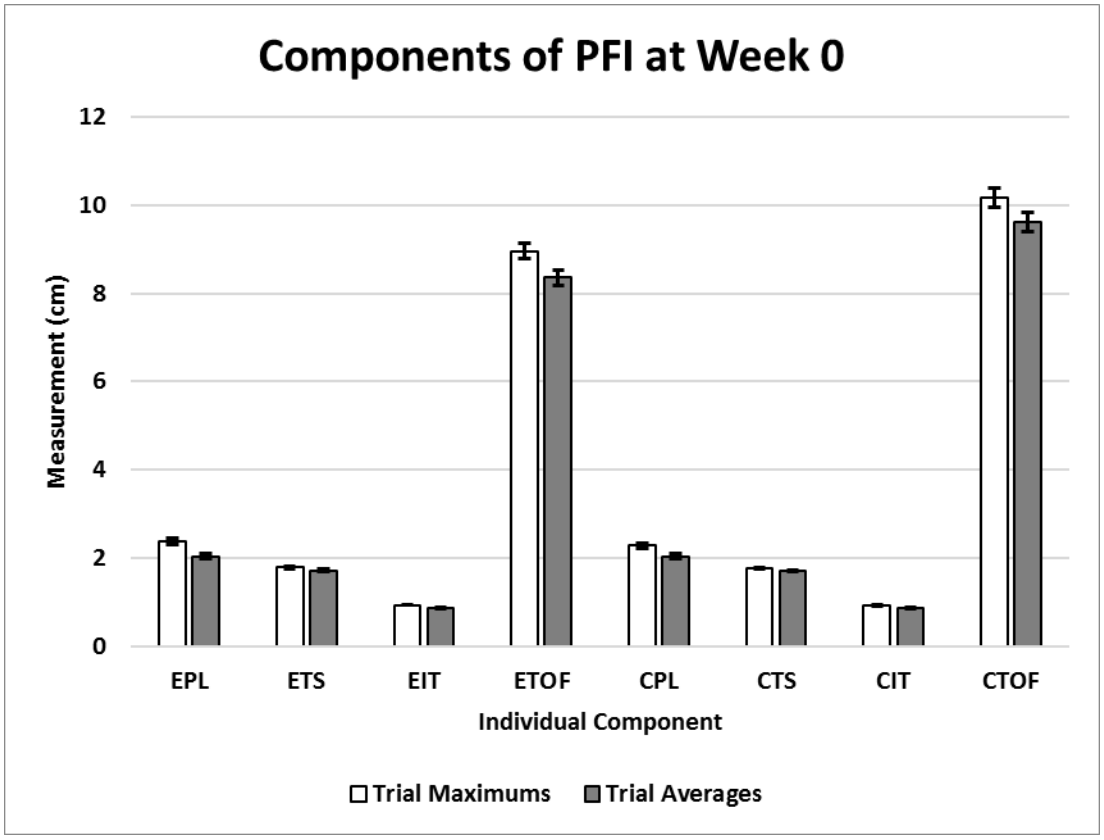

Figure 39: Mean PFI component measurements for week 0
The mean of all week 0 measurements for all experimental subjects is shown for both trial maximum and trial average component measurements. As expected, averages 'trial average' measurements are slightly smaller than averages 'trial maximum' measurements. However, standard error is also slightly smaller for averaged components. Error bars represent standard error of the mean. PL = print length factor, TS = toe spread factor, IT = intermediate toe spread factor, and TOF = distance to the opposite foot factor. E = experimental and C = contralateral.

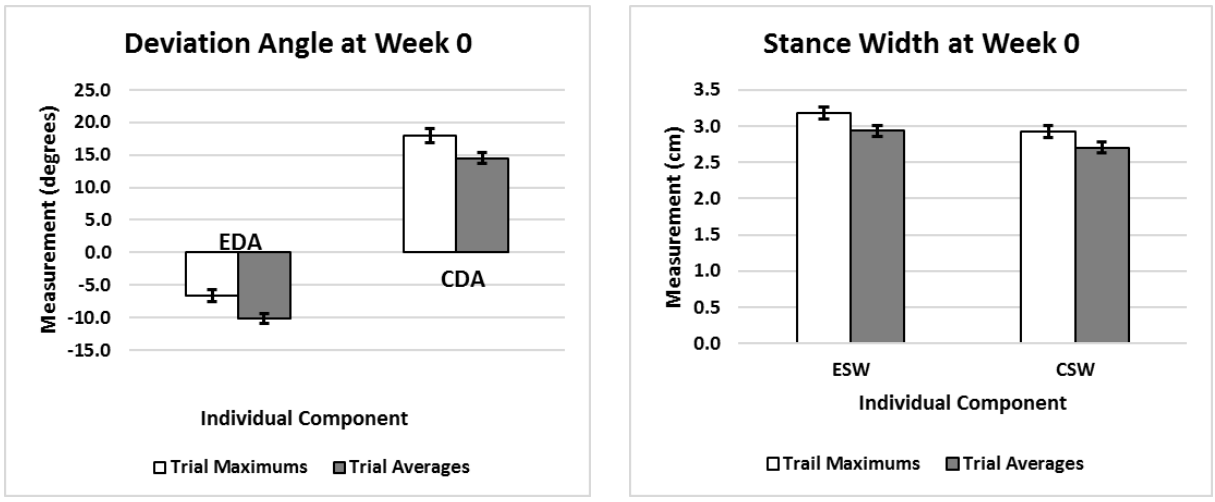

Figure 40: Simple Deviation Angle and Stance Width Week 0 Averages
The average measurements for deviation angle (DA) and stance width (SW) have relatively small differences between individual rats at week 0 for both the experimental (left) limb (E) and the contralateral limb (C).

Calculated 'Factors' for Common Peroneal Function Index (Maximum Measurements)

When calculated using the traditional method (using contralateral limb measurements to normalize the experimental measurements), and using maximum measurements for each trial, the calculated factors for PL, TS, IT, and TOF were all significantly affected by time ($p < 0.0001$ for all, ANOVA, Figure 41). PL factor was the lowest pre-operatively (at week 0) and increased immediately after transection (at week 1). Over the course of the experimental time frame, it decreased toward but did not achieve the pre-operative low (Figure 41). The TS factor only had two significantly distinct groups: a pre-operative maximum at week 0 and a sharp post-operative decrease starting at week 1 that persisted through at all other time points (Figure 41). The IT factor also had a pre-operative maximum at week 0 that decreased to reach a post-operative minimum at week 3. It increased again over the next 21 weeks to approach but not achieve the pre-operative maximum (Figure 41). Finally, the TOF factor had a pre-operative maximum and a minimum at week 3 post-operatively, with all other time points intermediate to the two extremes (Figure 41).

When the factors were calculated using the variant method (using week 0 average data to normalize experimental measurements), and using maximum measurements for each trial, time had a significant effect on the PL, TS, IT and TOF factors for the experimental (left) limb ($p < 0.0001$ for all,

ANOVA, Figure 42). The PL factor had a pre-operative (week 0) minimum measurement and a gradual increase to its maximum value at week 3. The factor then decreased over the remaining experimental time frame toward but not reaching,the pre-operative minimum (Figure 42). The TS and IT factors were both divided into significant pre- and post-operative groups but post-operative time points were not significantly different from each other (Figure 42). The TOF factor was longest pre-operatively and, similar to the PL factor, gradually decreased to a nadir at week 3. It then increased again, and by week 12 had reached the pre-operative level. However, it then decreased toward the week 3 nadir again over the remainder of the experimental time-frame (Figure 42).

For the variant method with maximum component measures on the contralateral limb, only the IT factor was significantly affected by time ($p = 0.0003$, ANOVA, Figure 43). The PL, TS, and TOF factors were not significantly affected by time ($p = 0.067$, $p = 0.97$, and $p = 0.069$ respectively, ANOVA, Figure 43). The IT factor started near zero, yet positive, at week 0 and then increased at week 1 post-transection. It then decreased, becoming negative, over the remainder of the experimental time-frame (Figure 43).

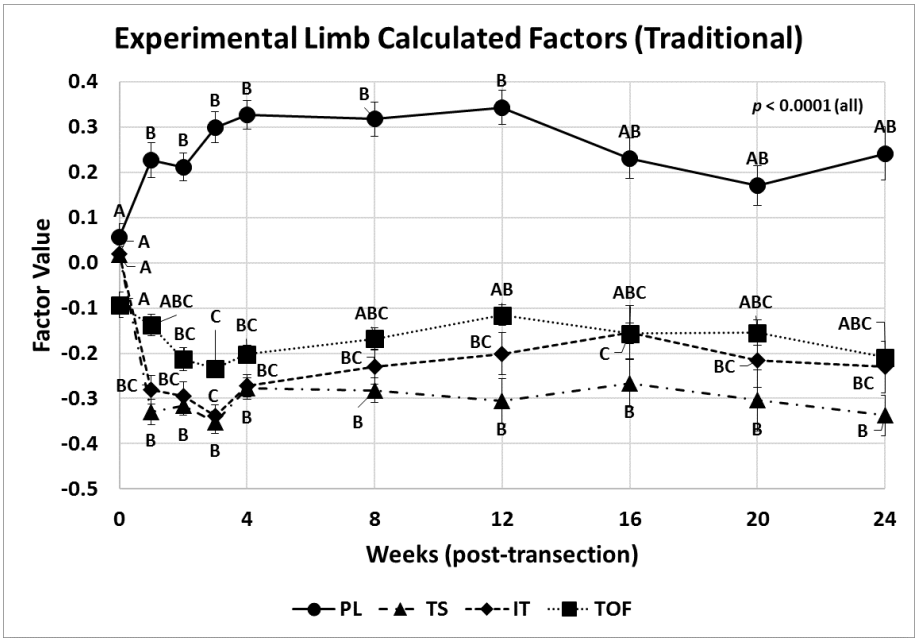

Figure 41: Calculated Maximum PFI Factors for the Experimental Limb (traditional method)
'Factors' calculated for the experimental limb using the traditional method of [(experimental limb measure – contralateral limb measure)/contralateral limb measure] and the maximum measures from each trial. All factors are significantly affected by time. PL = print length, TS = toe spread, IT = intermediate toe spread, and TOF = distance to the opposite foot. Letters represent distinct groups based on Tukey's HSD test (groups not connected by the same letter are significantly distinct). Data shown are the mean and standard error (SEM).

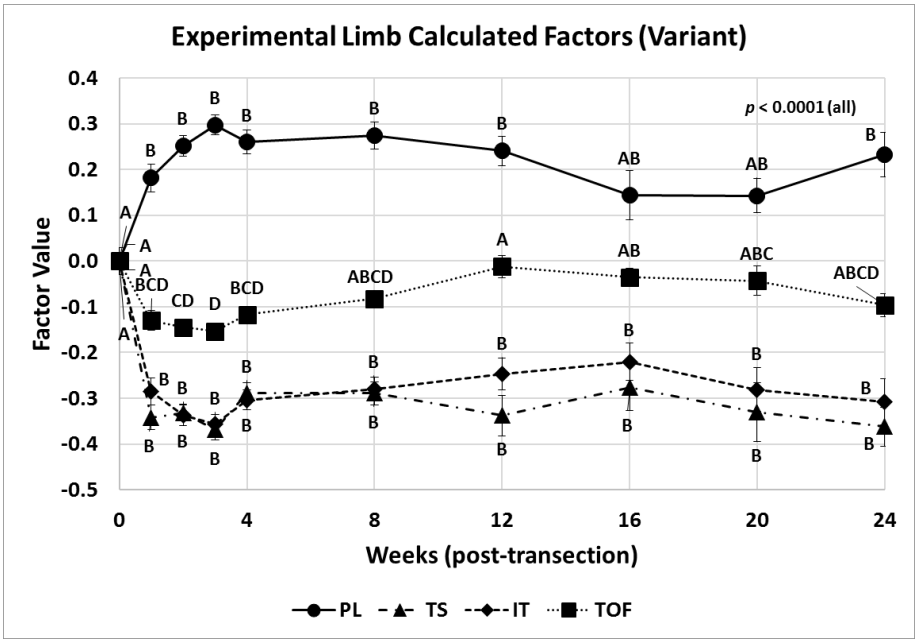

Figure 42: Calculated Maximum PFI Factors for the Experimental Limb (variant method)
'Factors' calculated for the experimental limb using the variant method of [(experimental limb measure – week 0 average limb measure)/week 0 average limb measure] and the maximum measures for each trial. All factors are significantly affected by time. PL = print length, TS = toe spread, IT = intermediate toe spread, and TOF = distance to the opposite foot. Letters represent distinct groups based on Tukey's HSD test (groups not connected by the same letter are significantly distinct). Data shown are the mean and standard error (SEM).

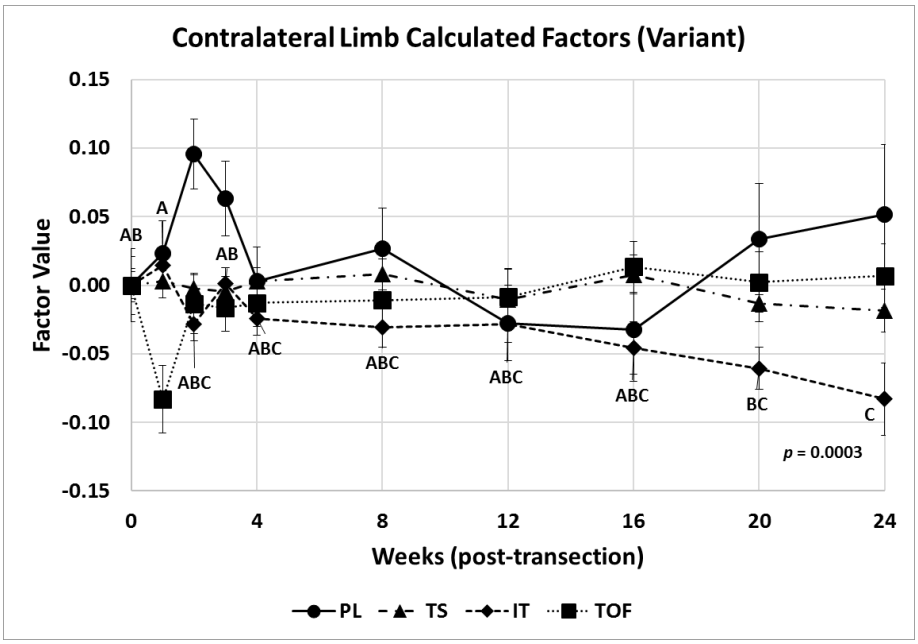

Figure 43: Calculated Maximum PFI Factors for the Contralateral Limb (variant method)
'Factors' calculated for the contralateral limb using the variant method of [(experimental limb measure – week 0 average limb measure)/week 0 average limb measure] and the maximum measures for each trial. Only the IT factor was significantly affected by time. PL = print length, TS = toe spread, IT = intermediate toe spread, and TOF = distance to the opposite foot. Letters represent distinct groups based on Tukey's HSD test (groups not connected by the same letter are significantly distinct). Letters only show for IT for clarity. Data shown are the mean and standard error (SEM).

Calculated 'Factors' for Common Peroneal Function Index (Average Measurements)

When calculated using the traditional method (using contralateral limb measurements to normalize the experimental measurements), and using average measurements for each trial, the calculated factors for PL, TS, IT, and TOF were all significantly affected by time ($p < 0.0001$ for PL, TS, and IT, and $p = 0.0008$ for TOF, ANOVA, Figure 44). The PL factor had its smallest value at week 0 (pre-operative) and increased to its maximum value by 4 weeks post-surgery. Then, it gradually decreased over the remaining experimental time frame but never achieved the pre-operative low (Figure 44). The TS, IT and TOF factors all had maximum values pre-operatively (at week 0) and then decreased to their respective nadir by week 3 following surgery. Each factor then gradually increased over the experimental time frame. None of these factors ever achieved their respective pre-operative maximums (Figure 44).

When the PL, TS, IT, and TOF factors were calculated using the variant method (using week 0 average data to normalize experimental measurements), and using average measurements for each trial, time had a significant effect on the PL, TS, IT and TOF factors for the experimental (left) limb ($p < 0.0001$ for all, ANOVA, Figure 45). The PL factor had a pre-operative (week 0) minimum measurement and a gradual increase to its maximum value at week 3. The factor then decreased over the remaining experimental time frame toward but not reaching the pre-operative minimum (Figure 45). The TS, IT and TOF factors all had maximum values at their pre-operative evaluation (week 0). Each of the factor decreased to their lowest level by week 3 post-transection and then gradually increased over the remaining experimental time frame. The TS and IT factors never achieved their pre-surgical maximum but TOF reached its maximum at week 12 post-surgery (Figure 45).

For the variant method with average component measures for PL, TS, IT, and TOF on the contralateral limb, only the PL factor was significantly affected by time ($p = 0.020$, ANOVA, Figure 46). The TS, IT, and TOF factors were not significantly affected by time ($p = 0.96$, $p = 0.072$, and $p = 0.37$ respectively, ANOVA, Figure 46). The PL factor had its lowest value at week 0, increased to its maximum by week 3 post-transection, and then gradually decreased over the experimental time frame. It never achieved its pre-operative level (Figure 46).

Both the DA and SW factors calculated for the experimental (left) limb, using the variant method (normalized with time 0 measurements) with trial average measurements, were significantly affected by time ($p < 0.0001$ for both, ANOVA, Figure 47). The DA factor had a pre-surgical low that increased by week 1 following surgery. Post-surgical groups, however, were not able to be differentiated significantly (Figure 47). The SW factor had a pre-surgical high value at zero, which decreased to a nadir at 2 weeks post-transection. The factor then increased over the remainder of the experimental time period, becoming positive and thus exceeding pre-operative levels at week 20 (Figure 47).

For the contralateral limb, using the same methods, the DA factor was not significantly affected by time ($p = 0.97$, ANOVA, Figure 48). However, the SW factor was significantly affected by time ($p < 0.0001$, ANOVA, Figure 48). Similar to the experimental limb, the contralateral limb SW had a value of zero at week 0. It also decreased following surgical transection and coaptation. However, it did not reach its lowest level until week 4. It then increased over the remainder of the experimental time period, exceeding pre-operative levels at week 20 (Figure 48).

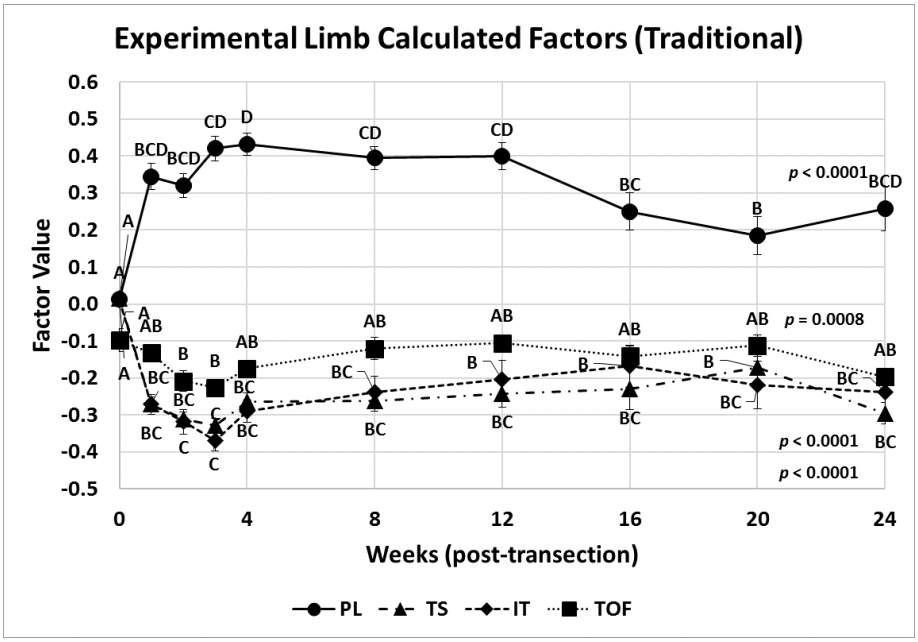

Figure 44: Calculated Averaged PFI Factors for the Experimental Limb (traditional method)
'Factors' calculated for the experimental limb using the traditional method of [(experimental limb measure – contralateral limb measure)/contralateral limb measure] and the average measurement from each trial. All factors are significantly affected by time. PL = print length, TS = toe spread, IT = intermediate toe spread, and TOF = distance to the opposite foot. Letters represent distinct groups based on Tukey's HSD test (groups not connected by the same letter are significantly distinct). Data shown are the mean and standard error (SEM).

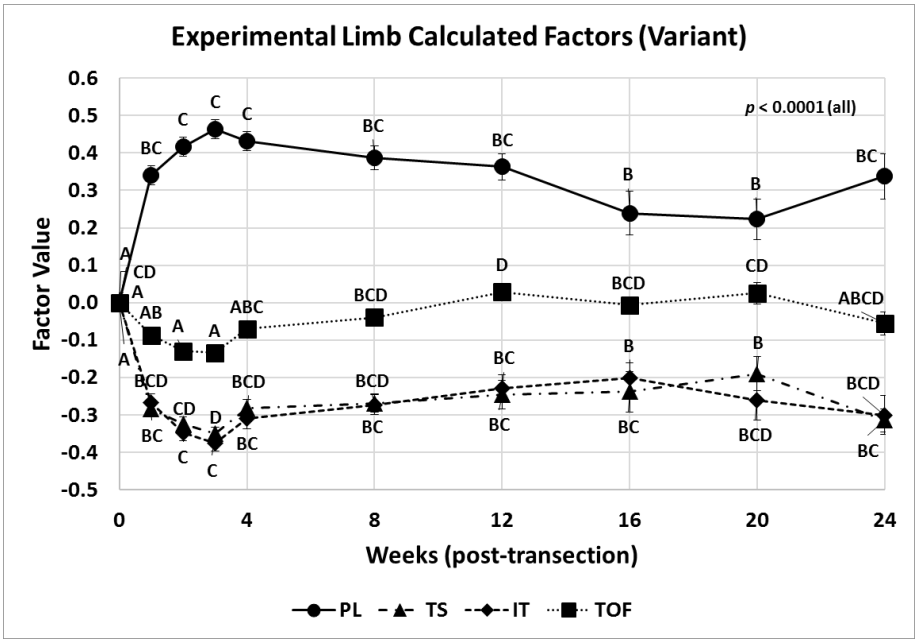

Figure 45: Calculated Averaged PFI Factors for the Experimental Limb (variant method)
'Factors' calculated for the experimental limb using the variant method of [(experimental limb measure – week 0 average limb measure)/week 0 average limb measure] and the average measures for each trial. All factors are significantly affected by time. PL = print length, TS = toe spread, IT = intermediate toe spread, and TOF = distance to the opposite foot. Letters represent distinct groups based on Tukey's HSD test (groups not connected by the same letter are significantly distinct). Data shown are the mean and standard error (SEM).

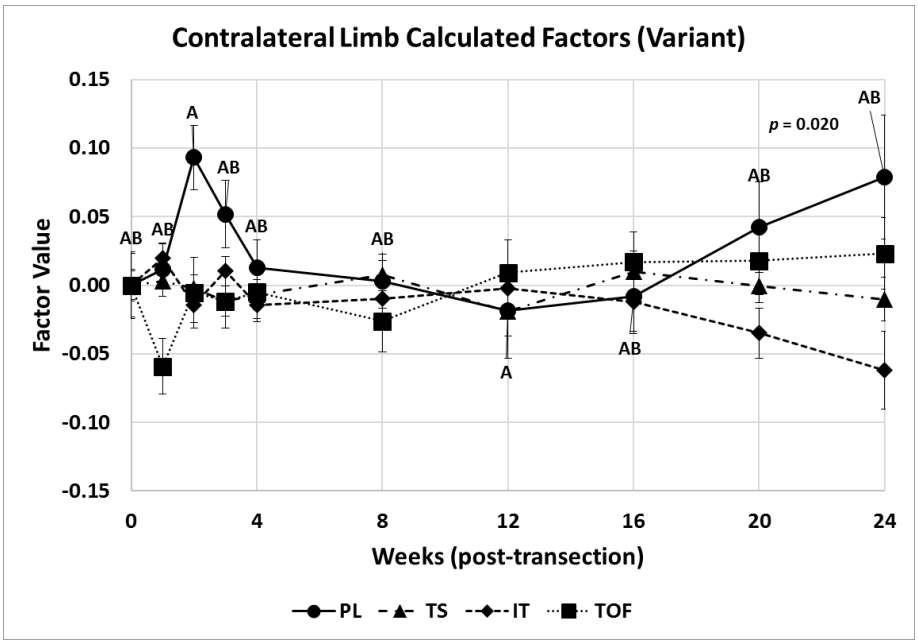

Figure 46: Calculated Averaged PFI Factors for the Contralateral Limb (variant method)
'Factors' calculated for the contralateral limb using the variant method of [(experimental limb measure – week 0 average limb measure)/week 0 average limb measure] and the average measures for each trial. Only the PL factor was significantly affected by time. PL = print length, TS = toe spread, IT = intermediate toe spread, and TOF = distance to the opposite foot. Letters represent distinct groups based on Tukey's HSD test (groups not connected by the same letter are significantly distinct). Letters only show for IT for clarity. Data shown are the mean and standard error (SEM).

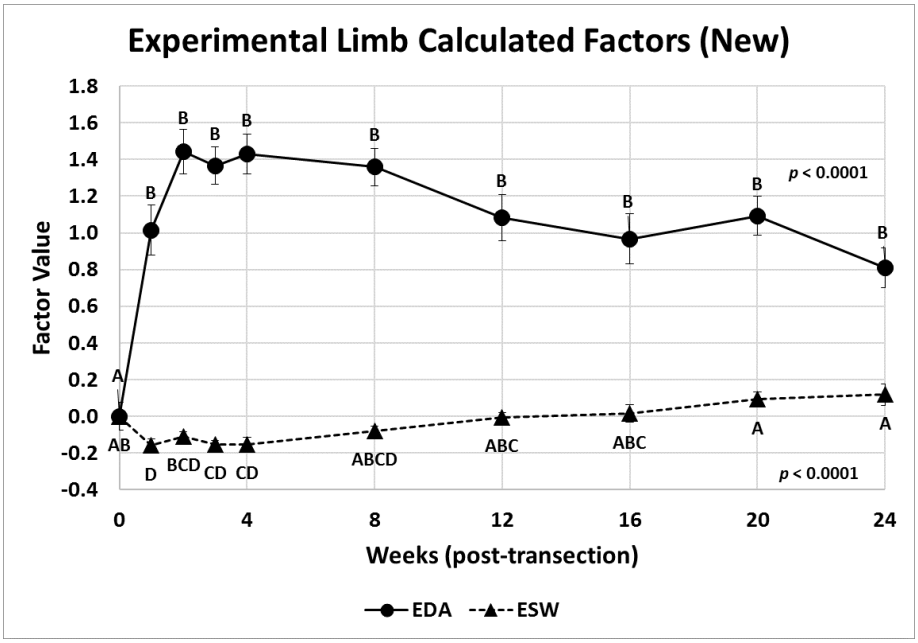

Figure 47: Calculated Averaged New PFI Factors for the Experimental Limb (variant method)
'Factors' calculated for the experimental limb using the variant method of [(experimental limb measure – week 0 average limb measure)/week 0 average limb measure] and the average measures for each trial for the new factors, DA and SW. Both factors are significantly affected by time. Letters represent distinct groups based on Tukey's HSD test (groups not connected by the same letter are significantly distinct). Data shown are the mean and standard error (SEM).

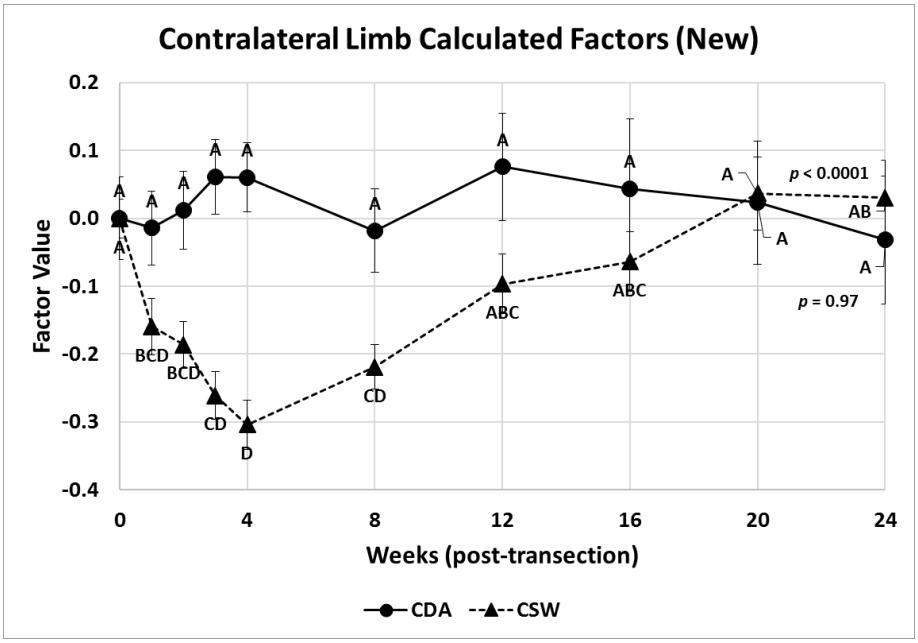

Figure 48: Calculated Averaged New PFI Factors for the Contralateral Limb (variant method)
'Factors' calculated for the experimental limb using the variant method of [(experimental limb measure – week 0 average limb measure)/week 0 average limb measure] and the average measures for each trial for the new factors, DA and SW. Both factors are significantly affected by time. Letters represent distinct groups based on Tukey's HSD test (groups not connected by the same letter are significantly distinct). Data shown are the mean and standard error (SEM).

Calculated Peroneal Function Index

There was a significant effect of time on peroneal function index (PFI), as calculated using the BMH method, with factors normalized using the contralateral limb, and using the largest measurement for each component within trials (BMH, $p = 0.014$, ANOVA, Figure 49). The PFI calculated using the variant method of normalizing factors using the week 0 average component measurements was also significantly affected by time for the experimental ($p = 0.0004$, ANOVA, Figure 49). Both methods yielded a PFI for the experimental limb at week 0 that was near 0, as expected. However, in the subsequent few post-surgical weeks the index improved (become more positive), rather than become more impaired (more negative). Finally, around week 8 or 12 the index began to decline, becoming negative and surpassing the pre-surgical values. The contralateral limb PFI (calculated using the variant method) was not significantly affected by time ($p = 0.099$, ANOVA, Figure 49).

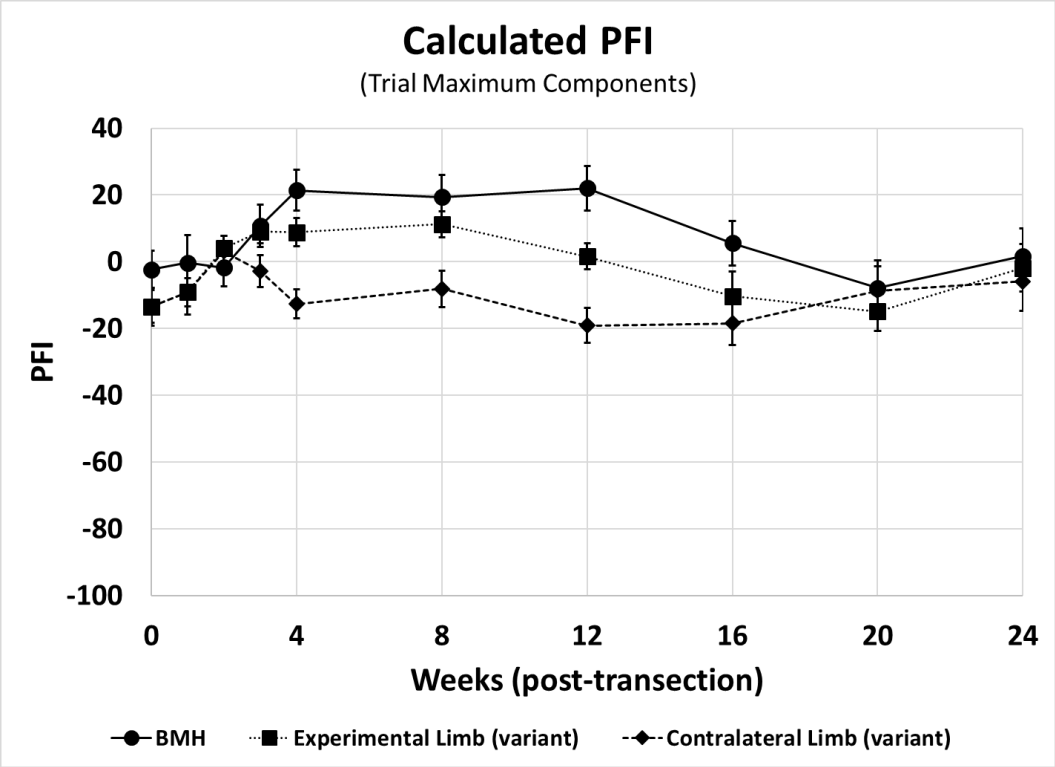

Figure 49: Calculated PFI (BMH Equation with Trial Maximum Component Measures)
*The PFI calculated using the BMH equation with trial component maximum measures and both the traditional ((E-C)/C) method and the variant method (using week 0 average measures) for normalizing the experimental measures was significantly affected by time (*p *= 0.014 and* p *= 0.0004, respectively, ANOVA). However, the index did not behave as expected, showing an improvement, rather than impairment, following surgical transection. The contralateral limb PFI (using the variant method) was not significantly affected by time (*p *= 0.099, ANOVA).*

Similarly, there was a significant effect of time on the peroneal functional index, when calculated using trial average measurements to normalize the measured components, for both the traditional (BMH) and variant methods of calculation ($p < 0.0001$ for both methods, ANOVA, Figure 50). Both methods yielded indices that also displayed the unexpected behavior of improving in the early few weeks following surgery rather than becoming more impaired, then declined in the later weeks of the experimental time frame (Figure 50). In contrast to using the maximum values for each trial, the method of using the average measurement for each component within a trial yielded a calculated PFI for the contralateral limb that was significantly affected by time ($p = 0.039$, ANOVA, Figure 50). However, this index also displayed the aberrant behavior previously described for the other calculated indices; it improved over the first two weeks then declined again to approximately the pre-surgical level (Figure 50).

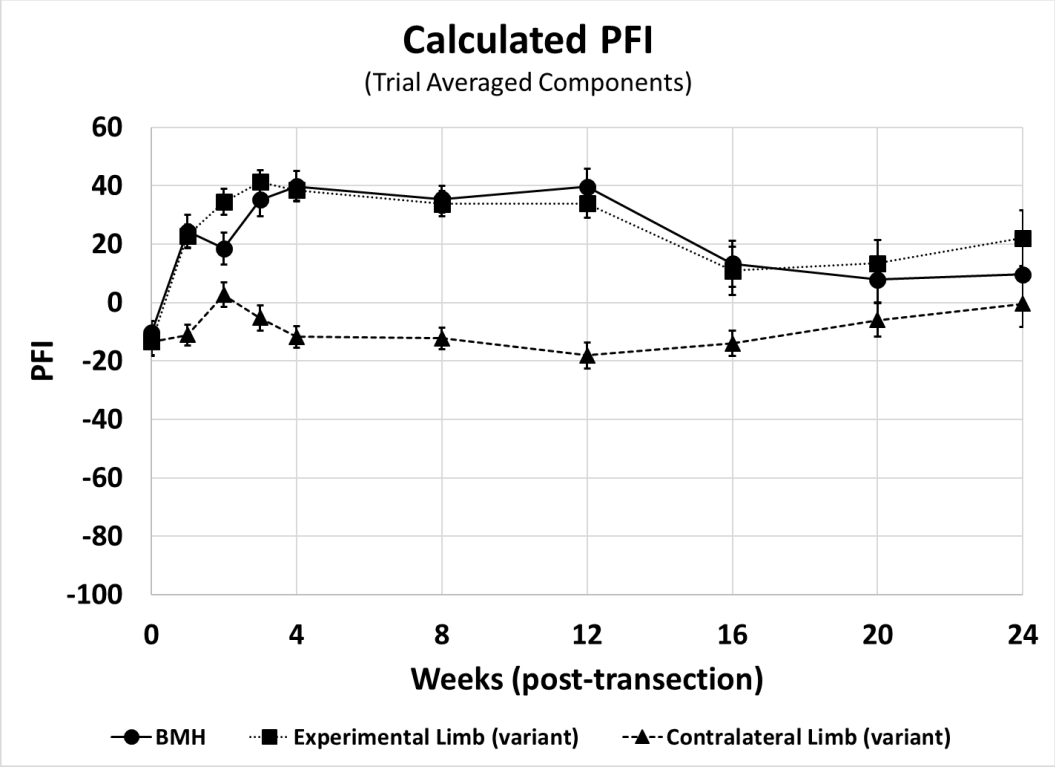

Figure 50: Calculated PFI (BMH Equation with Trial Average Component Measures)
The PFI calculated using the BMH equation with trial component average measures and both the traditional ((E-C)/C) method and the variant method (using week 0 average measures) for normalizing the experimental measures was significantly affected by time ($p < 0.0001$ for both, ANOVA). However, the index did not behave as expected, showing an improvement, rather than impairment, following surgical transection. Using this method, the contralateral limb PFI (using the variant method) was also significantly affected by time ($p = 0.039$, ANOVA).

A new CP function index

Screening of CP PFI factors revealed that only a subset of the factors were correlated with changes observed between week 0 and weeks 3 and 4 following transection and coaptation (Table 5). ETS, EDA, EPL, and CDA had significant individual *p*-values ($p < 0.0001$ for all) and also significant simultaneous *p*-values ($p < 0.0001$ for ETS, EDA and CDA, and $p = 0.0010$ for CDA). CPL, ETOF, and CTOF had significant individual *p*-values ($p = 0.0010$, $p = 0.0068$, and $p = 0.049$, respectively) but their simultaneous *p*-values within the model were not significant ($p = 0.16$, $p = 0.55$, and $p = 0.99$, respectively).

Table 5: Significant components for a new PFI formula
Three models were made based on the significance levels of these components: 1) those with significant individual p-*values, 2) those with individual* p-*values <0.005, and 3) only those with significant individual* and *significant simultaneous* p-*values*

Component	Individual p
ETS	<0.0001
EDA	<0.0001
EPL	<0.0001
CDA	<0.0001
CPL	0.0010
ETOF	0.0068
CTOF	0.049

The first model (7 factors, Model 1, Figure 51) included all components with a significant individual *p*-value (EPL, ETS, EDA, ETOF, CPL, CDA, and CTOF). The second model (5 factors, Model 2, Figure 51) included only those components with an individual *p*-value less than 0.005 (EPL, ETS, EDA, CPL and CDA). The third model (4 factors, Model 3, Figure 51) included only those components with significant individual *p*-values less than 0.05 (EPL, ETS, EDA, and CDA). All models had *p*-values < 0.0001 and high adjusted r^2 values (Model 1: 0.78, Model 2: 0.77, and Model 3: 0.76). PFI was then calculated for all time points using each of the three models.

$$Model\ 1 = -65.07(EPL) + 82.51(ETS) + 35(ETOF) - 14.24\ (EDA) + 44.36(CPL) - 8.35\ (CTOF) - 19.34(CDA) - 13.24$$

$$Model\ 2 = -67.25(EPL) + 85.44(ETS) - 14.46(EDA) + 39.55(CPL) - 20.07(CDA) - 13.9$$

$$Model\ 3 = -51.15(EPL) + 90(ETS) - 16.63(EDA) - 20.68(CDA) - 14.8$$

Figure 51: Models obtained from individual PFI component assessment.
These models were obtained using multiple linear regression analysis. Components (e.g. ETS, EDA, etc.) of these models reflect factors created for each component by subtracting each component's measurement from the component's week 0 average and dividing the resultant difference by the week 0 average for that component.

Time had a significant effect on the PFI calculated using each of the new models ($p < 0.0001$ for all three models, ANOVA, Figure 52). Mean PFI at time 0 (prior to surgery) was close to -14 for all three models (Model 1, 7 factors: -12.78 ± 3.14, Model 2, 5 factors: -13.90 ± 3.23, and Model 3, 4 factors: -13.24 ± 3.17; Figure 52). For each of the models, PFI decreased immediately following surgery to a the nadir at week 3, with means near -95 (Model 1, 7 factors: -95.03 ± 3.41, Model 2, 5 factors: -92.15 ± 3.5, and Model 3, 4 factors: 93.50 ± 3.44; Figure 52). All models showed a gradual increase in PFI from week 3 through week 20, though pre-surgical PFI was never attained by any of the models. At week 20, Model 1 (7 factors) had a mean PFI of -49.49 ± 4.97, Model 2 (5 factors) had a mean PFI of -56.33 ± 5.10, and Model 3 (4 factors) had a mean PFI of -53.58 ± 5.02. These means represent a recovery of lost function of ~60% for Model 1 (7 factors), ~72% for Model 2 (5 factors), and ~67% for Model 3 (4 factors).

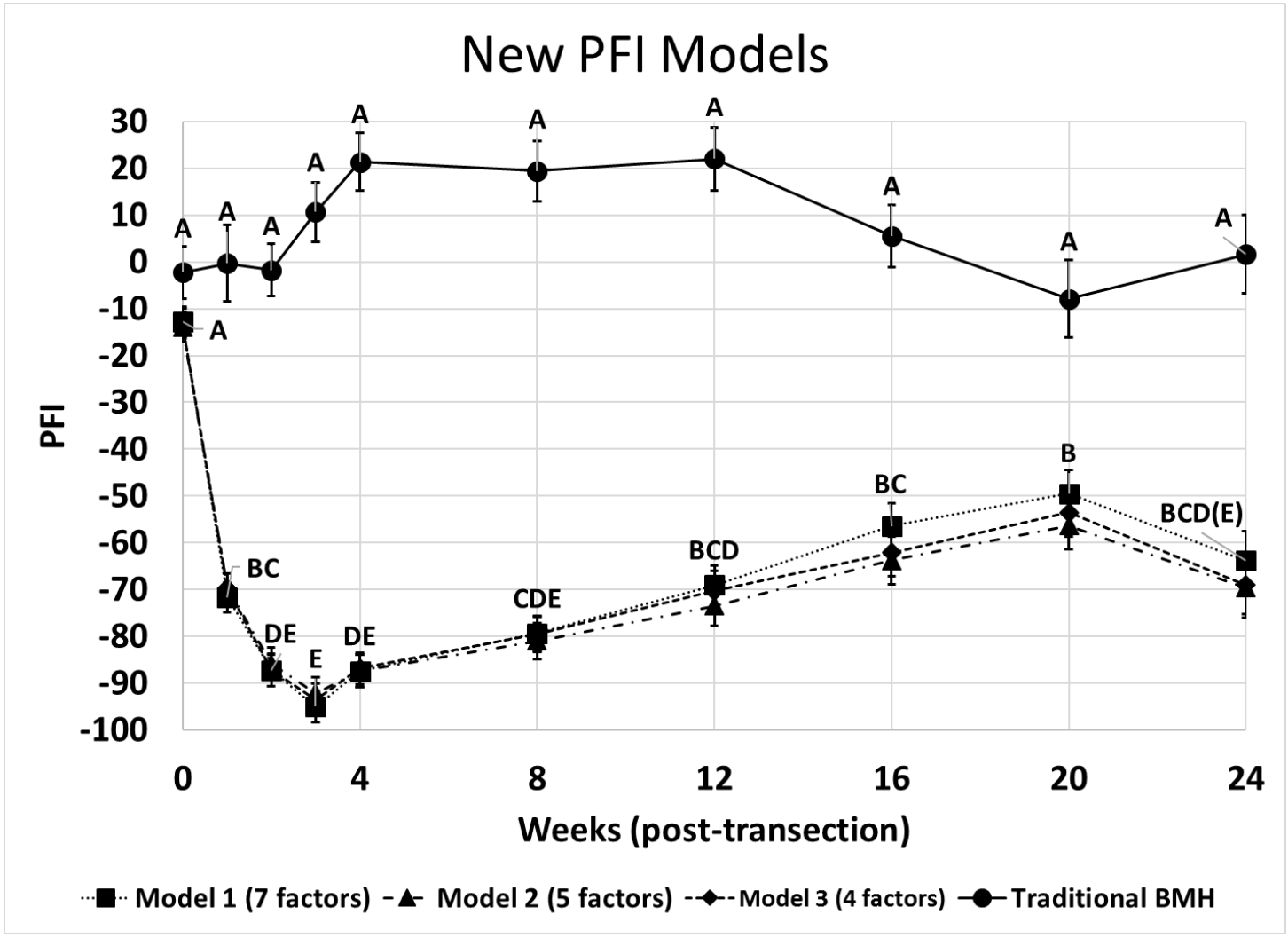

Figure 52: PFI derived from multiple linear regression analysis of all components.
There was a significant effect of time for all three new models for PFI ($p < 0.0001$ for all). All models had similar patterns of near zero week 0 PFI, nadir PFI at week 3, increasing PFI trends through week 20 and a drop in PFI at week 24. Letters represent distinct groups based on Tukey's HSD test (groups not connected by the same letter are significantly distinct). For week 24, Model 1 = BCD, Models 2 and 3 = BCDE. Data shown are the mean and standard error (SEM). Shown with the BMH PFI for comparison (no letters assigned).

Stationary Toe Spread Factor Components

Time had a significant effect on stationary TS, used to calculate the stationary TSF, for the experimental (left) limb ($p < 0.0001$, ANOVA, Figure 53). Stationary TS for the experimental limb had its widest measurement at week 0 and its narrowest measurement at week 2, with a gradual increase in width towards but never reaching pre-operative levels over the remaining experimental timeline. There was no significant effect of time on the stationary TS for the contralateral limb ($p = 0.21$, ANOVA, Figure 53).

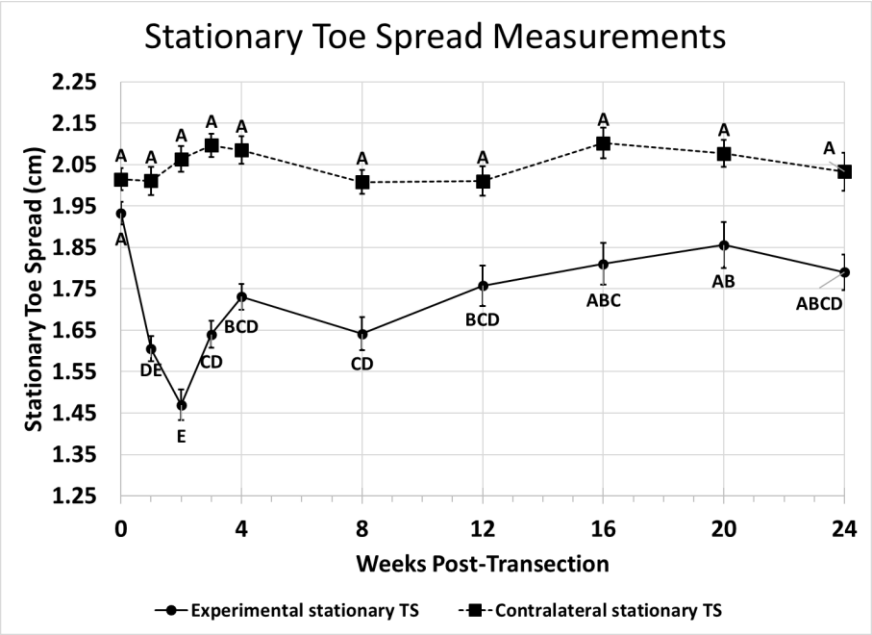

Figure 53: Variation in stationary toe spread (STS) over time for the CP functional recovery study
There was a significant effect of time on the experimental limb stationary TS ($p < 0.0001$, ANOVA) but not contralateral limb stationary TS ($p = 0.21$, ANOVA). Letters represent distinct groups based on Tukey's HSD test (groups not connected by the same letter are significantly distinct). Data shown are the mean and standard error (SEM).

Calculated Toe Spread Factor

There was significant variation of stationary TSF, calculated using the BMH method, over time ($p < 0.0001$, ANOVA, Figure 54). This trend was similar to the trend observed in the stationary TS measurement for the experimental limb from which it was derived; the largest measurement was at week 0 (pre-operative) and the smallest was at week 2 (post-operatively) with a gradual increase that approached but never reached pre-operative values by week 24. The stationary TSF for the experimental (left) limb that was calculated using the variant method also showed a pattern of variation with time that was similar to the standard BMH stationary TSF (E (variant), $p<0.0001$, ANOVA, Figure 54); the largest measurement was at week 0 (pre-operative) and the smallest was at week 2 (post-operatively) with a gradual increase that approached but never reached pre-operative values by week 24. The stationary TSF for the contralateral limb, also calculated using the variant method, showed no significant variation over time (C (variant), $p = 0.20$, ANOVA, Figure 54).

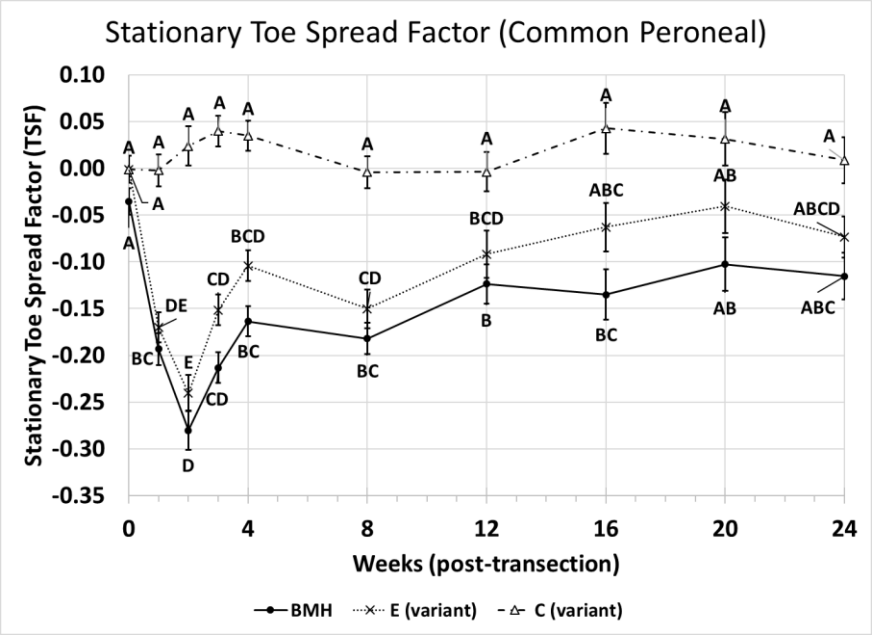

Figure 54: Variation in TSF over time for the CP functional recovery study.
There was a significant effect of time on TSF calculated using the BMH method (BMH TSF, $p < 0.0001$, ANOVA). There was also a significant effect of time on the TSF calculated for the experimental (left) limb using variant method (E (variant), *$p < 0.0001$). The contralateral (right) limb TSF calculated using the variant method showed no significant variation over time (C (variant), $p = 0.20$). Letters represent distinct groups based on Tukey's HSD test (groups not connected by the same letter are significantly distinct). Data shown are the mean and standard error (SEM).*

Skilled Locomotion Analysis

There was significant variation in velocity over time in each zone, and in all zones taken together, for skilled locomotion trials ($p < 0.0001$ for all, ANOVA, Figure 55). All zones showed a significant decrease in velocity at week 1 post-surgery with no significant change over the remainder of the experimental timeline.

Fixed effect modeling of SR for zone 1 showed an effect of time on the LF and RH SR ($p = 0.012$ and $p = 0.026$, respectively, Figure 56) but no effect of time on the RF or LH SR ($p = 0.067$ and $p = 0.059$, respectively, Figure 56). All limbs showed a trend of decreased SR over the first four weeks following surgery (in comparison to pre-surgical SR), that then increased modestly over the remainder of the experimental timeline.

For zone 2, fixed effect modeling showed that there was no significant effect of time on any of the limbs (by limb: RF, $p = 0.74$; LF, $p = 0.11$; RH, $p = 0.57$; LH, $p = 0.22$, Figure 57). Forelimb SR for this zone appeared to have an increasing trend as the experimental timeline progressed, whereas the hindlimb SR appear to have a decreasing trend.

Zone 3 fixed effect modeling of SR showed a significant effect of time on the LH ($p = 0.0052$, Figure 58). An immediate increase in LH slip rate at week 1 following surgery was immediately followed by the lowest SR over weeks 2 and 3, with the remainder of the experimental timeline falling somewhere between these two limits. The SR of the other limbs were not significantly affected by time (by limb: RF, $p = 0.27$; LF, $p = 0.62$; RH, $p = 0.062$, Figure 58), and produced no apparently meaningful trends.

Taking all zones summed together, fixed effect modeling of SR showed significant differences over time for the LF and LH SR ($p = 0.0074$ and $p = 0.026$, respectively, Figure 59). The LF slip rate decreased immediately following surgery (week 1) and increased to a peak at week 16. The LH similarly decreased and increased over the timeline. There was no effect of time on the RF or RH ($p = 0.50$ and $p = 0.074$, respectively, Figure 59), and no discernible pattern to their trends.

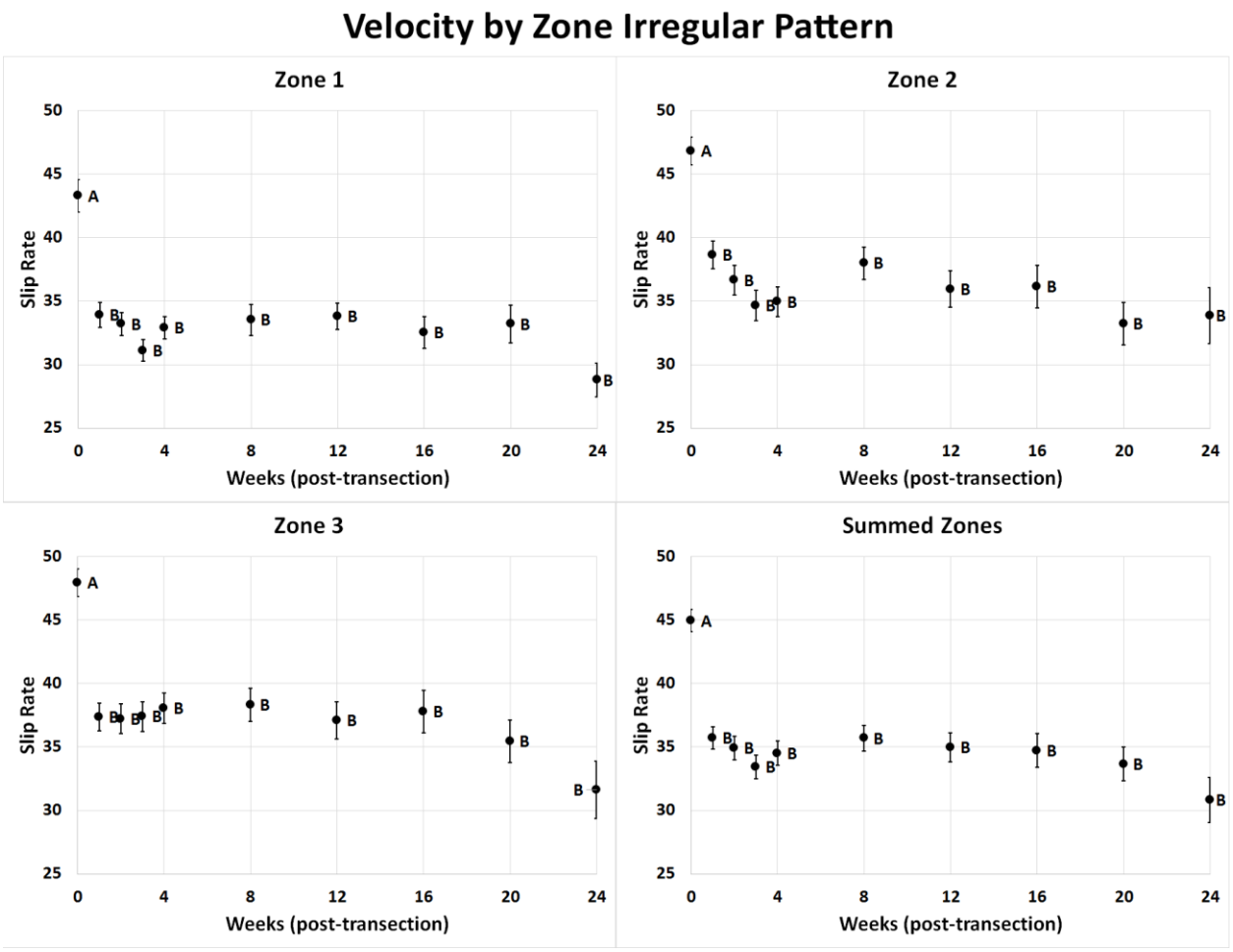

Figure 55: Variation in SL velocity (by zone and pattern) over time for CP recovery study.
Time affected velocity in all zones ($p < 0.0001$ for all). However, velocity decreased sharply immediately after transection-coaptation surgery but failed to change significantly over the remainder of the experimental time frame. Letters represent distinct groups based on Tukey's HSD test (groups not connected by the same letter are significantly distinct). Data shown are the mean and standard error (SEM).

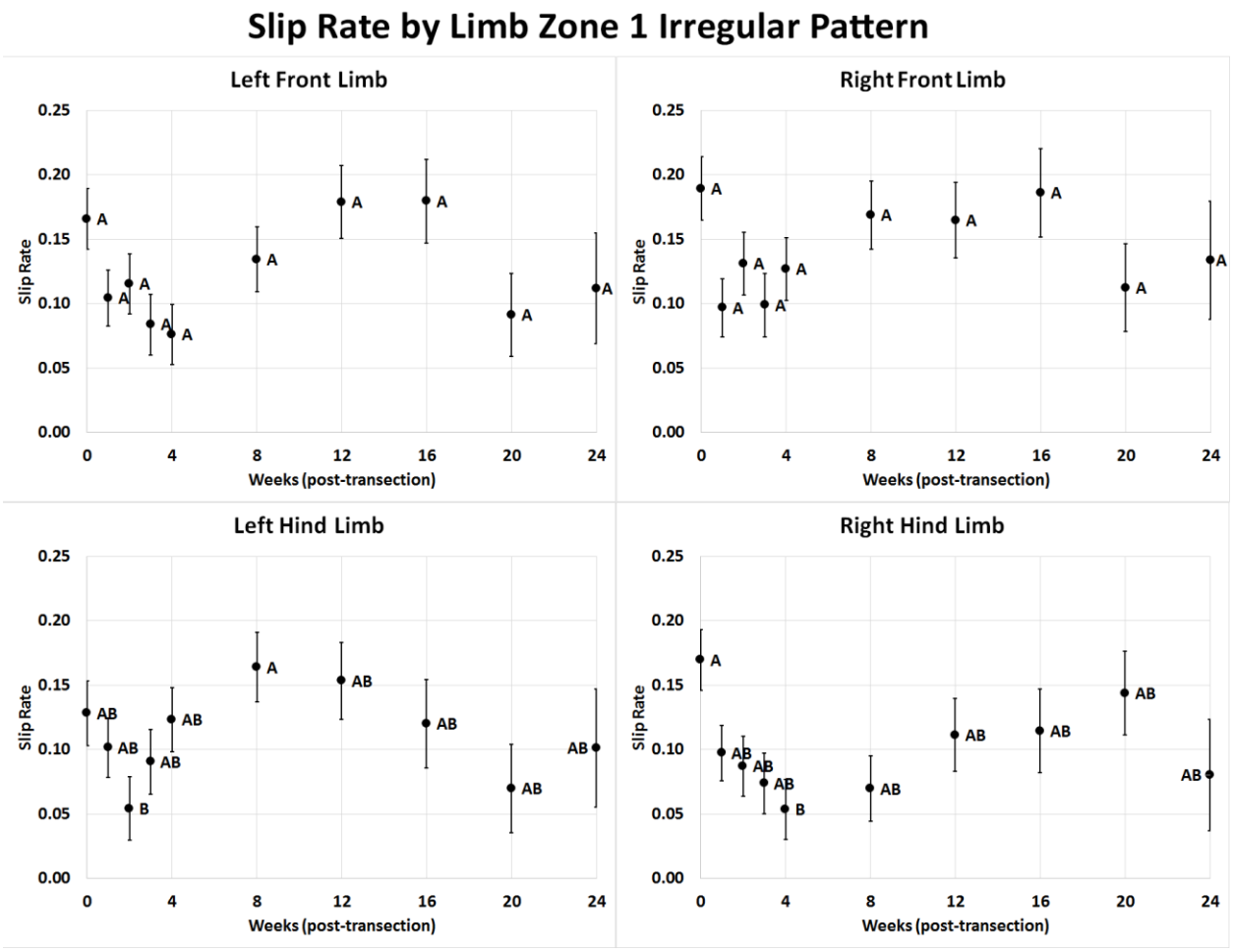

Figure 56: Zone 1 SR (by limb and pattern) for CP functional recovery study.
There was no effect of time on RF or LH SR (p = 0.067 and 0.059, respectively). However, time did have an effect on LF and RH SR (p = 0.012 and 0.026, respectively). Letters represent distinct groups based on Tukey's HSD test (groups not connected by the same letter are significantly distinct). Data shown are the mean and standard error (SEM).

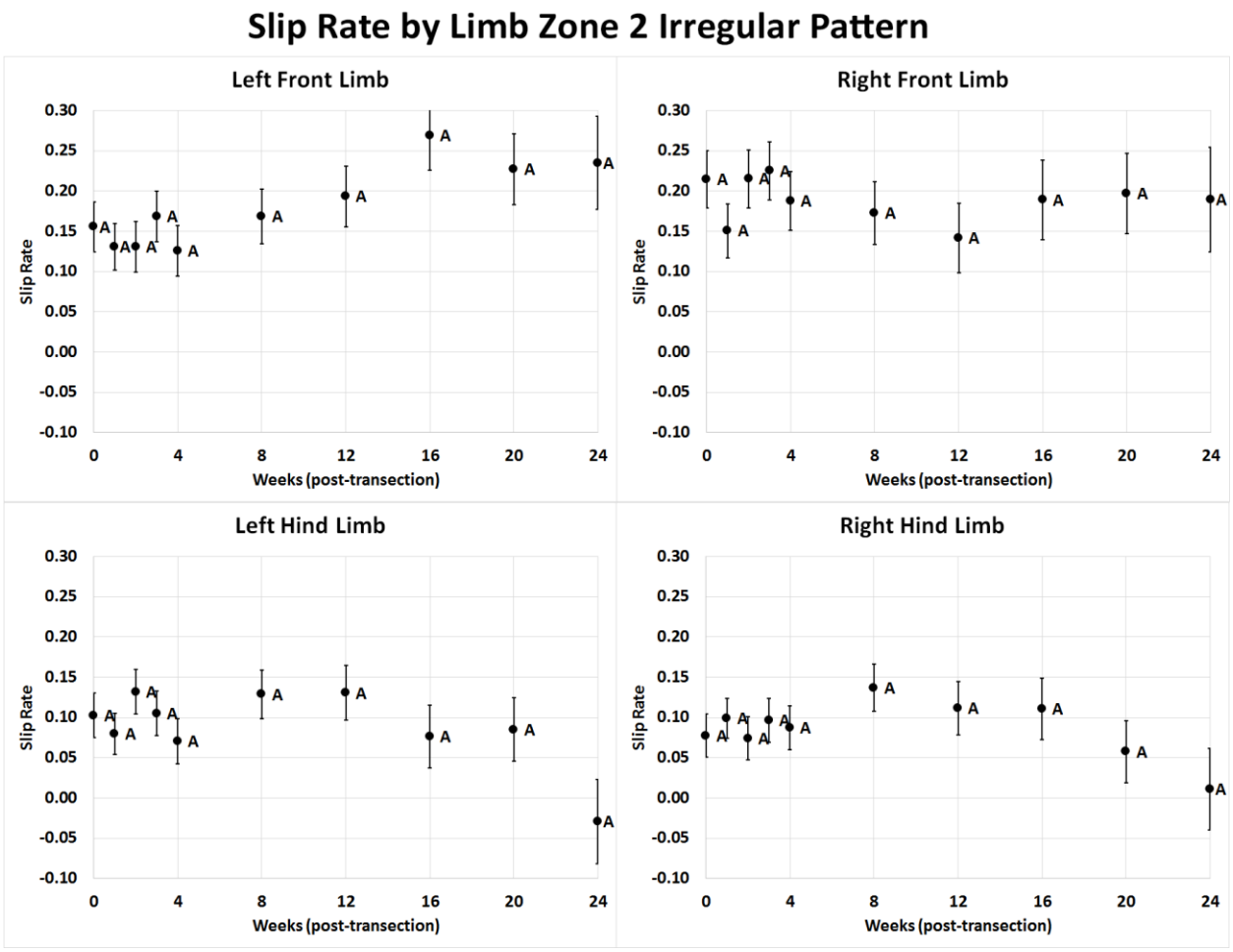

Figure 57: Zone 2 SR (by limb and pattern) for CP functional recovery study.
There was no significant effect of time on SR for any limb (RF, p = 0.74; LF, p = 0.11; RH, p = 0.57; LH, p = 0.22), though the forelimb SR trended towards an increase and hindlimb SR trended toward a decrease over the experimental time frame. Letters represent distinct groups based on Tukey's HSD test (groups not connected by the same letter are significantly distinct). Data shown are the mean and standard error (SEM).

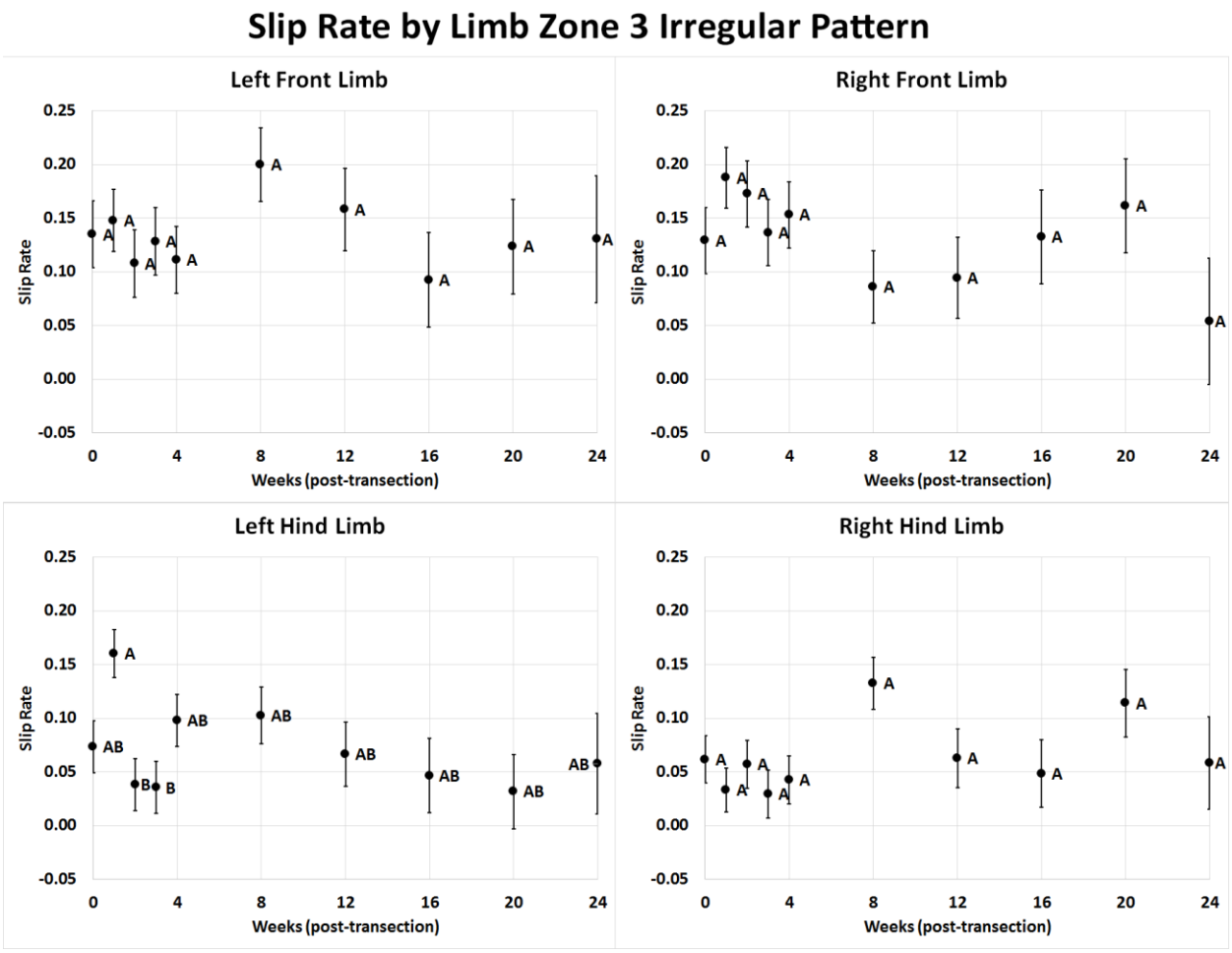

Figure 58: Zone 3 SR (by limb and pattern) for CP functional recovery study.
Time had a significant effect on the LH SR (p = 0.0052) but SR of all other limbs were not significantly affected (RF, p = 0.27; LF, p = 0.62; RH, p = 0.062). Letters represent distinct groups based on Tukey's HSD test (groups not connected by the same letter are significantly distinct). Data shown are the mean and standard error (SEM).

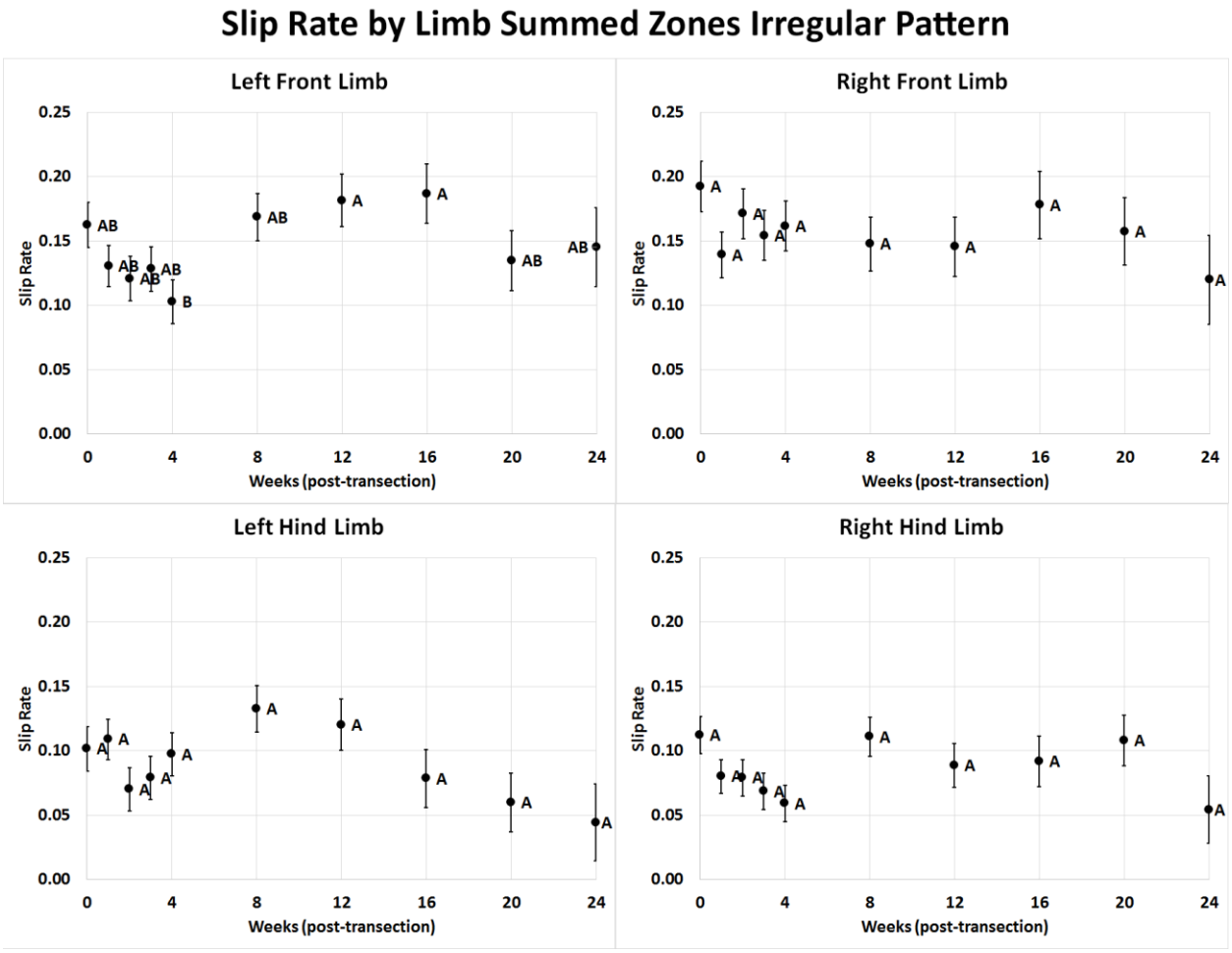

Figure 59: Combined zones SR (by limb and pattern) for CP functional recovery study.
The SR for the LF and LH were significantly affected by time (p = 0.0074 and 0.026, respectively) but RF and RH SR were not significantly affected (p = 0.50 and 0.074, respectively). Letters represent distinct groups based on Tukey's HSD test (groups not connected by the same letter are significantly distinct). Data shown are the mean and standard error (SEM).

Motor Neuron Counts

Comparison of Counting Methods

Comparing the number of labeled motor neurons (MN) counted using either a semi-automated algorithm (Volocity, PerkinElmer, Waltham, MA) or manual counting, repeatability was high, with low bias between methods (Table 6, Figure 60). The trend toward increasingly larger counts using the software algorithm as MN counts increased was significant ($p = 0.005$).

Table 6: Comparison of MN counting methods (semi-automated vs. manual) for PFI study.
The mean and SE of the labeled MN counts, with the mean and SE of the difference between the counts achieved through semi-automated and manual counting methods and the trend toward bias between methods.

	N	Mean	SE	Mean Diff	SE of Mean Diff	Trend Toward Bias
MN Count	25	887.88	75.83	-187.76	87.82	0.005

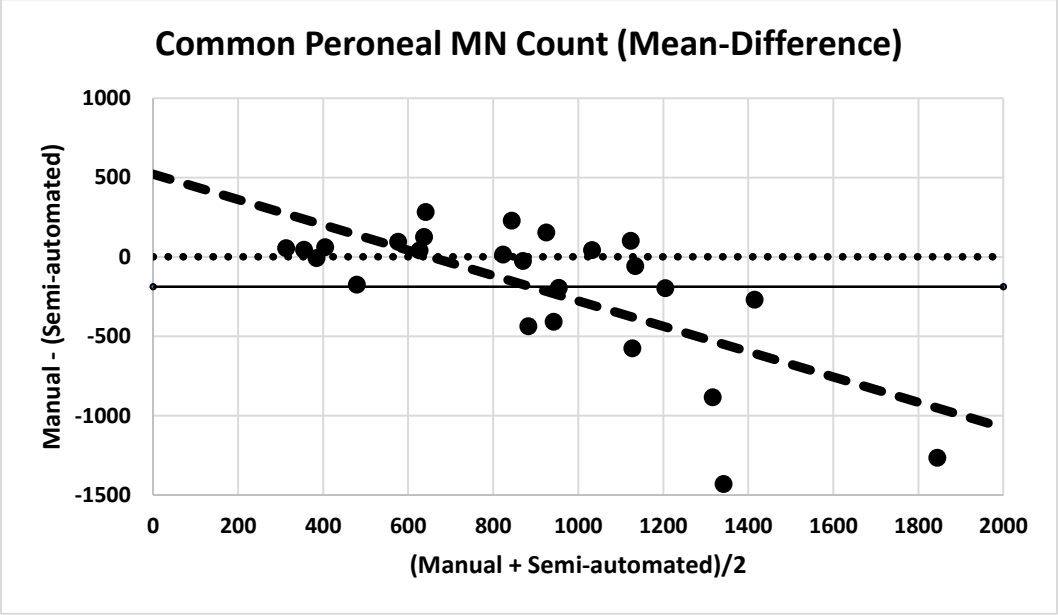

Figure 60: Mean-Difference plots for CP functional recovery MN counts.
Semi-automated counting trends toward increased counts as the population increases in size. Mean count (solid horizontal line), limits of agreement (± 1.96 x SD, paired horizontal dashed lines), and trend toward bias (fit dashed line) for sciatic nerve MN cell bodies.

Motor Neuron Count as a Function of Time

Time did not have a significant effect on MN counts over time (p = 0.061, ANOVA, Figure 61). However, the trends appear as expected with a sharp decrease in counts at week 1 following surgical transection-coaptation followed by a trend of increasing mean counts as recovery proceeded over the experimental timeline (Figure 61).

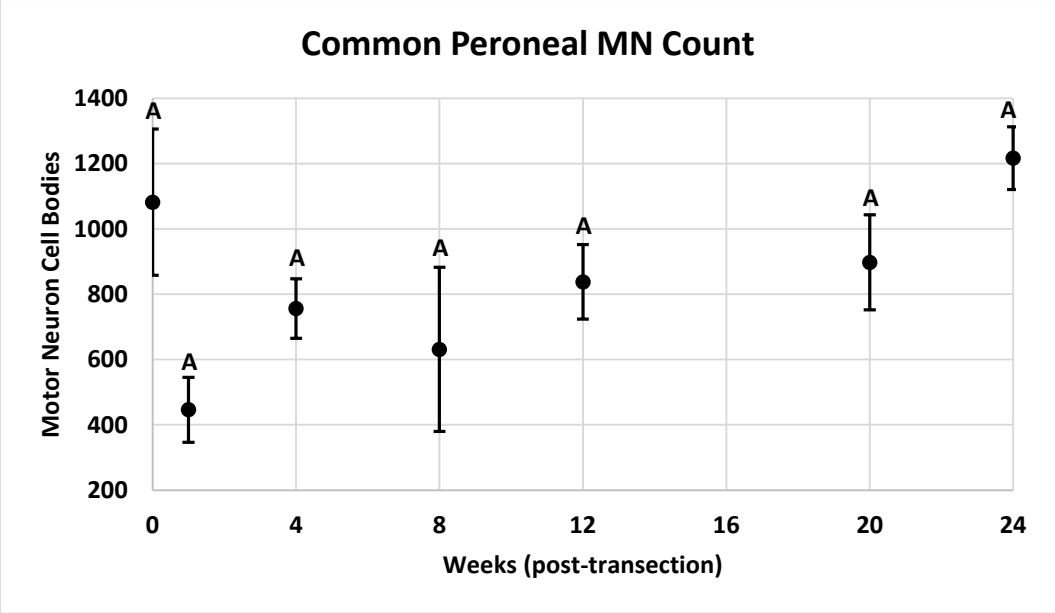

Figure 61: Variation of CP functional recovery MN count over time.
Trends appear as expected for MN count, with a decrease in counts at week 1 post transection-coaptation and a trend towards increased counts over the experimental timeline. However, there was no significant difference in counts, likely due to the large error in the week 0 and week 8 counts. Letters represent distinct groups based on Tukey's HSD test (groups not connected by the same letter are significantly distinct). Data shown are the mean and standard error (SEM).

Peroneal Function Index and Toe Spread Factor as Functions of Motor Neuron Count

There were no significant relationships between motor neuron (MN) count and PFI calculated using the BMH method (BMH PFI, $p = 0.51$, Figure 62), PFI calculated using the variant method (E (variant) PFI, $p = 0.39$, Figure 62), or in the contralateral (right) limb PFI calculated using the variant method (C (variant) PFI, $p = 0.98$, Figure 62). Similarly, no significant relationships were found between MN count and stationary TSF calculated using the BMH method (BMH TSF, $p = 0.74$, Figure 62), stationary TSF calculated using the variant method (E (variant) TSF, $p = 0.52$, Figure 62), or in the right limb stationary TSF calculated using the variant method (C (variant) TSF, $p = 0.56$, Figure 62). Interestingly, the PFI and the variant PFI for the experimental (left) limb showed trends toward negative correlations between MN count and function. The contralateral (right) week 0 index showed no discernible trend at all between MN count and function. All of the stationary TSF indices had trends toward a positive correlation with MN count.

Similarly, there were no significant relationships between motor neuron (MN) count and PFI calculated using any of the three new models (Model 1, 7 factors: $p = 0.25$; Model 2, 5 factors: $p = 0.28$; Model 3, 4 factors: $p = 0.29$, Figure 63). However, in contrast to the established method of calculating PFI, all three models showed positively trending relationships.

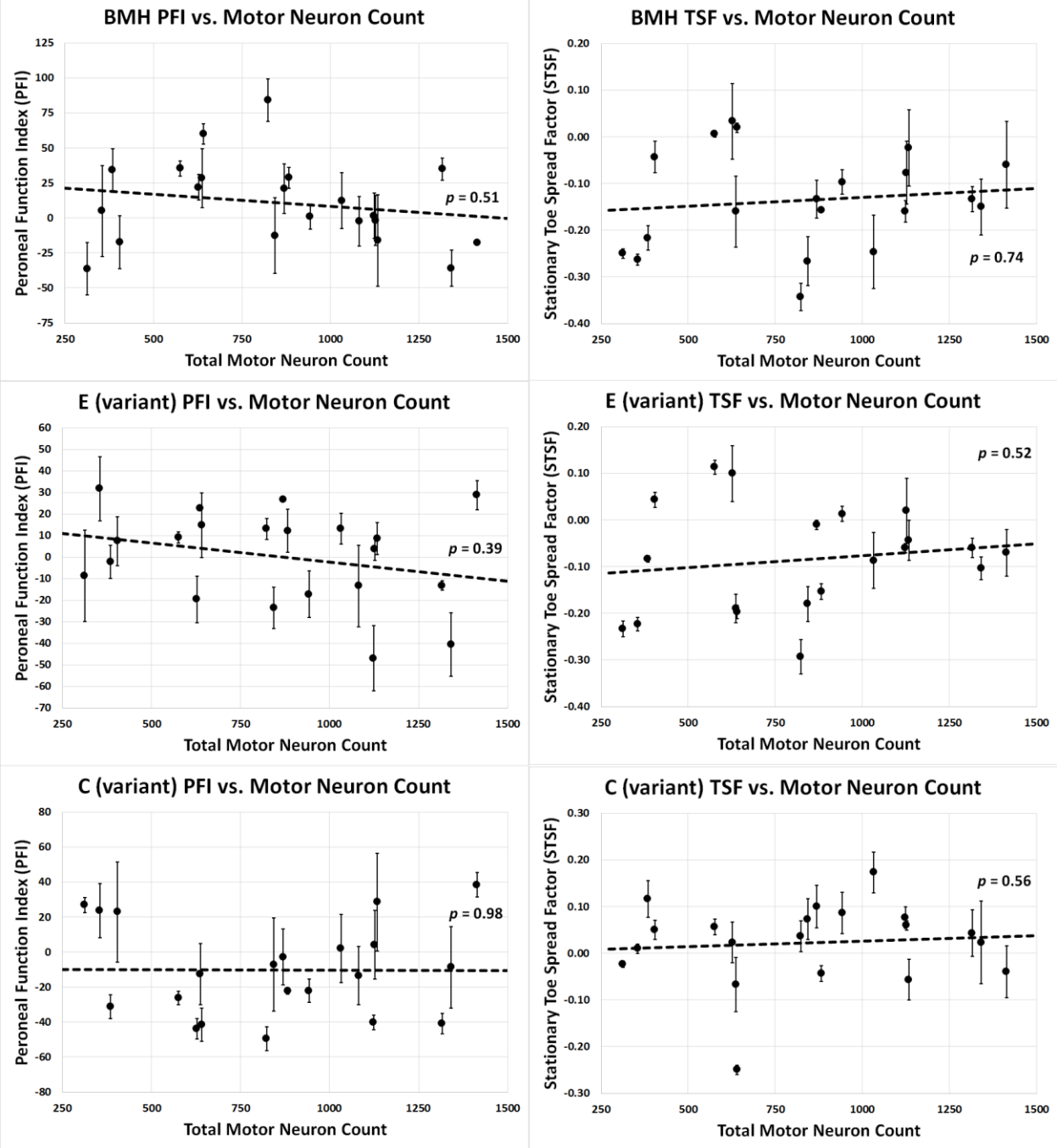

Figure 62: Variation in PFI and TSF as functions of MN count for CP functional recovery study.
No significant relationships were found between MN counts and PFI or TSF for either limb using either of the calculation methods. Interestingly, the SFI and the variant SFI for the experimental limb showed negative correlation trends between MN count and function. The C (variant) PFI showed no discernible trend at all between MN count and function. All TSF indices had trends toward a positive correlation with MN count. Data shown are the mean indices and standard error of those means (SEM).

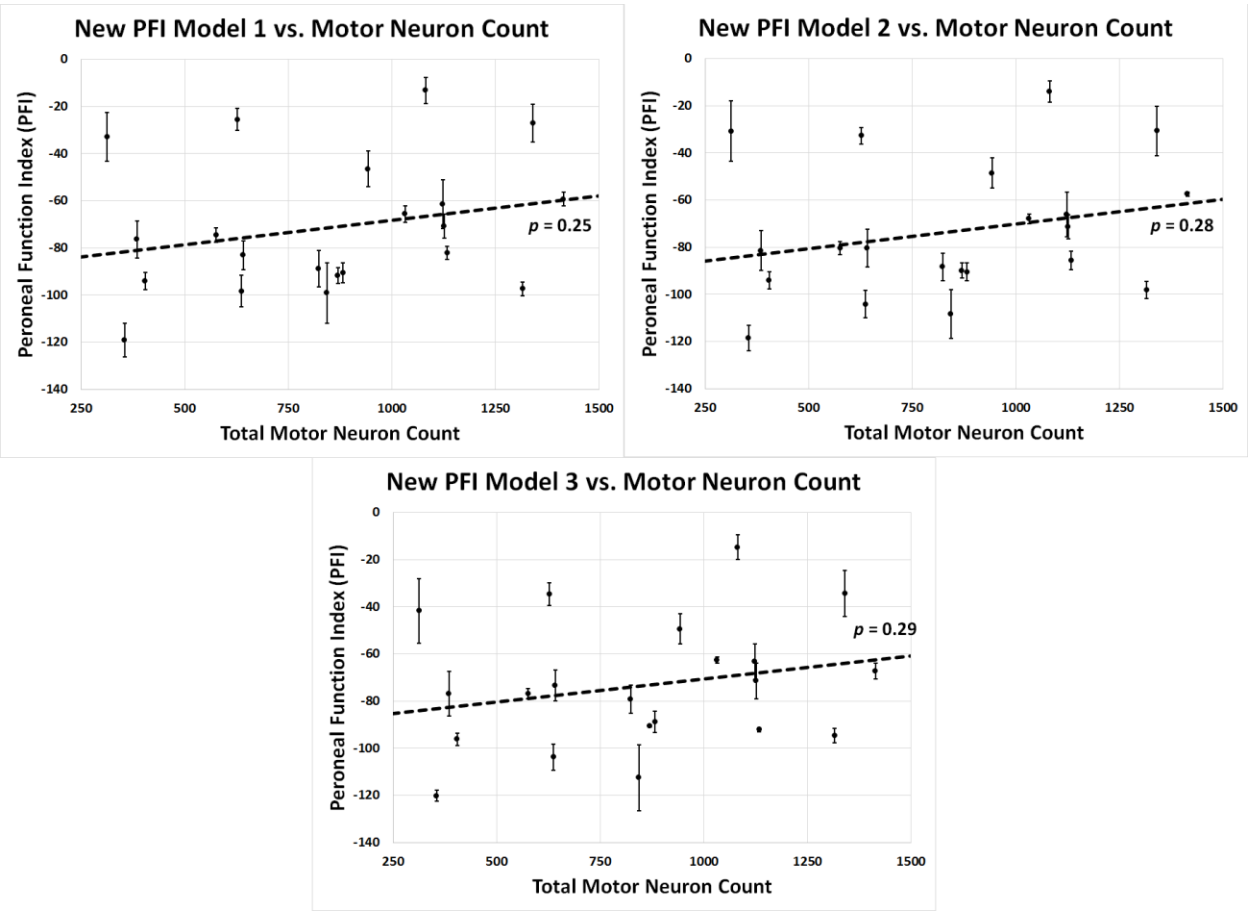

Figure 63: Variation in new PFI models as functions of MN count for CP functional recovery study.
All three of the new PFI models showed positive trends but no significant relationships were found between MN counts and the models. Data shown are the mean indices and standard error of those means (SEM).

Skilled Locomotion Slip Rate as a Function of Motor Neuron Count

The mean SR calculated using all zones summed together and using fixed effect modeling (as previously described) was not found to be significantly related to total MN counts for any limb (RF, p = 0.85; LF, p = 0.57; RH, p = 0.63; LH, p = 0.064, data shown only for LH: Figure 64). While not found to be significant, a negative trend existed that was similar to that observed in the sciatic nerve functional recovery study, where SR tended to decrease as MN counts increased.

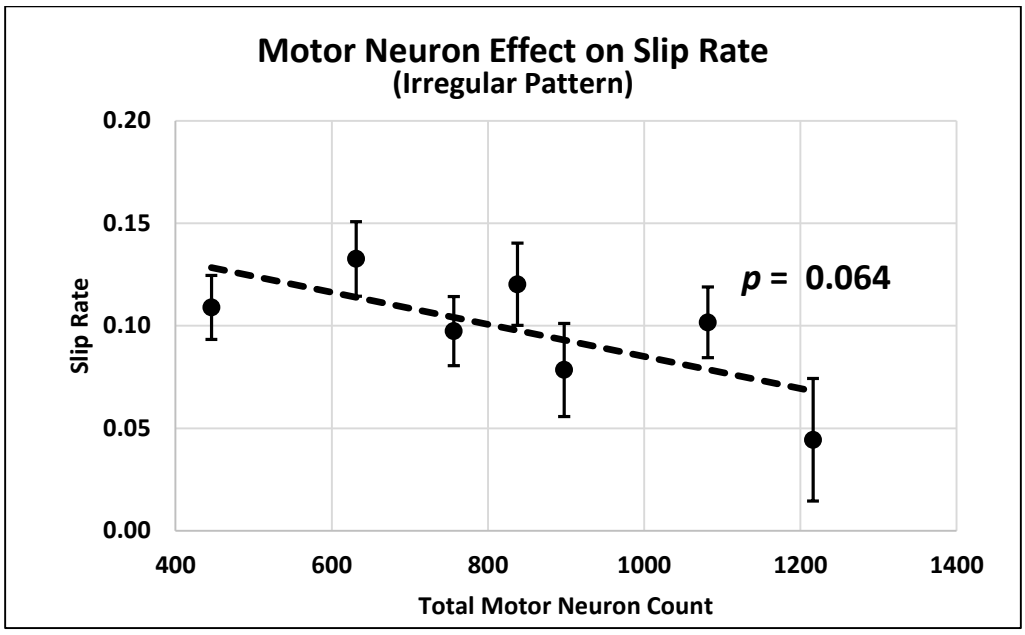

Figure 64: Variation in left hindlimb SR as a function of MN count for the CP study. While not significant, a negative trend existed between LH SR and total MN count, with SR decreasing as motor neurons increased.

Discussion and Conclusions

Sciatic Function Index

Footprint analysis has been used for a considerable period of time (since at least 1979[68]) to attempt to describe the function of the nerves that are required for making those footprints. As previously mentioned, the rat sciatic nerve regeneration model, in general, and the sciatic function index (SFI), in particular, is fairly ubiquitous in the literature with regard to peripheral nerve regeneration research[81,54,86,85,87–91,77,79,80,78,82,83,43,84]. There is no question that the work of researchers such as Hruska, de Medinaceli, Carlton, and Bain-Mackinnon-Hunter has contributed enormously to our understanding of functional recovery of peripheral nerve injuries. However, a variety of problems have plagued walking track analysis as a method of assessing functional recovery since its inception. These include failures to make readable tracks (due to print smearing, trail dragging, or other contamination[58,93,94] or as a result of anatomic changes following injury such as autotomy[92] or contractures[95]), pausing of the subject in a trial[96], weight gain, rat strain used[60], and non-selective innervation as a result of axonal misdirection[52] (especially in nerves with mixed fascicular populations, such as the sciatic nerve).

Despite the problems presented with walking track analysis to date, our calculated SFI results are very similar to those observed in the literature[58–60,20], showing roughly a 20% recovery over 16 weeks following nerve transection and coaptation (Figure 20). Even the interobserver repeatability within our lab was high with a low bias (Table 2), which matches previous observations that intra-institutional repeatability is typically high[20]. In addition, the results of our data were consistent whether we used the empirical de Medinaceli equation or the equation derived by BMH through multiple linear regression (Figure 20), though only the BMH equation differentiated between post-surgical groups.

Despite these observations, deeper analysis of the data underlying the calculated index did not agree with the results that we expected or observed in our calculated indices. For example, examination of our raw measurements from which the SFI is derived via ANOVA revealed that time had a significant effect on TS, IT, and TOF for the experimental limb (Figure 14). However, raw PL was not significantly affected by time. Further inspection of the data showed that though TS and IT were significantly different

between pre- and post-surgical groups, the post-surgical groups themselves could not be differentiated. In addition, 'factors' calculated for these raw measurements, using the traditional method of using the contralateral limb measurements to normalize experimental limb measurements, did not change this observation. PL factor was not significantly different over time, and TS and IT post-surgical groups were statistically the same (Figure 17). TOF, therefore, and its derived factor were the only measured parameters that statistically showed change over the entire course of the experiment. This is exactly the opposite result that we would expect given that BMH previously reported that TOF measurements were highly variable and did not contribute significantly to their regression equation[59]. In fact, the TOF measurement is not included in the BMH equation for SFI as a result of this determination, whereas our data suggest that PL is not a significant component, and TS and IT are barely so.

In addition, we also observed significant differences over time in contralateral limb IT and TOF, both between pre- and post-surgical groups and within post-surgical groups alone. This is in direct conflict with the both authors' reports that no significant differences were found in the contralateral limb measurements over time[58,59]. However, others have reported that there are indications of compensatory changes in the contralateral limb prints as a result of nerve injury, specifically in Sprague-Dawley rats[60]. Our data are supportive of this observation. This is a very strong argument against the use of contralateral limb print measurements as a basis for normalization. Therefore, we calculated new 'factors' based on week 0 average measurements.

These new 'factors' were calculated for each of the four original de Medinaceli SFI parameters (PL, TS, IT, and TOF). Pre-operative (time 0) averages of our PL, TS, IT, and TOF measurements were very consistent with very small variation for both the experimental and contralateral limbs. Furthermore, the week 0 measurements taken for the peroneal functional recovery group was similarly consistent, with only tiny variation (both studies are summarized in Figure 16). One advantage presented by this method of normalization was that contralateral limb measurements can be normalized against their pre-surgical measurements, as well, in order to detect changes in contralateral limb measures over time. Interestingly, normalization of experimental limb measurements at each time point with averaged week 0 experimental

limb measurements still did not reveal significant differences over time for PL or between post-surgical groups for TS and IT (Figure 18). Therefore, TOF remained the only factor to be significantly affected by time over the whole experimental time frame. This method of normalization did, however, reveal significant variation over time for contralateral limb IT and TOF (Figure 19).

Interestingly, the calculated SFI using the time 0 normalized factors performed similarly to the de Medinaceli SFI. There was a significant difference between pre-surgical and post-surgical time points using both methods but neither method differentiated between post-surgical time points. In contrast, the traditional BMH SFI (with contralateral limb normalized factors) was the only method that differentiated between post-surgical time points. A SFI was calculated for the contralateral limb, however, using the BMH equation and time 0 normalized contralateral limb measurements. This calculated index also showed significant differences between both pre- and post-surgical time points (Figure 20). In fact, it showed a relatively steady, if small, decline in function. Perhaps, as the rat comes to rely on its contralateral limb, there are changes that develop over time as a result of bearing more weight. This explicitly shows that contralateral limb changes are significant, and the BMH equation does not factor in TOF, which was the most reliably and significantly changed factor for either limb.

It is worth mentioning that, though other authors have also suggested SFI is not a reliable test of functional recovery because it does not account for velocity[92,105,104], our data clearly show that the velocity at which rats traversed the short distance used to measure SFI in the corridor apparatus did not vary over the experimental time frame (Figure 17).

Finally, we also had difficulty with autotomy in our experimental rats, losing 7 out of 24 total rats intended for the sciatic functional recovery study, despite the use of a bittering agent to deter chewing. As other authors have mentioned, this is a particularly common, although it apparently can be largely avoided if Lewis rats are used[113,114].

In summary, despite numerous differences in our experimental data from our expectations, the SFI as defined by BMH appears to have been successful. However, amongst other previously described problems, we have described a number of issues not previously considered. It is apparent from our data

that consideration of the contralateral limb and its changes over time are fundamental aspects of devising a complete functional index, at least for use in Sprague-Dawley rats. The variation in contralateral limb print measurements, taken together with the very consistent time 0 averages for all rats in this study are strong arguments for the use of pre-operative (week 0) average measurements to normalize experimental measurements instead of using the contralateral measurements, as has been done historically. This method would also allow observation of the changes in the contralateral limb and the inclusion of these variations in a more appropriate index. Ultimately, it seems that a new and more appropriate SFI should be devised using these alterations.

Common Peroneal Function Index

Peroneal function index is far less common in the literature, and while the couple of papers that include PFI show reasonable results[73,59,60,78,98,99], they often are accompanied by complaints regarding the difficulty obtaining reasonable prints, especially in the early stages of the experiment (soon after initial surgery). In fact, BMH stresses the use of stationary TS factor in lieu of PFI in the early weeks following surgery specifically because of this problem. While the literature does not reveal it, the author has heard (in personal communications) of other laboratories that have had difficulty getting PFI to 'work' at all.

In contrast to the results of the sciatic functional study (in terms of walking track analysis), our results for calculated PFI were completely unlike any results found in the literature. In fact, our calculated PFI (using the BMH equation) suggested that there was *improvement* in function immediately following surgery, that then decreased over the experimental time frame (Figure 49). The high repeatability between methods with a low bias suggested that digital method was acceptable for measurement but also verified that our measurements were probably not the root of the problem.

The BMH PFI equation is even more stripped down than the SFI equation, making use of only PL and TS. Analysis of our data revealed that there was a large variation in PL in the experimental limb over time (close to 1 cm). In comparison, in the sciatic functional recovery study PL varied by less than 0.5 cm. Additionally, TS decreased significantly immediately following surgery, but post-surgical groups could not be differentiated from each other. Furthermore, the 'factors' calculated from the raw

measurements showed that PL factor varied by approximately 0.35, and that the TS 'factor', like its raw measurement, only differentiated between pre- and post-surgical groups (Figure 41). The variation in PL was likely overpowering (mathematically) the relatively minor and insignificant contributions of TS in the BMH PFI computation.

Somewhat by accident, our PFI data was then processed through the BMH SFI equation (instead of the PFI equation). The results appeared astonishingly similar to our expectations, and nothing at all like our PFI results (not shown). As a result of this, and given the problems we had already observed in our examination of the SFI, we decided the most prudent course of action would be development of a new PFI. However, we first wanted to characterize some of the changes we had already thought about while analyzing the sciatic functional recovery study.

For example, as in their SFI calculations, BMH used the contralateral limb measurements to normalize the experimental limb measurements. However, our data revealed that there were significant differences between pre- and post-surgical groups and among post-surgical groups in contralateral limb PL, IT, and TOF. Therefore, we also normalized our experimental measurements for PFI using averaged time 0 component measurements to create variant 'factors'. As previously mentioned, the time 0 measurements for the common peroneal functional recovery study and sciatic functional recovery study were both very consistent with very small variation (Figure 16). As in the sciatic functional recovery study, there was generally smaller error within groups for the week 0 normalized 'factors'. However, there were also dramatic differences in the 'factors' themselves (compare Figure 41 and Figure 42). Primarily, the size of the PL and TOF 'factors' significantly decreased, although the significant differences in post-surgical IT were also lost. In addition, analysis of changes to the contralateral limb 'factors' was possible. Interestingly, only the contralateral IT 'factor' was significantly affected by time.

BMH also mentioned print angle (PA) and TOF when analyzing their data for their SFI, PFI and TFI[59] but they declined to include them in any of their formulae claiming that they were too variable and/or insignificant. De Medinaceli et al. also mentioned 'width between feet' that they rejected due to high variability[58]. In our common peroneal functional recovery study, as with the sciatic functional

recovery study, the TOF was significantly affected by time for the contralateral as well as the experimental limb (Figure 34). Furthermore, the calculated 'factors' for TOF were also significantly affected by time, both using the contralateral limb normalization (Figure 41) and week 0 normalization (Figure 42). Given the surprising contributions of TOF thus far, we decided to look at DA and SW. Both DA and SW were shown to be significantly affected by time in the experimental limb and differentiated both pre- and post-surgical groups (Figure 35). SW in the contralateral limb was similarly significantly affected by time. Contralateral limb DA was not affected by time.

Finally, we were concerned about the fundamental method by which all measurements were taken by previous authors. De Medinaceli and BMH both describe in their methods that for each trial the longest measurement of each parameter was recorded for the trial[58,59]. When considering the practical application of footprint measurement as a marker of anatomic and physiologic function, this does not make sense for all parameters. Furthermore, each of these factors should be considered in reference to the nerve being 'tested'. In this case, the common peroneal nerve is responsible for tarsal flexion and digital extension. Therefore, increases in TS and IT would certainly represent an increase in function. However, longer PL does not necessarily have the same representation, since rats do not prefer to drop their hocks naturally. Therefore, a longer PL would indicate loss of function, rather than a gain. Furthermore, taking the maximum measurement may mask the effects of smaller parameters, as seems to be the case in the BMH PFI calculations. Taking the longest measurement (or even the shortest measurement) does not accurately represent how the rat's limb is typically working. The gold standard for assessing the 'usual' function of things is generally assessed by looking at the average function. Therefore, we calculated average measurements for each trial (using the digitized prints).

Using average measurements for each trial, all parameters (PL, TS, IT, TOF, DA, and SW) were significantly affected by time in the experimental limb (Figure 37 and Figure 38). Furthermore, in each case time 0 measurements were significantly different from those at post-operative time points and post-operative time points were significantly different from each other. Similarly, in the contralateral limb, PL and SW were significantly different, both pre- and post-operatively (Figure 37 and Figure 38). Other

measurements were not significantly affected by time in the contralateral limb. Week 0 averages derived from the trial averaged measurements were very consistent, with small variations, consistent with the pattern observed for trial maximums (Figure 39 and Figure 40). 'Factors' calculated from the trial averaged measurements, using week 0 normalization, revealed that PL, TS, IT, TOF, SW, and DA were significantly affected by time both pre- and post-operatively (Figure 45 and Figure 47). For the contralateral limb, PL and SW were significantly affected by time both pre- and post-operatively (Figure 46 and Figure 48). TS, IT, TOF, and DA were not significantly affected by time. In general, the use of trial average measurements resulted in groups with less error. Often groups that were not significantly different for trial maximum data became significant (e.g. post-surgical experimental limb TS and IT, contralateral limb PL, TS and IT 'factors' for the experimental limb, etc.).

Velocity was analyzed and found to be significantly affected by time, both pre- and post-operatively (Figure 36). Therefore, unlike SFI, velocity must be considered when deriving a new functional index for peroneal functional recovery.

Multiple linear regression was performed on the trial averaged week 0 normalized factors. Velocity was included and subject # was included as a random effect. Ultimately, three different models were generated based on various levels of significance of the contributing factors (Figure 51). We prefer Model 2, as it uses measurements from both the experimental and contralateral limbs, yet has a very tight significance requirement (all factors have p-value < 0.005). The results of all three models, along with our calculated BMH PFI, are shown in Figure 52. They appear as expected for a typical functional recovery index, and are all very similar in appearance and exact in significant differences between groups. There is a significant loss of function post-operatively for all models that reaches its nadir at week 3 post-operatively. There is a gradual increase among significantly distinguishable groups throughout the remainder of the experimental time frame, with an ultimate recovery of 40-50% (model dependent) within the confines of the experimental time frame. Finally, none of the models used velocity as its effect within each model was not significant enough to include it.

In summary, we found that the BMH PFI cannot be appropriately used in Sprague-Dawley rats with common peroneal transection injury. Problems with poor print production and contracture are reported. However, we found that over-emphasis of PL and a failure to include other factors such as TOF and DA to be more representative of the problems with this index. In addition, we used week 0 averages to normalize our factors, an approach we feel is superior to contralateral limb normalization due to changes in the contralateral limb prints following injury. It remains to be seen whether this is true in all strains of rat. Additionally, we used averaged component measurements within trials rather than trial maximums. We feel this method is superior because it decreases error within groups and does not mask the effects of smaller parameters. Finally, based on our data, SW and velocity do not appear to have significant enough effects to be included in a model of PFI. As a result of our analysis, we have presented three models for the calculation of PFI from walking tracks.

Stationary Toe Spread Factor

For the sciatic functional recovery study, the stationary toe spread raw measurements were significantly affected by time for both the experimental and contralateral limbs (Figure 21). However, the calculated stationary TS factor, whether normalized using contralateral limb measurements or week 0 average measurements, did not reliably show recovery of function over the entire experimental time frame (Figure 22). It did show a significant decrease at 1 and 4 weeks post-operatively, which then increased at week 8. However, over the last 8 week of the experiment, it decreased again to the lowest level (the same as at 4 weeks post-operatively). Therefore, it does not represent a reliable means of estimating recovery in a sciatic transection model in Sprague-Dawley rats.

For the common peroneal functional recovery study, the stationary toe spread measurements were significantly affected by time, both in pre- and post-surgical groups, only in the experimental limb (Figure 53). The calculated stationary TS factor showed a significant decrease that reached its lowest level at week 3, followed by a gradual increase over the experimental time frame, with a maximum at 20 weeks post-operatively (Figure 54). The pattern was similar for factors calculated with contralateral limb normalization and factors calculated with week 0 normalization, though the initial decrease was less

dramatic in week 0 normalized factors. The recovery was approximately the same, so week 0 normalized factors showed recovery that was closer to pre-operative levels. This may be an effective method of estimating recovery of function for common peroneal transection in Sprague-Dawley rats. However, the estimated recovery was approximately 70-80% (depending on normalization method) and therefore represented the highest estimation of recovery of all the methods tested.

Skilled Locomotion Over a Ladder

In the sciatic recovery study, both regular and randomized irregular patterns were used to assess slip rates of rats recovering from sciatic nerve transection-coaptation. Both patterns produced similar results (Figure 24 through Figure 27). However, the randomized irregular patterns seem to be more sensitive. For example, on the regular pattern, significant differences over time were detected in the left hind limb in zone 1 and 3, and both the right and left hind limbs in zone 2 and when all zones were combined. In contrast, on the randomized irregular patterns, significant differences over time were detected in the left hind and right front limbs in zone 1, in both hind limbs and the right front in zone 2, and in all limbs in zone 3 and when all zones were combined. We selected the left hind limb for further analysis because, interestingly, all other significantly affected limbs showed progressive improvement (decrease in slip rate) following surgery with no preceding loss of ability (increase in slip rate).

For both studies (and on both pattern types for the sciatic functional recovery study), velocity was significantly affected by time (Figure 23 and Figure 55). In all cases, there was a dramatic decrease in velocity at week 1, immediately following transection-coaptation surgery. Interestingly, there was no significant differentiation between post-surgical groups for either study or on either ladder pattern. Taken together with the decreasing slip rates in all limbs other than the left hind limb, and that velocity on the randomized irregular patterns were generally slower, this presents an interesting argument that Sprague-Dawley rats slow down and step more carefully when presented with difficult terrain and/or significant injury to one of their limbs. It also adds some credibility to the rapid increase in slip rate in the left hind limb immediately after surgery followed by a slow decrease over time. However, it may also represent a confounding factor in this method since it is difficult to determine how much of the decrease in slip rate

over time is due to recovery and how much is due simply to increased care in limb placement. In order to account for velocity, slip rates were modeled using velocity and week as fixed effects and subject number as a random effect in both studies.

For the sciatic functional recovery study, this method suggested the highest level of recovery of all the methods (approximately 43% on the regular pattern and approximately 41% on the randomized irregular pattern). This may be a result of the increased care with which the rats learned to traverse the ladders over time. For the common peroneal functional recovery study, the left hind limb varied significantly in zone 1 and zone 3 but not zone 2 or when all zones were combined (Figure 56 through Figure 59). The only other limb that varied significantly was the right hind limb, and then only in zone 1. Apparently, skilled locomotion across a ladder with randomly assigned irregular rung patterns is not an effective way to estimate functional recovery in Sprague-Dawley rats recovering from common peroneal transection-coaptation.

Retrograde Labeled Motor Neuron Counts

For both the sciatic functional recovery study and the common peroneal functional recovery study, the repeatability was high between manual and semi-automated (using Volocity® software) counting methods. However, in both studies there was a bias towards higher counts using the semi-automated method than the manual method as total motor neuron counts got higher (Figure 29 and Figure 60). This indicates that, though the semi-automated method is a reasonable replacement for the manual method, the protocol for counting needs some improvement.

It is generally accepted that the sciatic nerve contains between 1600 and 2100 total MN (our mean was 3090 for normal rats), the tibial branch contains roughly 1000 MN (our mean was ~2000 for normal rats, 550 of which were double-labeled), and the common peroneal branch contains approximately 600-650 (our mean for the sciatic functional recovery study was ~1630 for normal rats, 550 of which were double-labeled)[115,116]. Absolute MN counts for time 0 (non-surgical rats) in the common peroneal functional recovery study are somewhat lower (1082 ± 224).

The trends displayed by the MN counts appear appropriate; MN counts decrease immediately following surgery (to near zero in the sciatic functional recovery study populations) and then increase as the nerve regenerates. However, these were only statistically significant for the sciatic functional recovery study (Figure 30 and Figure 61).

One troubling feature of the sciatic functional recovery study was that 17.8% of the total MN population of the non-surgical positive controls were double-labeled. This indicates that some error in our method resulted in the double-labeling and confounds interpretation regarding axonal misdirection. Therefore, no significance can be attached to double-labeling in the experimental groups.

For the sciatic functional recovery study, recovery of the sciatic nerve based on back-labeled motor neurons alone is estimated to be 61%. This is higher than even the highest of the estimations made by functional assessments (Skilled Locomotion; 41-43%). Motor neuron counts had a significant positive relationship with calculated SFI, calculated with either contralateral limb or time 0 normalized 'factors' (Figure 31). However, as expected, it had no relationship at all with calculated TSF. Finally, total MN counts had a negative relationship with skilled locomotion slip rates for the left hind limb when all zones were combined on both the regular and irregular patterns (Figure 32). These data provide further evidence of the appropriateness of these models for assessing functional recovery but provide no argument for which method is more accurate.

Due to the lack of significant differences in MN count groups, there was no significant relationship between MN counts and PFI (any method), stationary TS factor (any method), or skilled locomotion.

APPENDIX

Corridor

A corridor apparatus was designed and built specifically so that animals would be subjected to similar experimental conditions for assessment of both walking tracks and skilled locomotion (Figure 65). The corridor itself was constructed of polymethyl methacrylate (Plexiglas®, Ridout Plastics, San Diego, CA) and consisted of a platform (120 cm x 10cm) raised approximately 15 cm above the bench-top upon which the rats run, and walls that rise approximately 15 cm on either side and at each 'end' of the platform. At the 'start' end of the corridor was placed a hinged door that facilitates placing a rat into the apparatus. At the 'finish' end of the corridor a hole permits entry down a ramp into a 'dark box' (also composed of Plexiglas® but opaque black in color) that contains the rat's home cage. This particular arrangement allows the rat to travel downward, in the dark, to a region that has the safe and familiar scent of their ordinary living space. The cover for the 'dark box' was also hinged to facilitate removal of the rat between trials. Beneath the platform a sheet of mirrored Plexiglas® was positioned, angled at 45° to permit visualization and video recording of the underside of the rat in addition to the left side (and potentially the right side, though the right side was not recorded for this study).

Figure 65: Corridor apparatus with ladder insert.
The apparatus was composed entirely of Plexiglas® and included a hinged door at the 'start' end and an exit, down a ramp, into a dark box that contained the rat's home cage. Four photoreceptor sensors triggered events that recorded the timing of each trial and started and stopped video recording. The apparatus was well lit with 1000W of halogen light. The apparatus is shown here with a ladder insert that could be removed to facilitate walking track analysis trials.

Command, control and timing

Four photoreceptor sensors (M12 series polarized retroreflective, Banner Engineering Corp., Minneapolis, MN) were placed at adjustable intervals along the length of the corridor. These sensors were wired to a LED timer (CUB5T, Red Lion Controls, York, PA) and a 12-bit data acquisition device (USB-6008, National Instruments Corporation, Austin, TX) that relayed the photoreceptor trigger events to a PC. The LED timer was programmed to reset to 0 and initiate timing when the first sensor was triggered and to stop timing when the fourth sensor was triggered. The timer itself was placed behind the corridor apparatus in an enclosure assembled by KOM Automation (Liverpool, NY) so that visualization was possible below the mirror. The photoreceptor sensors broke the length of the corridor into three zones (zone 1 to 3 from right to left; Figure 66).

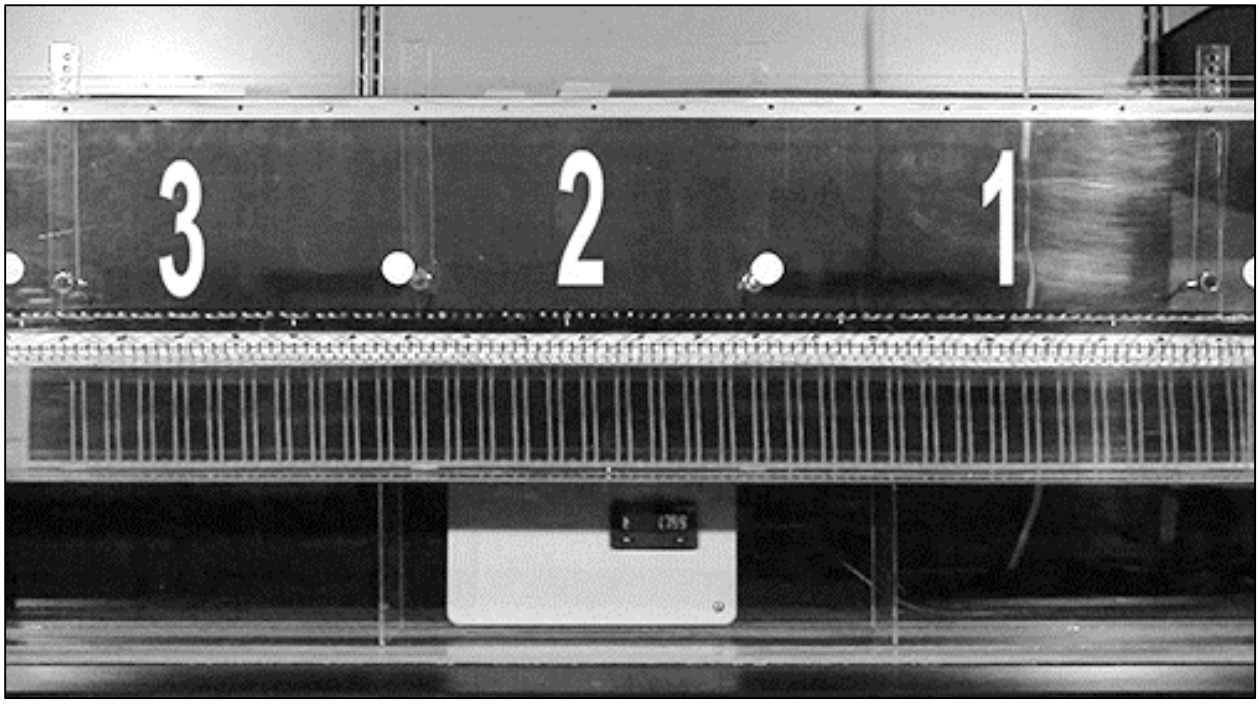

Figure 66: Typical view of video recording (with zones labeled).
This is the typical view through the camera that recorded video of each trial. Zones are shown in red numerals between the reflective dots used by the photoreceptors to trigger timing and video recording. The apparatus is shown here with the ladder insert and the 'regular' ladder pattern (two rungs in and one out, repeating). Also visible is a LED timer that corroborated the time recordings on the computer.

Custom software was written using Matlab® 2013 (Mathworks®, Natick, MA) to interpret the DAQ signals into time recordings on the PC as each of the photoreceptor sensors was triggered and to end recording when the last sensor was triggered (to avoid excess null video data). The photoreceptor sensors were placed at fixed intervals and, together with the time recordings, the software was able to calculate velocity in each of the three distinct zones created by the photoreceptor sensors.

Ladder insert

A specially constructed ladder insert was created to place inside the corridor for testing skilled locomotion. The walls of the ladder insert were also composed of Plexiglas®. The rungs were removable and composed of 1/8" (3 mm) diameter stainless steel wire (Speedy Metals, New Berlin, WI). The walls of the ladder were also 120 cm in length (the length of the corridor) but rungs were loaded only in the first 109 cm of the insert in order to allow the rat to step off the ladder before entering the 'dark box'. Holes for the rungs were spaced 1 cm apart.

As previously described by Metz and Winshaw[102], ladder rung arrangements were modified to test under two different conditions: one using a regular pattern of rungs and one using an irregular pattern of rungs. The 'regular pattern' (a simple repeating 'two rungs in and one rung out' pattern) was used to allow the rats to 'learn' the rung positions, whereas a randomized 'irregular' pattern was used as a means to remove the effects of pattern memorization.

For the 'irregular pattern' trials in our studies, the ladder was divided into five regions of 21 cm each. Five distinct irregular patterns were derived (Figure 67) so that, when placed end to end, no rat would ever be required to stretch further than 4 cm between rungs (no more than 3 empty rung-holes in a row). Given 5 possible positions, and 5 distinct irregular pattern segments, there were 120 possible permutations that would result in absolutely unique 109 cm long irregular ladder rung arrangements ('irregular' patterns). A random number generator was used to arrange these permutations into a randomly ordered list. For each group and at each time point, new irregular patterns were selected from this list, and no pattern was recycled.

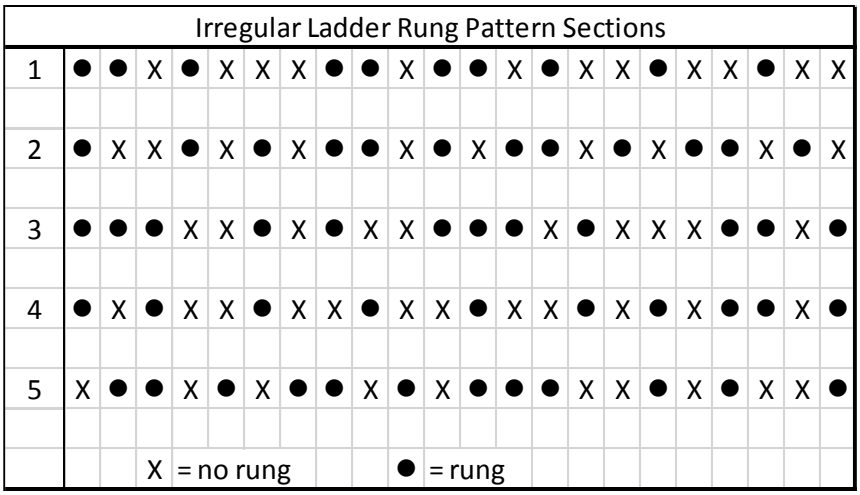

Figure 67: Irregular ladder rung pattern sections
The ladder was divided into five regions of 21 cm each, requiring that all 5 patterns be used in each trial. However, the five possible positions allowed for 120 possible combinations, thus allowing each study to proceed without repeating combinations.

Video recording

Video recording was accomplished using a Canon EOS Rebel T4i DSLR camera (Canon USA, Inc., Melville, NY) that was attached to the PC via universal serial bus (USB) and controlled by small C language programs [written using a software development kit (SDK) provided by Canon USA, Inc.] that were called by functions in the Matlab® program. Video was recorded at a resolution of 1920 x 1088 using a frame rate of 60 fps, and a high shutter speed (1/640s, f4.5, ISO800) to minimize blurring between frames (Figure 68). The entire apparatus was well lit by two 500W work lamps positioned above and at either end of the apparatus on the opposite side of the room (to minimize glare artifact).

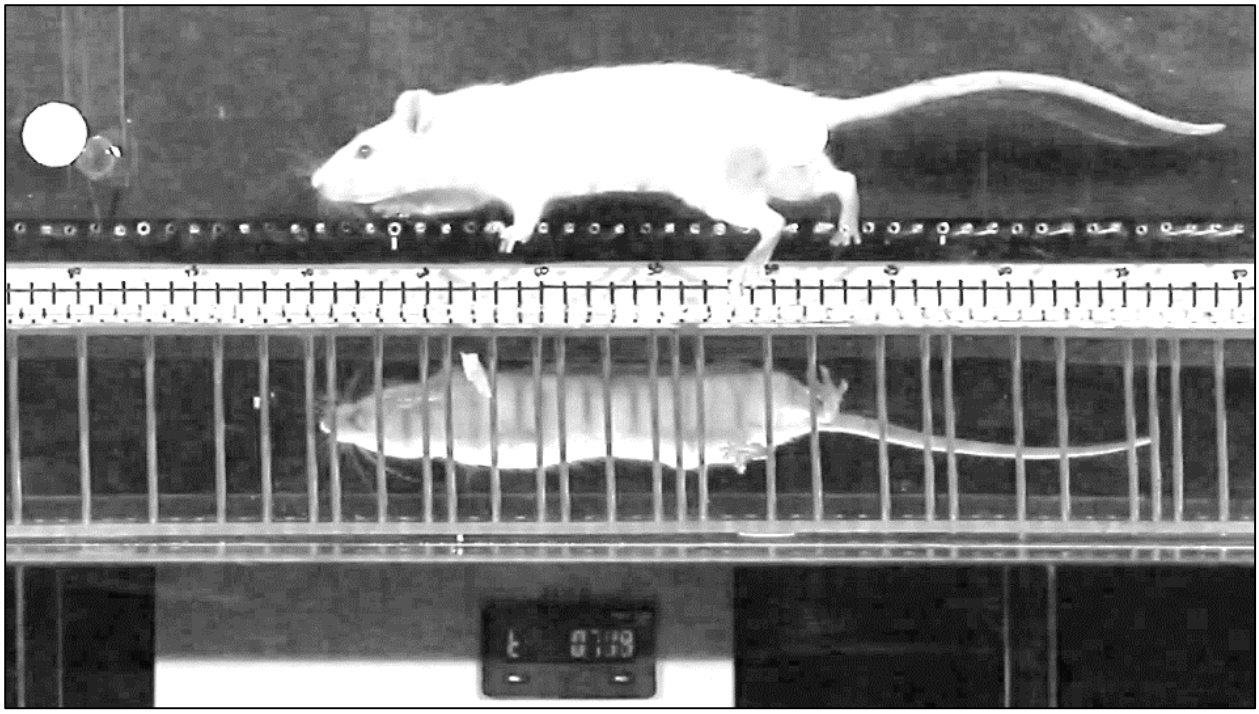

Figure 68: Typical still frame quality of captured video showing a slipped step of the left hind limb

WORKS CITED

1. Ide, C. Peripheral nerve regeneration. *Neurosci. Res.* **25,** 101–21 (1996).

2. Burnett, M. G. & Zager, E. L. Pathophysiology of peripheral nerve injury: a brief review. *Neurosurg. Focus* **16,** E1 (2004).

3. Welch, J. A. Peripheral nerve injury. *Semin. Vet. Med. Surg. (Small Anim).* **11,** 273–84 (1996).

4. Brushart, T. M. *Nerve Repair*. (Oxford University Press, 2011). doi:10.1093/med/9780195169904.001.0001

5. Sunderland, S. The anatomy and physiology of nerve injury. *Muscle Nerve* **13,** 771–84 (1990).

6. *Neuroscience*. (Sinauer Associates, Inc., 2012).

7. Hall, S. Nerve repair: a neurobiologist's view. *J. Hand Surg. Br.* **26,** 129–36 (2001).

8. Gilbert, S. F. *Developmental Biology*. (Sinauer Associates, Inc., 2010).

9. Maggi, S. P., Lowe, J. B. & Mackinnon, S. E. Pathophysiology of nerve injury. *Clin. Plast. Surg.* **30,** 109–126 (2003).

10. De Medinaceli, L., Wyatt, R. J. & Freed, W. J. Peripheral nerve reconnection: mechanical, thermal, and ionic conditions that promote the return of function. *Exp. Neurol.* **81,** 469–87 (1983).

11. Waller, A. On the section of the glossopharyngeal and hypoglossal nerves of the frog, and observations of the alterations produced thereby in the structure of their primitive fibres. *... Trans. R. Soc. ...* **140,** 423–429 (1850).

12. Rotshenker, S. Wallerian degeneration: the innate-immune response to traumatic nerve injury. *J. Neuroinflammation* **8,** 109 (2011).

13. Taskinen, H. S. *et al.* Peripheral nerve injury induces endoneurial expression of IFN-gamma, IL-10 and TNF-alpha mRNA. *J. Neuroimmunol.* **102,** 17–25 (2000).

14. Bendszus, M. & Stoll, G. Caught in the act: in vivo mapping of macrophage infiltration in nerve injury by magnetic resonance imaging. *J. Neurosci.* **23,** 10892–6 (2003).

15. Perry, V. H., Brown, M. C. & Gordon, S. The macrophage response to central and peripheral nerve injury. A possible role for macrophages in regeneration. *J. Exp. Med.* **165,** 1218–23 (1987).

16. Dahlin, L. B. Prevention of macrophage invasion impairs regeneration in nerve grafts. *Brain Res.* **679,** 274–80 (1995).

17. Baichwal, R. R., Bigbee, J. W. & DeVries, G. H. Macrophage-mediated myelin-related mitogenic factor for cultured Schwann cells. *Proc. Natl. Acad. Sci. U. S. A.* **85,** 1701–5 (1988).

18. Lee, S. K. & Wolfe, S. W. Peripheral nerve injury and repair. *J. Am. Acad. Orthop. Surg.* **8,** 243–52 (2000).

19. Fu, S. Y. & Gordon, T. The cellular and molecular basis of peripheral nerve regeneration. *Mol. Neurobiol.* **14,** 67–116 (1997).

20. Wood, M. D., Kemp, S. W. P., Weber, C., Borschel, G. H. & Gordon, T. Outcome measures of peripheral nerve regeneration. *Ann. Anat.* **193,** 321–33 (2011).

21. Fawcett, J. W. & Keynes, R. J. Peripheral nerve regeneration. *Annu. Rev. Neurosci.* **13,** 43–60 (1990).

22. Seckel, B. R. Enhancement of peripheral nerve regeneration. *Muscle Nerve* **13,** 785–800 (1990).

23. Belkas, J. S., Shoichet, M. S. & Midha, R. Peripheral nerve regeneration through guidance tubes. *Neurol. Res.* **26,** 151–60 (2004).

24. Valero-Cabré, A., Tsironis, K., Skouras, E., Navarro, X. & Neiss, W. F. Peripheral and spinal motor reorganization after nerve injury and repair. *J. Neurotrauma* **21,** 95–108 (2004).

25. Gutmann, B. Y. E., Guttmann, L. & Medawar, B. The rate of regeneration of nerve. *J. Exp. Biol.* **19,** 14–44 (1942).

26. Wujek, J. R. & Lasek, R. J. Correlation of axonal regeneration and slow component B in two branches of a single axon. *J. Neurosci.* **3,** 243–251 (1983).

27. Jacob, J. M. & McQuarrie, I. G. Axotomy accelerates slow component b of axonal transport. *J. Neurobiol.* **22,** 570–582 (1991).

28. Jacob, J. M. & McQuarrie, I. G. Acceleration of axonal outgrowth in rat sciatic nerve at one week after axotomy. *J. Neurobiol.* **24,** 356–67 (1993).

29. Love, F. M. & Thompson, W. J. Schwann cells proliferate at rat neuromuscular junctions during development and regeneration. *J. Neurosci.* **18,** 9376–85 (1998).

30. Gordon, T., Hegedus, J. & Tam, S. L. Adaptive and maladaptive motor axonal sprouting in aging and motoneuron disease. *Neurol. Res.* **26,** 174–85 (2004).

31. Jonsson, S. *et al.* Effect of delayed peripheral nerve repair on nerve regeneration, schwann cell function and target muscle recovery. *PLoS One* **8,** e56484 (2013).

32. Dayawansa, S. *et al.* Allotransplanted DRG neurons or Schwann cells affect functional recovery in a rodent model of sciatic nerve injury. *Neurol. Res.* **36,** 1020–7 (2014).

33. Kouyoumdjian, J. A. Peripheral nerve injuries: A retrospective survey of 456 cases. *Muscle and Nerve* **34,** 785–788 (2006).

34. Portincasa, A. *et al.* Microsurgical treatment of injury to peripheral nerves in upper and lower limbs: A critical review of the last 8 years. *Microsurgery* **27,** 455–462 (2007).

35. Scholz, T. *et al.* Peripheral nerve injuries: an international survey of current treatments and future perspectives. *J. Reconstr. Microsurg.* **25,** 339–44 (2009).

36. Taylor, C. a, Braza, D., Rice, J. B. & Dillingham, T. The incidence of peripheral nerve injury in extremity trauma. *Am. J. Phys. Med. Rehabil.* **87,** 381–5 (2008).

37. Noble, J., Munro, C. A., Prasad, V. S. & Midha, R. Analysis of upper and lower extremity peripheral nerve injuries in a population of patients with multiple injuries. *J. Trauma* **45,** 116–22 (1998).

38. Selecki, B. R., Ring, I. T., Simpson, D. A., Vanderfield, G. K. & Sewell, M. F. Trauma to the central and peripheral nervous systems: Part I: an overview of mortality, morbidity and costs; N.S.W. 1977. *Aust. N. Z. J. Surg.* **52,** 93–102 (1982).

39. Christie, K. J. & Zochodne, D. Peripheral axon regrowth: new molecular approaches. *Neuroscience* **240,** 310–24 (2013).

40. Nichols, C. M. *et al.* Effects of motor versus sensory nerve grafts on peripheral nerve regeneration. *Exp. Neurol.* **190,** 347–55 (2004).

41. Mackinnon, S. E., Doolabh, V. B., Novak, C. B. & Trulock, E. P. Clinical outcome following nerve allograft transplantation. *Plast. Reconstr. Surg.* **107,** 1419–29 (2001).

42. Pfister, B. J. *et al.* Biomedical engineering strategies for peripheral nerve repair: surgical applications, state of the art, and future challenges. *Crit. Rev. Biomed. Eng.* **39,** 81–124 (2011).

43. Whitlock, E. L. *et al.* Processed allografts and type I collagen conduits for repair of peripheral nerve gaps. *Muscle Nerve* **39,** 787–99 (2009).

44. Richmond, F. J. *et al.* Efficacy of seven retrograde tracers, compared in multiple-labelling studies of feline motoneurones. *J. Neurosci. Methods* **53,** 35–46 (1994).

45. Brushart, T. M. & Mesulam, M. M. Alteration in connections between muscle and anterior horn motoneurons after peripheral nerve repair. *Science* **208,** 603–5 (1980).

46. Tam, S. L., Archibald, V., Jassar, B., Tyreman, N. & Gordon, T. Increased neuromuscular activity reduces sprouting in partially denervated muscles. *J. Neurosci.* **21,** 654–67 (2001).

47. Major, L. A., Hegedus, J., Weber, D. J., Gordon, T. & Jones, K. E. Method for counting motor units in mice and validation using a mathematical model. *J. Neurophysiol.* **97,** 1846–56 (2007).

48. McComas, a J., Fawcett, P. R., Campbell, M. J. & Sica, R. E. Electrophysiological estimation of the number of motor units within a human muscle. *J. Neurol. Neurosurg. Psychiatry* **34,** 121–31 (1971).

49. Cragg, B. G. & Thomas, P. K. Changes in conduction velocity and fibre size proximal to peripheral nerve lesions. *J. Physiol.* **157,** 315–27 (1961).

50. Davis, L. A., Gordon, T., Hoffer, J. A., Jhamandas, J. & Stein, R. B. Compound action potentials recorded from mammalian peripheral nerves following ligation or resuturing. *J. Physiol.* **285,** 543–59 (1978).

51. Navarro, X., Udina, E., Ceballos, D. & Gold, B. G. Effects of FK506 on nerve regeneration and reinnervation after graft or tube repair of long nerve gaps. *Muscle Nerve* **24,** 905–15 (2001).

52. Gramsbergen, a, IJkema-Paassen, J. & Meek, M. F. Sciatic nerve transection in the adult rat: abnormal EMG patterns during locomotion by aberrant innervation of hindleg muscles. *Exp. Neurol.* **161,** 183–193 (2000).

53. Gordon, T., Yang, J. F., Ayer, K., Stein, R. B. & Tyreman, N. Recovery potential of muscle after partial denervation: a comparison between rats and humans. *Brain Res. Bull.* **30,** 477–82 (1993).

54. Chen, C.-J. *et al.* Transplantation of bone marrow stromal cells for peripheral nerve repair. *Exp. Neurol.* **204,** 443–53 (2007).

55. Kemp, S. W. P. *et al.* Dose and duration of nerve growth factor (NGF) administration determine the extent of behavioral recovery following peripheral nerve injury in the rat. *Exp. Neurol.* **229,** 460–70 (2011).

56. Walsh, S. K., Gordon, T., Addas, B. M. J., Kemp, S. W. P. & Midha, R. Skin-derived precursor cells enhance peripheral nerve regeneration following chronic denervation. *Exp. Neurol.* **223,** 221–8 (2010).

57. Brenner, M. J., Dvali, L., Hunter, D. a, Myckatyn, T. M. & Mackinnon, S. E. Motor neuron regeneration through end-to-side repairs is a function of donor nerve axotomy. *Plast. Reconstr. Surg.* **120,** 215–23 (2007).

58. De Medinaceli, L., Freed, W. J. & Wyatt, R. J. An index of the functional condition of rat sciatic nerve based on measurements made from walking tracks. *Exp. Neurol.* **77,** 634–43 (1982).

59. Bain, J. R., Mackinnon, S. E. & Hunter, D. A. Functional evaluation of complete sciatic, peroneal, and posterior tibial nerve lesions in the rat. *Plast. Reconstr. Surg.* **83,** 129–38 (1989).

60. Hare, G. M. *et al.* Walking track analysis: a long-term assessment of peripheral nerve recovery. *Plast. Reconstr. Surg.* **89,** 251–8 (1992).

61. Rupp, A. *et al.* Electrophysiologic assessment of sciatic nerve regeneration in the rat: surrounding limb muscles feature strongly in recordings from the gastrocnemius muscle. *J. Neurosci. Methods* **166,** 266–77 (2007).

62. Couto, P. a *et al.* A comparison of two-dimensional and three-dimensional techniques for the determination of hindlimb kinematics during treadmill locomotion in rats following spinal cord injury. *J. Neurosci. Methods* **173,** 193–200 (2008).

63. Kemp, S. W. P., Alant, J., Walsh, S. K., Webb, A. a & Midha, R. Behavioural and anatomical analysis of selective tibial nerve branch transfer to the deep peroneal nerve in the rat. *Eur. J. Neurosci.* **31,** 1074–90 (2010).

64. Varejão, A. S. P. *et al.* Motion of the foot and ankle during the stance phase in rats. *Muscle Nerve* **26,** 630–5 (2002).

65. Zumwalt, A. C., Hamrick, M. & Schmitt, D. Force plate for measuring the ground reaction forces in small animal locomotion. *J. Biomech.* **39,** 2877–81 (2006).

66. Howard, C. S., Blakeney, D. C., Medige, J., Moy, O. J. & Peimer, C. a. Functional assessment in the rat by ground reaction forces. *J. Biomech.* **33,** 751–7 (2000).

67. Clarke, K. A. Differential fore- and hindpaw force transmission in the walking rat. *Physiol. Behav.* **58,** 415–9 (1995).

68. Hruska, R. E., Kennedy, S. & Silbergeld, E. K. Quantitative aspects of normal locomotion in rats. *Life Sci.* **25,** 171–9 (1979).

69. Zellem, R. T., Miller, D. W., Kenning, J. a, Hoenig, E. M. & Buchheit, W. a. Experimental peripheral nerve repair: environmental control directed at the cellular level. *Microsurgery* **10,** 290–301 (1989).

70. Lowdon, I. M., Seaber, a V & Urbaniak, J. R. An improved method of recording rat tracks for measurement of the sciatic functional index of de Medinaceli. *J. Neurosci. Methods* **24,** 279–81 (1988).

71. Shen, N. & Zhu, J. Application of sciatic functional index in nerve functional assessment. *Microsurgery* **16,** 552–5 (1995).

72. De Medinaceli, L., DeRenzo, E. & Wyatt, R. J. Rat sciatic functional index data management system with digitized input. *Comput. Biomed. Res.* **17,** 185–92 (1984).

73. Carlton, J. & Goldberg, N. Quantitating integrated muscle function following reinnervation. *Surg. Forum* **37,** 611 (1986).

74. Hoogeveen, J. F., Troost, D., Wondergem, J., van der Kracht, a H. & Haveman, J. Hyperthermic injury versus crush injury in the rat sciatic nerve: a comparative functional, histopathological and morphometrical study. *J. Neurol. Sci.* **108,** 55–64 (1992).

75. Kuypers, P. D., van Egeraat, J. M., van Briemen, L. J., Godschalk, M. & Hovius, S. E. A magnetic evaluation of peripheral nerve regeneration: II. The signal amplitude in the distal segment in relation to functional recovery. *Muscle Nerve* **21,** 750–5 (1998).

76. Kuypers, P. D., Walbeehm, E. T., Heel, M. D., Godschalk, M. & Hovius, S. E. Changes in the compound action current amplitudes in relation to the conduction velocity and functional recovery in the reconstructed peripheral nerve. *Muscle Nerve* **22,** 1087–93 (1999).

77. Clavijo-Alvarez, J. a *et al.* Comparison of biodegradable conduits within aged rat sciatic nerve defects. *Plast. Reconstr. Surg.* **119,** 1839–51 (2007).

78. De Ruiter, G. C. *et al.* Two-dimensional digital video ankle motion analysis for assessment of function in the rat sciatic nerve model. *J. Peripher. Nerv. Syst.* **12,** 216–22 (2007).

79. Kim, S.-M., Lee, S.-K. & Lee, J.-H. Peripheral nerve regeneration using a three dimensionally cultured schwann cell conduit. *J. Craniofac. Surg.* **18,** 475–88 (2007).

80. Meek, M. F., Ijkema-Paassen, J. & Gramsbergen, A. Functional recovery after transection of the sciatic nerve at an early age: a pilot study in rats. *Dev. Med. Child Neurol.* **49,** 377–9 (2007).

81. Nie, X. *et al.* Improvement of peripheral nerve regeneration by a tissue-engineered nerve filled with ectomesenchymal stem cells. *Int. J. Oral Maxillofac. Surg.* **36,** 32–8 (2007).

82. Monte-Raso, V. V., Barbieri, C. H., Mazzer, N., Yamasita, A. C. & Barbieri, G. Is the Sciatic Functional Index always reliable and reproducible? *J. Neurosci. Methods* **170,** 255–61 (2008).

83. Dinh, P., Hazel, A., Palispis, W., Suryadevara, S. & Gupta, R. Functional assessment after sciatic nerve injury in a rat model. *Microsurgery* **29,** 644–9 (2009).

84. Chen, J., Chu, Y. F., Chen, J. M. & Li, B. C. Synergistic effects of NGF, CNTF and GDNF on functional recovery following sciatic nerve injury in rats. *Adv. Med. Sci.* **55,** 32–42 (2010).

85. Wood, M. D. *et al.* Fibrin matrices with affinity-based delivery systems and neurotrophic factors promote functional nerve regeneration. *Biotechnol. Bioeng.* **106,** 970–9 (2010).

86. Matsuda, K. *et al.* Retrograde axonal tracing using manganese enhanced magnetic resonance imaging. *Neuroimage* **50,** 366–74 (2010).

87. Nagao, R. J., Lundy, S., Khaing, Z. Z. & Schmidt, C. E. Functional characterization of optimized acellular peripheral nerve graft in a rat sciatic nerve injury model. *Neurol. Res.* **33,** 600–8 (2011).

88. Bittner, G. D. *et al.* Rapid, effective, and long-lasting behavioral recovery produced by microsutures, methylene blue, and polyethylene glycol after completely cutting rat sciatic nerves. *J. Neurosci. Res.* **90,** 967–80 (2012).

89. Penna, V., Wewetzer, K., Munder, B., Stark, G. B. & Lang, E. M. The long-term functional recovery of repair of sciatic nerve transection with biogenic conduits. *Microsurgery* **32,** 377–82 (2012).

90. Xu, L. *et al.* Neural stem cells enhance nerve regeneration after sciatic nerve injury in rats. *Mol. Neurobiol.* **46,** 265–74 (2012).

91. Lee, J.-Y. *et al.* Functional evaluation in the rat sciatic nerve defect model: a comparison of the sciatic functional index, ankle angles, and isometric tetanic force. *Plast. Reconstr. Surg.* **132,** 1173–80 (2013).

92. Shenaq, J. M., Shenaq, S. M. & Spira, M. Reliability of sciatic function index in assessing nerve regeneration across a 1 cm gap. *Microsurgery* **10,** 214–9 (1989).

93. Maeda, T. *et al.* Regeneration across ‘stepping-stone’ nerve grafts. *Brain Res.* **618,** 196–202 (1993).

94. Meek, M. F., den Dunnen, W. F., Robinson, P. H., Pennings, A. J. & Schakenraad, J. M. Evaluation of functional nerve recovery after reconstruction with a new biodegradable poly (DL-lactide-epsilon-caprolactone) nerve guide. *Int. J. Artif. Organs* **20,** 463–8 (1997).

95. Dellon, A. L. & Mackinnon, S. E. Sciatic nerve regeneration in the rat. Validity of walking track assessment in the presence of chronic contractures. *Microsurgery* **10,** 220–5 (1989).

96. Dellon, E. S. & Dellon, a L. Functional assessment of neurologic impairment: track analysis in diabetic and compression neuropathies. *Plast. Reconstr. Surg.* **88,** 686–694 (1991).

97. Meek, M. F., Den Dunnen, W. F., Schakenraad, J. M. & Robinson, P. H. Long-term evaluation of functional nerve recovery after reconstruction with a thin-walled biodegradable poly (DL-lactide-epsilon-caprolactone) nerve guide, using walking track analysis and electrostimulation tests. *Microsurgery* **19,** 247–53 (1999).

98. Chen, B., Song, Y. & Liu, Z. Promotion of nerve regeneration in peripheral nerve by short-course FK506 after end-to-side neurorrhaphy. *J. Surg. Res.* **152,** 303–10 (2009).

99. Wong, K.-H. *et al.* Peripheral Nerve Regeneration Following Crush Injury to Rat Peroneal Nerve by Aqueous Extract of Medicinal Mushroom Hericium erinaceus (Bull.: Fr) Pers. (Aphyllophoromycetideae). *Evid. Based. Complement. Alternat. Med.* **2011,** 580752 (2011).

100. Galtrey, C. M. & Fawcett, J. W. Characterization of tests of functional recovery after median and ulnar nerve injury and repair in the rat forelimb. *J. Peripher. Nerv. Syst.* **12,** 11–27 (2007).

101. Metz, G. a & Whishaw, I. Q. Cortical and subcortical lesions impair skilled walking in the ladder rung walking test: a new task to evaluate fore- and hindlimb stepping, placing, and co-ordination. *J. Neurosci. Methods* **115,** 169–79 (2002).

102. Metz, G. a & Whishaw, I. Q. The ladder rung walking task: a scoring system and its practical application. *J. Vis. Exp.* 2–5 (2009). doi:10.3791/1204

103. Soblosky, J. S., Colgin, L. L., Chorney-Lane, D., Davidson, J. F. & Carey, M. E. Ladder beam and camera video recording system for evaluating forelimb and hindlimb deficits after sensorimotor cortex injury in rats. *J. Neurosci. Methods* **78,** 75–83 (1997).

104. Varejão, a S., Meek, M. F., Ferreira, a J., Patrício, J. a & Cabrita, a M. Functional evaluation of peripheral nerve regeneration in the rat: walking track analysis. *J. Neurosci. Methods* **108,** 1–9 (2001).

105. Walker, J. L., Evans, J. M., Meade, P., Resig, P. & Sisken, B. F. Gait-stance duration as a measure of injury and recovery in the rat sciatic nerve model. *J. Neurosci. Methods* **52,** 47–52 (1994).

106. PHS Policy on Humane Care and Use of Laboratory Animals. (2002). at <http://grants.nih.gov/grants/olaw/references/phspol.htm>

107. Guide for the Care and Use of Laboratory Animals. (2011). at <http://www.ncbi.nlm.nih.gov/books/NBK54050/>

108. Kilkenny, C., Browne, W. J., Cuthill, I. C., Emerson, M. & Altman, D. G. Improving bioscience research reporting: the ARRIVE guidelines for reporting animal research. *PLoS Biol.* **8,** e1000412 (2010).

109. Gerfen, C. R. Basic neuroanatomical methods. *Curr. Protoc. Neurosci.* **Chapter 1,** Unit 1.1 (2003).

110. Schofield, B. R. Retrograde axonal tracing with fluorescent markers. *Curr. Protoc. Neurosci.* **Chapter 1,** Unit 1.17 (2008).

111. Bland, J. M. & Altman, D. G. Statistical methods for assessing agreement between two methods of clinical measurement. *Lancet* **1,** 307–10 (1986).

112. Bland, J. M. & Altman, D. G. Measuring agreement in method comparison studies. *Stat. Methods Med. Res.* **8,** 135–60 (1999).

113. Weber, R. a, Proctor, W. H., Warner, M. R. & Verheyden, C. N. Autotomy and the sciatic functional index. *Microsurgery* **14,** 323–7 (1993).

114. Jin, J. *et al.* Peripheral nerve repair in rats using composite hydrogel-filled aligned nanofiber conduits with incorporated nerve growth factor. *Tissue Eng. Part A* **19,** 2138–46 (2013).

115. Schmalbruch, H. Fiber composition of the rat sciatic nerve. *Anat. Rec.* **215,** 71–81 (1986).

116. Swett, J. E., Wikholm, R. P., Blanks, R. H., Swett, a L. & Conley, L. C. Motoneurons of the rat sciatic nerve. *Exp. Neurol.* **93,** 227–52 (1986).